Complementation of a bimolecular Antibody-Derivative within the context of the Immunological Synapse

Komplementierung eines bimolekularen Antikörper-Derivates im Kontext der Immunologischen Synapse

Doctoral thesis for a doctoral degree

at the Graduate School of Life Sciences,

Julius-Maximilians-Universität Würzburg,

Section Integrative Biology

submitted by

Dina Kouhestani

from

Neyshaboor, Iran

Würzburg 2019

Submitted on:

Members of the Promotionskomitee:

Chairperson: Prof. Dr. med. Georg Gasteiger

Primary Supervisor: Prof. Dr. Markus Sauer

Supervisor (Second): Prof. Dr. med. Hermann Einsele

Supervisor (Third): Dr. med. Thomas Bumm

Date of Public Defence: ……..……

Date of Receipt of Certificates: …….

Affidavit

I hereby confirm that my thesis entitled Complementation of a bimolecular Antibody-Derivative within the context of the Immunological Synapse is the result of my own work. I did not receive any help or support from commercial consultants. All sources and/ or materials applied are listed and specified in the thesis.

Furthermore, I confirm that this thesis has not yet been submitted as part of another examination process neither in identical nor in similar form.

Würzburg, 18 November 2019

Dina Kouhestani

Eidesstattliche Erklärung

Hiermit erkläre ich an Eides statt, die Dissertation Komplementierung eines bimolekularen Antikörper-Derivates im Kontext der Immunologischen Synapse eigenständig, d.h. insbesondere selbstständig und ohne Hilfe eines kommerziellen Promotionsberaters, angerfertigt und keine anderen als die von mir angegebenen Quellen und Hilfsmittel verwendet zu haben.

Ich erkläre außerdem, dass die Dissertation weder in gleicher noch in ähnlicher Form bereits in einem anderen Prüfungsverfahren vorgelegen hat.

Würzburg, 18 November 2019

Dina Kouhestani

Acknowledgements

First and foremost, I have to thank my research supervisors Prof. Dr. med. Gernot Stuhler, Prof. Dr. Markus Sauer and Dr. med. Thomas Bumm who supervised me during this project and gave me the opportunity to carry out this study within their group and laboratory. Without their assistance and dedicated involvement in every step throughout the process, this work would have never been accomplished. I would like to thank all of you very much for your support and understanding over these past four years. I would also like to thank Prof. Dr. med. Hermann Einsele, who agreed to supervise me during this study as second assessor.

I would also like to show gratitude to our Post docs, Dr. Tim Schnyder and Dr. Boris Nowotny for inspiring discussions and drawing attentions to many precious points in my project, and I hope that I have managed to address several of them here. I am also grateful for the good collaboration on the FCS (fluorescence correlation spectroscopy) experiments with Dr. Hannes Neuweiler and his doctoral student Julia Heiby. Their results are a part of our already submitted manuscript.

Getting through my dissertation required more than academic support, and I have many, many people to thank for listening to and, at times, having to tolerate me over the past four years. I cannot begin to express my gratitude and appreciation for their friendship, Dr. Maria Geis, Isabel Strömer and Annika Grimmer.

I must also thank Marc-Dominic Bohn and Keali Röhm for helping me for the improvement of my English texts, and Hannes Gotthardt for creating some of the gene illustrations.

Furthermore, I would like to thank the following peoples who supported me discovering the details of the hemibody binding behaviour using microscopy: Dr. Robert Blum, who not only give me permission to use their confocal laser scanning microscope, but also connected me with many knowledgeable persons and Dr. Thomas Andreska for giving me the introduction to use the microscope. Dr. Zeinab Mokhtari who gave me very helpful tips for the scientific processing of my microscopy images using software. Dr. Corrina Martin who assisted me during ca flux imaging and provided helpful material for these experiments. Prof. Dr. Katrin Heinze who gave me permission to use their time-lapse microscope and Mike Friedrich and Jürgen Pinnerker who assisted me making time-lapse films. Dr. Julian Rydzek who provided me the materials for transfection of Jurkat cells with ZAP70-GFP gene.

Moreover, I would like to thank the members of GSLS (graduate school of life science Würzburg) for their support, advice for the thesis submission, and their friendly welcome. Most importantly, none of this could have happened without my family. My uncle and his wife, who

offered their encouragement through phone calls every week. With their understanding, they have been kind and supportive to me over the last several years. To my parents, my brother and my boyfriend – it would be an understatement to say that, as a family, we have experienced some ups and downs in the past four years. Every time I was ready to quit, you did not let me, and I am forever grateful. This dissertation stands as a testament to your unconditional love and encouragement.

Table of contents

1 Abstract

Cancer is a disease of uncontrolled cell proliferation and migration. Downregulation of antigen-presenting major histocompatibility complex (MHC) and co-stimulatory molecules are two of the most commonly used pathways by cancer cells to escape from immune surveillance. Therefore, many approaches have been developed for restoring the immune surveillance in cancer patients. One approach is to redirect the patient's own T cells for tumor cell destruction. For T cell function it is important to induce a durable and robust cytotoxic response against target cells and to generate memory T cells, after MHC-mediated recognition of foreign intracellular antigens presented on the surface of antigen presenting cells (APC). Because of these cytotoxic properties, T cell mediated immunotherapy has been established as an effective and durable anti-neoplastic treatment. Different T cell mediated therapies for cancer treatment exist. One of them is using bispecific antibody fragments, so called bi-sepcific T cell engagers (BiTEs), for retargeting of T cells against single antigen positive tumor cells. The BiTE antibodies have two antigen binding domains, one against a target on the target cell, the second against CD3 on the T cells, facilitating cell-to-cell interactions. However, suitable single tumor antigens are limited, which restricts this approach to very few tumor types. To overcome this limitation, we have developed T cell-engaging antibody derivatives, termed hemibodies.

Hemibodies exist as two complementary polypeptide chains. Each consists of two specific domains. On one end there is a single-chain variable fragment (scFv) against a target protein and on the other end there is either the heavy chain variable domain (VH) or light chain variable domain (VL) of an anti-CD3 binding antibody. Only when both hemibodies bind their respective antigens on the same tumor cell, the complementary anti CD3 VH and VL domains become aligned and reconstitute the functional CD3 binding-domain to engage T cells.

For targeting malignant cells of hematopoietic origin, we used hemibodies against CD45 and HLA-A2. They were expressed in CHO cells, then purified via Strep-tag. To get more insight into the hemibody mechanism of T cell mediated target cell killing, we analyzed the biochemical and functional properties of hemibodies in more detail.

Our main finding indicates that VLαCD3-scFvαHLA-A2 and VHαCD3-scFvαCD45 hemibodies induce an atypical immunological synapse characterized by a co-localization of HLA-A2 and CD45 out of the target cell -T cell interface. Nevertheless, hemibodies induce a high caspase activity in target cells in a concentration-dependent manner at nanomolar concentrations *in vitro*. Looking at ZAP70, which is usually recruited from the cytoplasm to the CD3 receptor in

the middle of the cell-cell interface, we were able to detect activated ZAP70 outside of the cell-cell interface in the presence of hemibodies. In contrast cells treated with BiTEs show a central recruitment in the cell-cell interface as expected.

We looked also at the interaction of hemibodies with soluble recombinant CD3 epsilon/gamma protein in the absence of target cells. The binding could be measured only at very high concentration out of the therapeutic window.

This work contributes to the mechanistic understanding, which underlies the hemibody technology as a new dual antigen restricted T cell-mediated immunotherapy of cancer.

Kurzbeschreibung

Krebs ist eine Krankheit mit unkontrollierter Zellproliferation und -migration. Die Herunterregulierung des antigen-präsentierenden Haupthistokompatibilitätskomplexes (MHC) und der co-stimulierenden Moleküle sind zwei der am häufigsten verwendeten Wege von Krebszellen, um der Immunüberwachung zu entkommen. Daher wurden viele Ansätze zur Wiederherstellung der Immunüberwachung bei Krebspatienten entwickelt. Ein Ansatz besteht darin, die eigenen T-Zellen des Patienten zur Zerstörung von Tumorzellen anzuleiten. T-Zellen zeichnen sich durch ihre schnelle Expansion nach MHC-vermittelter Erkennung von fremden intrazellulären Antigenen auf der Oberfläche von Antigen-präsentierenden Zellen (APC) aus. Darüber hinaus sind eine dauerhafte und robuste zytotoxische Immunantwort und die Erzeugung von Gedächtnis-T-Zellen wichtige Merkmale von T-Zellen. Aufgrund dieser Eigenschaften hat sich die T-Zell-vermittelte Immuntherapie als wirksame antineoplastische Behandlung in den letzten Jahren etabliert. Es gibt verschiedene Ansätze T-Zellen zur Krebsbehandlung zu nutzen. Ein Ansatz verwendet bispezifische Antikörperfragmente, sogenannte bi-sepezifische T-Zell-Engager (BiTEs), zum Retargeting von T-Zellen gegen Antigen-positive Tumorzellen. Die BiTE-Antikörper besitzen zwei Antigen-Bindungsdomänen. Eine ist gegen ein Antigen auf der Zielzelle gerichtet und die zweite ist gegen CD3 auf T-Zellen gerichtet, was zu einer direkten Rekrutierung der T-Zelle an die Zielzelle führt. Geeignete einzelne Tumorantigene, die nur auf Tumorzellen zu finden sind und nicht auf gesundem Gewebe sind jedoch begrenzt, was diesen Ansatz auf sehr wenige Tumortypen einschränkt. Um diese Einschränkung zu überwinden, haben wir bispezifische T-Zell-rekrutierende Antikörper-Derivate entwickelt, sogenannte Hemibodies.

Hemibodies sind „single chain“ Polypeptidketten. Jeder Hemibody besitzt zwei spezifische Antigen bindende Domänen. Eine Domäne besteht aus einem „single chain variable Fragment“ (scFv) und ist gegen ein Zielantigen gerichtet und zweite Effektor-Domäne besteht entweder aus der variablen Domäne der schweren Kette (VH), oder die variable Domäne der leichten Kette (VL) eines Anti-CD3-Antikörpers. Nur wenn zwei komplementierende Hemibodies ihr jeweiliges Antigen auf der Oberfläche derselben Zielzelle binden, können die beiden anti-CD3-VH- und anti-CD3-VL-Domänen komplementieren und erst jetzt die funktionelle anti-CD3-Bindungsdomäne ausbilden um T-Zellen zu binden und zu aktivieren.

Zur Therapie von bösartigen Zellen hämatopoetischen Ursprungs haben wir Hemibodies gegen CD45 und HLA-A2 hergestellt. Sie wurden in CHO-Zellen exprimiert und dann über

Strep-Tag gereinigt. Um mehr über den Hemibody-Mechanismus der T-Zell-vermittelten Abtötung von Zielzellen zu erfahren, haben wir die biochemischen und funktionellen Eigenschaften von Hemibodies genauer analysiert.

Unser Arbeit zeigt, dass VLαCD3-scFvαHLA-A2- und VHαCD3-scFvαCD45-Hemibodies eine atypische immunologische Synapse ausbilden. Diese ist gekennzeichnet durch die gemeinsame Verdrängung von HLA-A2 und CD45 aus dem „interface“ zwischen Zielzelle und T-Zelle. Dennoch können Hemibodies selbst bei Konzentrationen im nanomolaren Bereich in vitro eine Caspase-Aktivität in den Zielzellen induzieren. Betrachtet man ZAP70, dass bei T-Zell Aktivierung normalerweise vom Zytoplasma zum CD3-Rezeptor in der Mitte des Zell-Zell „interface“ rekrutiert wird, zeigt sich bei der Hemibody vermittelten T-Zell Aktivierung aktiviertes ZAP70 außerhalb des Zell-Zell „interface“. Im Gegensatz zu Hemibodies zeigen mit BiTEs aktivierte T-Zellen erwartungsgemäß eine zentrale Rekrutierung von ZAP70 im Zell-Zell „interface“.

Wir untersuchten auch die Wechselwirkung von Hemibodies mit löslichem rekombinantem CD3-Epsilon / Gamma-Protein in Abwesenheit von Zielzellen. Eine Bindung konnte nur bei sehr hoher Konzentration außerhalb des therapeutischen Fensters gemessen werden.

Diese Arbeit untersucht im Detail den T-Zell vermittelten Mechanismus der Hemibody Technologie. Die Ergebnisse ermöglichen uns den Wirkmechanismus der Hemibodies besser zu verstehen. Dies ist wichtig für die sichere Weiterentwicklung dieser neuen zielgerichteten T-Zell vermittelten Immuntherapie.

2 Introduction

2.1 Cancer

In contrast to healthy cells, cancer cells grow and divide in an uncontrolled manner. R.A. Weinberg has defined the hallmarks of cancer, which are important for the clonal evolution of a healthy cell into a cancer cell. They consist of sustaining proliferative signalling, escaping growth suppression, resisting programmed cell death, replicative immortality, activating angiogenesis, reprogramming of energy metabolism, escaping the immune system, inducing invasion, and finally metastasis. Genomic instability as a common feature in most cancer cells, gives rise to these hallmarks (Hanahan & Weinberg, 2011). A defect in the regulation of surveillance mechanisms, DNA damage checkpoints, and DNA repair machinery can lead to genomic instability (Yao & Dai, 2014). It has been reported that accumulation of genomic alterations within normal cells, and selection of aggressively growing cells contributes to the tumor initiation and progression (Nowell, 1976). As a consequence of genomic instability, the tumor cells are characterized by shorter cell cycle and/or can bypass intracellular and immunological checkpoints (Yao & Dai, 2014).

2.2 Cancer Treatment

Our growing understanding of the biology of cancer enables many possibilities to prevent and cure disease. One of the most important causes of cancer are external noxa like tobacco smoke or ultraviolet radiation and therefore, avoiding the teratogenic noxa is important to reduce the risk for specific cancer like lung cancer and malignant melanoma.

However, prevention teratogenic noxa or screening for early pre-cancerous tumor cells is not sufficient to prevent all cancer types. A recent publication concludes “that most cases of cancer are fundamentally unpreventable because they are the result of chance is unwarranted” (Ledford, H., 2016).

Finding new ways for a safer and more effective cancer therapy is important. Immunotherapy has revolutionized the cancer treatment in the last decade. In the last years antibodies

targeting immune checkpoints have shown great clinical success in some types of solid cancers (Zugazagoitia et al., 2016).

But despite all the success in cancer therapy in the last years, there is still a big medical need for many cancer entities. A major difficulty is in removing every single cancer cell. If a few cancer stem cells remain after therapy, they can proliferate again, causing the disease to relapse (Chang, 2016). Furthermore, the cancer cells are able to gain resistance mechanisms to traditional therapies. The mechanisms that promote drug resistance include drug inactivation, drug target alteration, drug efflux, DNA damage repair, cell death inhibition, and the epithelial-mesenchymal transition. Additionally, the epigenetic modifications have been reported to induce resistance (Housman et al., 2014).

Another drawback of current cancer therapy like radiation and chemotherapy, is the off-target effect on non-malignant healthy cell, resulting in side effects. The side effects can be dose-limiting, causing treatment failure and relapse of the malignant cell clone.

To reduce side effects and to increase the therapeutic effect, modern anticancer therapies need to focus their cytotoxic effect on the malignant cells. The two major columns for modern cancer therapy is 1) targeted therapy against the malignant cell clone, reducing the unwanted side effects 2) activating the cytotoxic potential of the patient own immune system to eliminate the malignant cells.

2.2.1 Cancer Immunotherapy

In the last twenty years, cancer immunotherapy developed to a new column in cancer therapy, next to surgery, chemotherapy, radiation therapy, and small molecule targeted therapy. Current anticancer immunotherapy strategies include tumor-targeting monoclonal antibodies (mAbs), oncolytic viruses, dendritic cell (DC)-based interventions, peptide-based vaccines, immunostimulatory cytokines, immunomodulatory mAbs, pattern recognition receptor (PRR) agonists, immunogenic cell death (ICD) inducers, and adoptive T cell transfer (Galluzzi et al., 2014). In this study, we focus on antibody-based immunotherapy, including our novel hemibody technology derived from the bispecific T cell engager class.

2.2.1.1 Antibody-based immunotherapy

The successful development of monoclonal antibodies for cancer therapy is often compared to Paul Ehrlich’s theory of the “magic bullet”. The “magic bullet” concept was developed by the

German Nobel laureate Paul Ehrlich and the Japanese microbiologist Kiyoshi Shiga in 1900 (Tan & Grimes, 2010). They proposed that it is possible to kill disease-causing microbes with a specific compound, they called “magic bullet”, without harming the body itself.

The first monoclonal antibodies were developed against antigens expressed on the cell surface of cancer cells. The antibodies should bind to the cancer cells and activate the patient’s immune system to destroy the cancer cell.

The first monoclonal antibodies were developed using the hybridoma technology by Georges Köhler and César Milstein (Kohler & Milstein, 2005). The way for the first antibodies from the laboratory to clinic was long. Many difficulties had to be managed like antibody immunogenicity and reduced ability to induce immune effector mechanisms. One of the first monoclonal antibodies in the clinic was Trastuzumab, a highly specific monoclonal antibodies (mAbs) targeting human epidermal growth factor receptor 2 (HER2) in patients with breast cancer (Strebhardt & Ullrich, 2008). Trastuzumab was later also successfully used in other solid cancer expressing the same cell surface antigen HER2 like gastric cancer (Gunturu, Woo, Beaubier, Remotti, & Saif, 2013).

Classic IgG based antibodies like Trastuzumab activate the immune system via the fragment crystallisable (Fc) portion of the antibody. After binding to the antigen-positive cell, different immune responses are initiated. 1) Activation of the complement system via the activation of the complement component, C1 that in turn initiates the classical complement system or via the activation of C3b resulting in induction of alternative complement pathways (Complement in Monoclonal Antibody Therapy of Cancer). 2) Stimulation of antibody-dependent cellular cytotoxicity (ADCC) by binding of the antibody via the Fc domain to the Fc gamma receptor expressed on immune effector cells like natural killer (NK) cells, neutrophils and γδT-cells (Griguolo, Pascual, Dieci, Guarneri, & Prat, 2019).

The cytotoxicity of monoclonal antibodies can be increased by conjugation the antibody to toxic chemicals like potent cytotoxins such as maytansinoid, auristatin, protein toxins like *Pseudomonas* exotoxin, and diphtheria toxin, cytolytic immunomodulatory protein like Fas ligand, biologically active peptide-like GLP-1 which extend the pharmacological half-life of the natural peptide, enzymes such as urease changing the biochemistry of the targeted microenvironment and finally radionuclides like 90Y, 111In (Kamada, H. et al., 2013).

All of these monoclonal antibodies have in common; they are targeting single antigens on tumor cells and do not activate T cells, the most potent cytotoxic cell of the immune system.

2.2.1.2 T cell activating antibody

To enhance the cytotoxic potential of antibodies, a new class of T cell engaging antibodies was developed. In contrast to NK cells or macrophages, the T cell response is more potent for cytotoxicity due to the T cell expansion after activation and the ability to generate immunologic memory cells.

Morrison and colleagues developed in 1997 the first recombinant bispecific immunoglobulin (Coloma & Morrison, 1997). They fused flexible linker peptides to the C-termini of the heavy chains of IgG followed by single-chain variable domains with different specificities.

The first tri-specific T cell activating antibody Catumaxomab was approved in the year 2009, for treating patients with malignant ascites. Catumaxomab is a trispecific antibody with dual specificity for the tumor antigen EpCAM and the T cell specific CD3 molecule. It binds to EpCAM positive tumor cells with one arm and with the second to T cells. With its constant Fc domain, it can also bind to Fc gamma receptor positive immune cells or activate the complement system. This activation of different immune cells is causing a massive cytokine release syndrome in the patient with severe side effects. The therapeutic window for Catumaxomab, the dosage difference between therapeutic effect and severe side effects, was so small that the antibody is not used in the clinic today anymore.

Since the 1980es different T cell recruiting antibodies have been developed. One class that made it all the way into clinic are the bispecific T-cell engagers (BiTEs) (Staerz, Kanagawa, & Bevan, 1985). BiTEs lack the Fc receptor. They consist of two single-chain variable fragments (scFvs) of two different antibodies, linked via a short serine-glycine linker to each other (Figure 1). This short and flexible linker allows the two scFv domains to rotate freely and to bind their respective antigens. One scFv is directed against an antigen on the target cell, and the other scFv domain is directed against the epsilon chain of the CD3 receptor on the T cell. The short 4 amino acid long linker brings the T cell and target cell closer together, resulting in a direct cell-cell contact.

The scFv based BiTE antibodies are small in size, around ~55 kDa, which is much smaller than a traditional antibody with a molecular weight of 146-160 kDa. As a consequence, the small size of these molecules and the lack of the Fc region lead to their rapid renal elimination. But also, the small size can be an advantage regarding solid tissue penetration. BiTEs are potent in vitro and in vivo and can induce specific antitumoral cytotoxicity at concentrations as low as 10 pg/ml, and the cell lysis is achieved at small effector-target cell ratios (Loffler et al., 2000). Furthermore, Bites are able to induce repeated rounds of target cell lysis by T cells (Hoffmann et al., 2005).

The scFv sequence of the first BiTEs is from the original anti-CD3 antibody clone OKT3. The OKT3 antibody is directed against the epsilon subunit of the CD3 receptor complex.

The binding of the antibody to the epsilon chain is activating the CD3 receptor and the T cells. Unlike the natural T cell activation which is controlled by major histocompatibility complex (MHC) recognition and distinct cell surface receptor interactions including costimulatory molecules, BiTE-mediated T cell activation is characterized by a lack of dependence upon T cell costimulation and MHC recognition. This property of BiTEs, to direct activate T cells for target cell killing, is unique for bispecific antibodies. It has been supposed that T cell activation may be achieved by alternate mechanisms such as activation by clustering of many TCRs within the induced immunological synapse (Haas et al., 2009).

Blinatumomab (AMG103, MT103) is the first bispecific T cell recruiting antibody approved from the regulatory authorities in the year 2014 in the USA and in 2015 in Europe, for the treatment of CD19 positive relapsed acute lymphoblastic leukaemia (ALL). Blinatumomab is directed against CD19 and CD3. Blinatumomab is active at very low concentration in nM range and works thru induction of T cell mediated redirected lysis of target cells. A phase III study has confirmed that Blinatumomab is active against CD19 positive B-cell non-Hodgkin's lymphoma and CD19 positive acute lymphoblastic leukaemia (ALL) (Topp, M.S. et al., 2008).

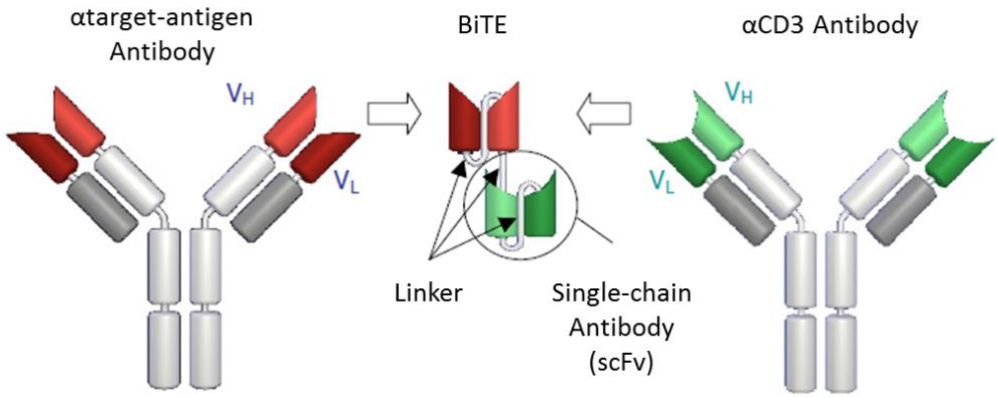

Figure 1 : Schematic construction of BiTE molecule. BiTE molecule is assembled from two monoclonal antibodies. Variables VH and VL domains of each antibody are fused into a single-chain antibody that is linked by a short peptide linker to complete the BiTE construct (Nagorsen, Kufer, Baeuerle, & Bargou, 2012).

2.3 The mode of T cell activation

2.3.1 Mechanism of TCR/CD3 activation

Understanding the mechanisms, by which T cell activating antibodies initiate the synapse formation between target cells and T cell requires a look into the natural T cell receptor (TCR) signaling and downstream signaling cascade which contributes to cellular response. The TCR consists of a multi-subunit receptor complex containing CD3γ, CD3δ, CD3ε, and TCRζ subunits. All of the CD3 receptor components form immunoreceptor tyrosine-based activation motifs (ITAMs) in their cytoplasmic domains. TCRαβ heterodimer recognize and bind to the peptides represented from the major histocompatibility complex (MHC) molecules on the surface of antigen-presenting cells (APCs) (van der Merwe & Dushek, 2011). Engagement of antigen-presenting cells (APC) is the first critical step in T cell activation. This engagement leads to TCR signaling initiation. For complete activation of the TCR signaling cascade, associated invariant CD3 and ζ chains are required (Courtney, Lo, & Weiss, 2018). T cell and APC contacts are classified into two different groups according to their dynamics in vivo: transient connection forming from promigratory junctions termed immunological kinapses and prolonged contacts from stable junctions called immunological synapses. Kinapses are formed when the T cell respond to self-peptide-major histocompatibility complex (pMHC) and looking for pathogen-derived pMHC, while synapses are induced by T cell receptor (TCR) interaction with agonist pMHC resulting in strong immune response which generate effector and memory T cells (Fooksman et al., 2010). T cells have highly efficient mechanisms, to recognize and discriminate antigen on MHC receptor. The T cell development occurs in the thymus, where they learn to distinguish self-peptides from the foreign antigens. During the multistep selection process in the thymus, each developing T cell express a unique TCR and goes thru a self-MHC restricted and self-tolerant T cell selection. Different signals in the thymus decide what will happen with the developing T cell. If T cells with their TCR react weakly to the self-antigens presented by thymocytes, they get a maturation signal which results in the generation of a functional T cell. This type of selection is termed a positive selection. In contrast, if T cells react strongly with self-antigens, they receive a death signal known as negative selection (Stepanek et al., 2014).

Mature T cells must have special properties for their correct function as immune cells. They must be able to detect activating peptide-MHC complexes, and they must be able to discriminate between weak peptide-MHC complexes, in the case of rare peptide-MHC ligands, and self-peptide MHC complexes. A failure to discriminate between these signals may lead to

severe consequences such as autoimmune reactions against the own tissue, and failure to recognize foreign pathogens causing severe infections. The TCR has the ability to identify multiple ligands with different affinities which lead to different responses depending on the strength of the binding. For example, if the T cells detect the low-affinity self-peptide-MHC molecule, they will not activate, while in the case of recognition of high-affinity non-self-peptide-MHC molecules, T cells will activate and proliferate (Fooksman et al., 2010).

The mechanisms by which TCR binding to a peptide-MHC complex is leading to biochemical changes in the cytoplasmic domains of the TCR-CD3 complex depends on if the primary mechanism is TCR-CD3 aggregation, conformational change, or segregation (Figure 2). (i) The aggregation model descripts the interaction between CD4 or CD8 coreceptors with the same agonist peptide-MHC complex as the TCR. This promotes the recruiting of intracellular coreceptor-associated lymphocyte-specific protein tyrosine kinase (LCK) into close distance with intracellular immunoreceptor tyrosine-based activation motifs (ITAMs) of the CD3 complex, resulting in ITAMs phosphorylation. Although some published data indicate that TCR triggering can occur in the absence of coreceptors (Locksley, Reiner, Hatam, Littman, & Killeen, 1993) (Schilham et al., 1993). They suggest that coreceptor heterodimerization is not critical for TCR triggering. (ii) The conformational change model postulates that peptide-MHC binding to the TCR contributes to mechanical effects which induce displacement of the TCR-CD3 complex (Alam et al., 1999) (Reich et al., 1997). This results in conformation changes of the CD3 cytoplasmic domains and following ITAM phosphorylation. (iii) The kinetic-segregation model postulates that TCR binding to peptide-MHC molecule induces the movement of TCR-CD3 complex to the close-contact zone which in turn leads to segregation of TCR-CD3 complex from inhibitory tyrosine phosphatase CD45 resulting in the phosphorylation of TCR-CD3 ITAMs.

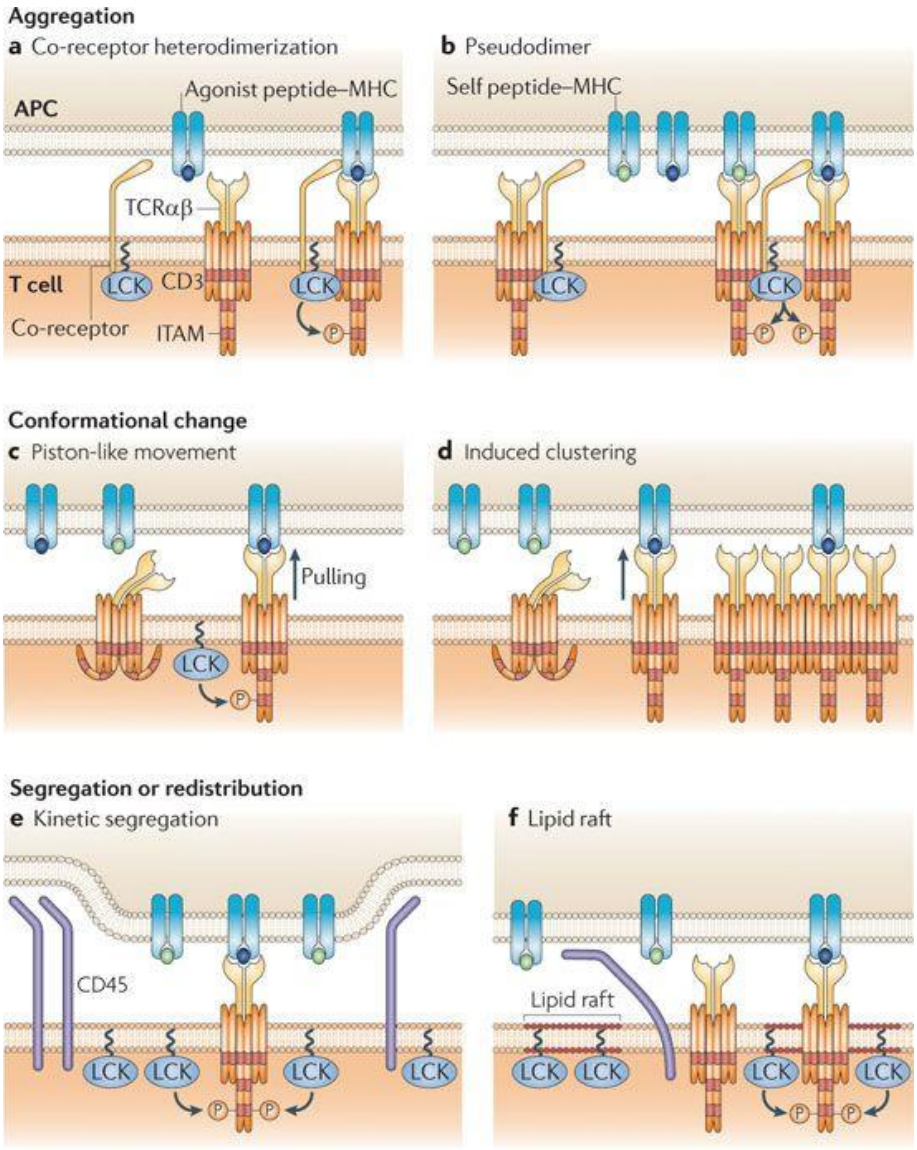

Figure 2: T cell receptor (TCR) triggering is categorized into three groups according to whether the primary mechanisms are aggregation, conformational change, or segregation. a) The co-receptor heterodimerization model postulates that after the binding of co-receptor to the same peptide-MHC complex as the TCR, recruits co-receptor-associated LCK close to the TCR-CD3 immunoreceptor tyrosine-based activation motifs (ITAMs). b) In the pseudodimer model, binding of two TCRs to low-affinity self (green) or high-affinity agonist (Bluemel et al.), brings them into the closest proximity with each other and the binding of the co-receptor to one TCR contributes to the formation of the agonist peptide-MHC complex resulting in the dimerization of TCRs. c) In the piston-like movement model, ITAM phosphorylation is achieved by the induction of the TCR-CD3 complex by the mechanical effects (primarily pulling; black arrow) of peptide-MHC binding to the TCR. d) In this model, the clustering of TCRs is promoted by dissociation of ITAMs from the membrane and conformational change in the TCR-CD3 complex. The conformational change facilitates kinase activity. e) The kinetic-segregation model suggests that phosphorylation of TCR-CD3 ITAMs by LCK is enabled by the segregation of the inhibitory tyrosine phosphatase CD45 from the TCR-CD3 complex. The segregation is promoted by TCR binding to peptide-MHC ligand leading to the recruiting of TCR-CD3 in close-contact zones. f) In the lipid raft model, reconstitution of peptide-MHC complex leads to the partitioning of the TCR-CD3 complex into regions of membrane, which are rich in LCK, and lacking CD45 (van der Merwe & Dushek, 2011).

Different theories such as the serial-triggering model (Valitutti, Muller, Cella, Padovan, & Lanzavecchia, 1995) and the kinetic proofreading model (McKeithan, 1995) (Rabinowitz, Beeson, Lyons, Davis, & McConnell, 1996) exist trying to explain how the initiation of the intracellular signaling cascade is activating the T cell. The scenario by Ven der Merwe et al. suggest: In resting T cells, constitutively active LCK at the TCR-CD3 complex phosphorylates tyrosine of ITAM, and the CD45 phosphatase as an opponent constitutively dephosphorylates the ITAM motifs. These two enzymes are working together in an equilibrium, causing the signaling cascade to be inhibited. Any mechanisms that increase the phosphorylation of ITAMs will tilt this balance in favour of phosphorylation resulting in TCR signaling. The formation of the peptide-MHC complex induces the aggregation of TCR-CD3 complexes and their exclusion from other membrane proteins leading to a decrease of the CD45 activity and an increase of LCK activity. TCR-CD3 aggregation is forming microclusters with 10-100 TCRs (van der Merwe & Dushek, 2011). After the T cell is activated the formation of a so-called immunologic synapse between T cell and APC is initiated. In the synapse, the TCR becomes concentrated at the center, and larger molecules such as the receptor-like protein tyrosine phosphatase CD45 is driven out of the interface to the periphery. CD4 or CD8 coreceptors colocalize with pMHC resulting in the recruitment of LCK to the TCR complex. The close proximity of LCK to the TCR, allows LCK to phosphorylate ITAM signaling motifs of the CD3 molecules. The phosphorylated ITAM motifs allows binding of SH2 domains of the Zap70 kinase. In resting cells, Zap70 localizes within the cytoplasm in an autoinhibited conformation. Upon TCR initiation, phosphorylated ITAMs provide a place for binding of LCK resulting in recruitment of Zap70 to the plasma membrane and disruption of autoinhibition. The kinase LCK is stabilizing the active form of Zap70 through phosphorylation of its interdomain linker and activation loop (Figure 3) (Wange & Samelson, 1996) (Palacios & Weiss, 2004). The recruited and activated Zap70 phosphorylates the linker for activation of T cells (LAT). LAT works as a signaling hub and contains four major Zap70 phosphorylation sites: Y132, Y171, Y191, and Y226. The Y132 side is responsible for the recruitment of phosphatidylinositol phospholipase C (PLC1) PCL1, in turn, mediates calcium signaling and the Rat sarcoma (Ras)/ Mitogen-activated-Protein-Kinase (MAPK) pathway. The phosphorylated Y171, -Y191, and –Y226 sides recruit the Growth factor receptor-bound protein 2 (Grb2) andGrb2-related adapter protein downstream of Shc (Gads) proteins, which act as adaptors to bind SOS and SLP-76, resulting in Ras, Rac, Rho GTPase activation (Balagopalan, Coussens, Sherman, Samelson, & Sommers, 2010) (Zhang et al., 2000) (Yablonski, Kuhne, Kadlecek, & Weiss, 1998). Also, the TCR and the CD28 costimulatory molecule activate Phosphoinositid-3-Kinasen (PI3K). Activated PI3K is phosphorylating phosphatidylinositol 4,5bisphosphate (PIP2) to phosphatidylinositol (3,4,5)-triphosphate (PIP3) which will recruit proteins like ITK and Lymphocyte cytosolic protein 2 (SH2 domain containing leukocyte protein of 76kDa (SLP-76) to the inner leaflet of the plasma

membrane (Andreotti, Schwartzberg, Joseph, & Berg, 2010). The IL2-inducible T-cell kinase (Kojima, Toda, & Sitkovsky) attach to PIP3 through its PH domain and SLP-76 through its SH3 domain resulting in its translocation to the plasma membrane and following activation. PLC1 is phosphorylated by activated ITK. PLC1 is responsible for hydrolyzing PIP2 and generation of secondary messengers' inositol 1,4,5triphosphate (IP3) and diacylglycerol (DAG). IP3 diffuses within the cytoplasm and binds to its receptor (IP3R) located in the endoplasmic reticulum (ER). It leads to the release of Ca^{2+} stores from the ER. This event, in turn, induces the influx of extracellular calcium through channels in the plasma membrane (Courtney et al., 2018). Ca^{2+} influx is activating a wide range of downstream proteins, including the transcription factor NFAT (nuclear factor of activated T cells). The cytoplasmic Ca^{2+} binds to calmodulin. This binding changes the conformation of calmodulin and allows it to activate different target enzymes. One of them calcineurin is a phosphatase that dephosphorylates the NFAT. This action enables the nuclear localization sequence to be detected by nuclear transporters resulting in the entry of NFAT into the nucleus (Murphy, 2011). DAG located within the plasma membrane promotes the activation of protein kinase C (PKC) and RasGRP, which activate Ras. Additionally, the recruitment of SOS to LAT via Grb2 causes the activation of the RAS pathway. The activation of RasGRP and SOS promotes a rapid and bistable amplification of Ras activation. In turn, Ras-mediated activation of Raf results in activation of MEK and the MAP kinase ERK pathway (Das et al., 2009) (Courtney et al., 2018).

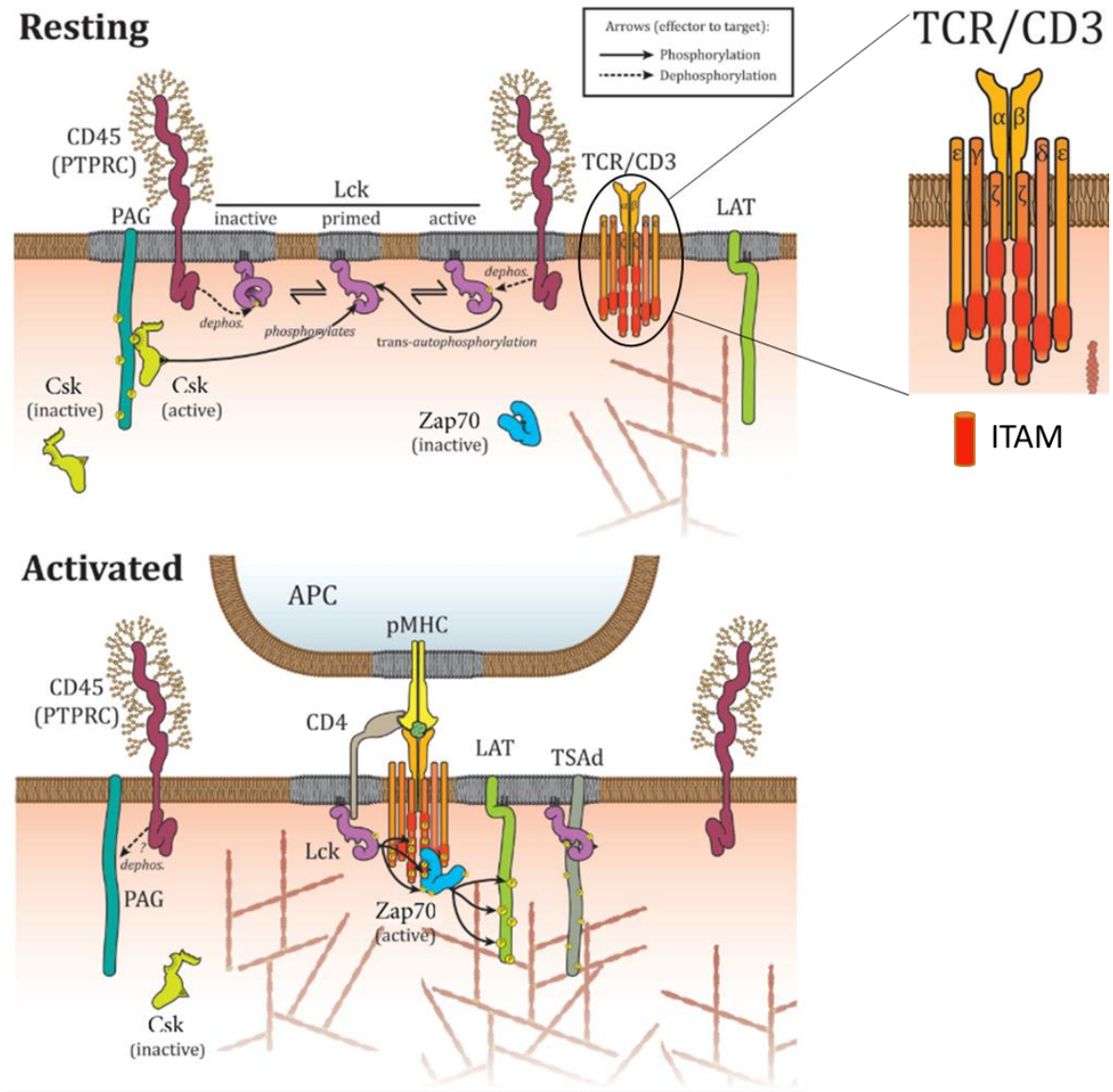

Figure 3: Initiation of TCR signaling. In resting cells, LCK is located in microdomains where it interacts directly with CD45 that plays both an inhibitory and activating role in LCK regulation. Csk limits LCK activity by targeting membrane microdomains by PAG. In resting cells, LCK is associated with membrane domains and interacts with inhibitory proteins, which prevent the constitutive activation of LCK and following TCR or ZAP70 phosphorylation. Upon activation, CD45 is excluded from membrane microdomains, and Csk detaches from the plasma membrane as a result of PAG dephosphorylation by CD45. LCK oligomerizes bind to immunoreceptor tyrosine-based activation motifs (ITAMS) of TCR/CD3 receptor and phosphorylate ITAMs and ZAP70. Phosphorylated ZAP70, in turn, phosphorylates LAT to mediate TCR signaling. Interactions of LCK with TSAd and CD4/8 enhances TCR binding and signaling. It is Adapted from (Rossy, Williamson, & Gaus, 2012).

2.3.2 Immunological synapse

The cellular arm of the adaptive immune system is characterized by its killing activity against infected cells and tumor cells. Natural killer (NK) cells and CD8+ αβ T cells mediate this process by distinct pathways. All of these pathways are promoted by a cytotoxic immunological synapse. Cajal described the neural synapse as the protoplasmic osculation (kiss). Following this model, the cytotoxic synapse has been called as a kiss of death (Dustin & Long, 2010). Neuronal- and an immunological-synapse differ in several aspects.

In contrast to neuronal synapses, immune cells form synapses which are more transient (Alarcon, Mestre, & Martinez-Martin, 2011). When a TCR on T cell recognizes a relevant pMHC ligand on APCs, the plasma membranes of two cells come into close apposition to transmit signals resulting in the formation of an immunological synapse (Basu & Huse, 2017). The concept of T-cell killing via an immunologic synapse was first descripted in 1984 (Monks, Freiberg, Kupfer, Sciaky, & Kupfer, 1998). In 1998 studies by Kupfer et al. indicated that adhesion receptors in the interface between the helper T cell and B cell (as APCs) are unusually segregated. His published data in 1998 introduced the term Supramolecular Activation Clusters (SMAC) into the immunology vocabulary. Kupfer et al. described the immunological synapse as a “bull’s eye” architecture which consists of two distinct micron-scale domains: a central cSMAC containing ligand-bound antigen receptors such as TCR and related signaling proteins like LCK. Furthermore, the cSMAC has been suggested to be the place where the downregulation of the CD3 molecule and following termination of TCR signaling occurs (Alarcon et al., 2011). The (c) cSMAC is surrounded by the peripheral (p) pSMAC, which function as a ring of LFA-1 adhesion receptors (Dustin & Long, 2010). The pSMAC is in turn, enclosed by a dense ring of filamentous actin (F-actin). This ring is called distal dSMAC (dSMAC). This distal ring is rich in proteins with large ectodomains such as CD43 and CD45 far from the cSMAC (Figure 4) (Basu & Huse, 2017) (Alarcon et al., 2011).

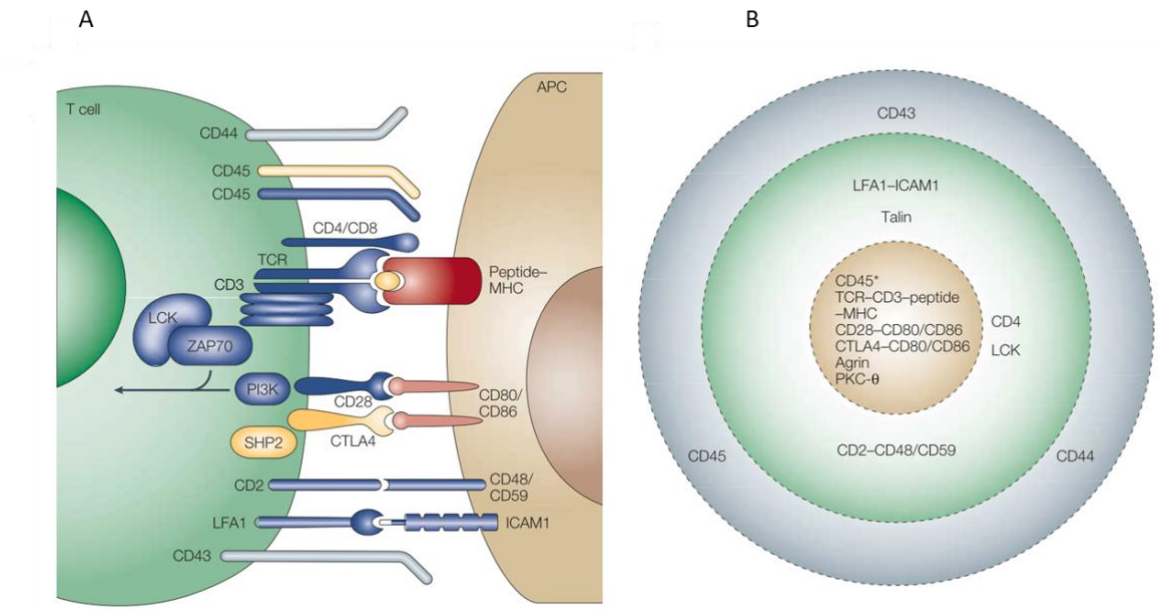

Figure 4: Overview of a mature T cell synapse. A) The profile view shows a selection of the key ligands pairs and signaling molecules involved in T cell recognition. The stimulatory peptide-MHC molecule is indicated in red, activating/co-stimulatory molecules are blue, while inhibitory molecules are yellow. In grey, molecules are presented that are not contributing to signaling. The arrow pointed to signals that lead to T cell activation. **B)** The face on view of the synapse with the characteristics 'bulls-eye' zone pattern. This region consists of the central region of the supramolecular activation complex (cSMAC) (yellow), the peripheral ring surrounding the cSMAC (pSMAC, green) and the distal region located outside the pSMAC (dSMAC, grey). The abbreviations of the molecules/ligand pairs within the SMAC regions: APC, antigen-presenting cell; CTLA4, cytotoxic T lymphocytes antigen 4; ICAM1, intercellular adhesion molecule 1; LFA1, leukocyte function-associated antigen 1; PI3K, phosphatidylinositol 3-kinase; SHP2, SRC homology 2-domain-containing protein tyrosine phosphatase 2; TCR, T-cell receptor; ZAP70, ζ-chain-associated protein 70. *CD45 goes in the cSMAC at a later stage (Huppa & Davis, 2003).

2.3.3 Different cytotoxic T lymphocytes killing

There are two major ways of CTL-mediated cell killing: (i) Ca^{2+}-dependent killing by perforin and serine proteases called granzymes (intrinsic apoptotic). (ii) Fas ligand (FasL)-mediated killing (extrinsic apoptotic) which is independent of Ca^{2+}. Both pathways induce apoptosis in the target cell by activation of caspase. However, the perforin pathway is usually faster (Dustin & Long, 2010). Perforin is an essential component in the granule exocytosis pathway for target cell apoptosis. The perforin mediated pathway is based on a highly conserved membrane injury response. Ca^{2+} flux triggers the repair response in which internal vesicles, including lysosomes and endosomes, donate their membranes to reseal the damaged membrane (Keefe et al., 2005).

The killing is induced by endosomal lysis which induces the granzymes into the target cell cytoplasm, and thus no specific receptor is needed. The synaptic cleft enhances the perforin-mediated killing through high local concentration of free perforin and granzyme and prevents harm to bystander cells. Moreover, since FasL and Fas are membrane proteins with a limited

distance of approximately 15 nm, the cell-cell contact (synapse) is important for their function (Dustin & Long, 2010).

How does the perforin-mediated target cell killing function? Upon T cell binding to the target cell, T cell discharge cytotoxic granules containing perforin co-packaged with granzymes into the synaptic cleft. Active granzymes are stored in association with negatively charged chondroitin sulfate proteoglycans, and they will dissociate from it once released into the synaptic cleft where the pH is neutral. After encountering extracellular Ca^{2+}, perforin binds to lipid moieties in the target-cell membrane through its C2 domain. Only in a sufficiently high concentration, perforin can polymerize into complement-like transmembrane pores with 10-20 nm in diameter. Through these pores, granzymes can diffuse into the target cell. Once granzyme B arrives at the cytosol, it mediates apoptosis pathways in the target cell by activating the mitochondrial (intrinsic) pathway. In the cytosol, granzyme B cleaves the pro-apoptotic BH3 (BCL-2-homology domain 3)-only protein BID (BH3-interacting-domain death agonist), and the BID C-terminal fragment induces mitochondrial outer-membrane permeabilization (MOMP). It leads to the release of SMAC (second mitochondrial-derived activator of caspase), cytochrome c and OMI. Finally, caspase is activated (Figure 5) (Voskoboinik, Smyth, & Trapani, 2006).

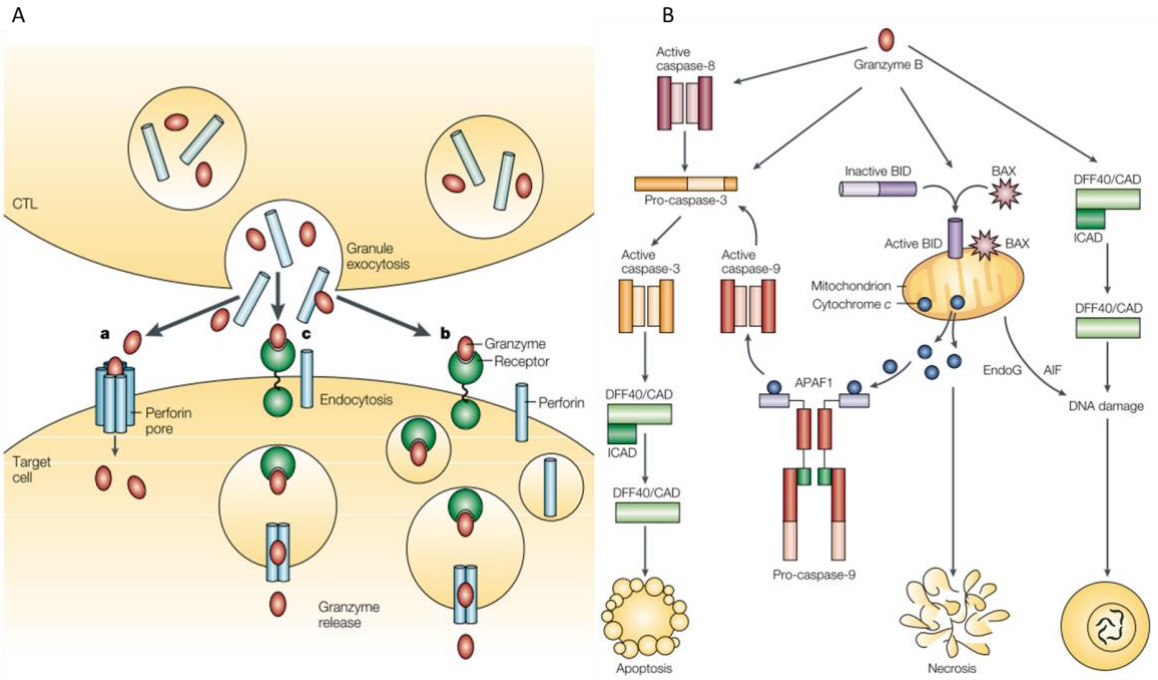

Figure 5: Pathways of entry for Granzyme B into the extracellular space between cytotoxic T lymphocytes (CTL) and a target cell and the following mediated cell death. A) a; The entry of granzyme B into the target cell is achieved by a pore consisting of polymerized perforin in the target cell membrane. **b;** A recent discovery has indicated that granzymes might be taken up by receptor-mediated endocytosis and that perforin helps to release bound granzymes with the endosomes into the cytosol of the target cell. **c;** Moreover, granzyme uptake into the target cell is succeeded by perforin-mediated damage to the membrane. **B)** Once granzyme B is released into the cytoplasm of the target cell, it induces apoptotic cell death through the direct cleavage of pro-caspase-3 or, indirectly, through caspase-8. Additionally, cleavage of BID leads to translocation of granzyme B, with other members of the pro-apoptotic BCL2-family such as BAX, to the mitochondria. This process promotes the release of cytochrome c and the activation of caspase-9 through interaction with the adaptor molecule apoptotic protease-activating factor 1 (APAF1). Alternatively, cell death can be achieved by caspase-independent pathways in the case of mitochondrial dysfunction. This can lead to necrotic death and the release of factors such as apoptosis-inducing factor (AIF) and endonuclease G (EndoG) which mediate caspase-independent cell death. Finally, granzyme B-mediated proteolysis of the inhibitor ICAD can directly activate DFF40/CAD (DNA fragmentation 40/caspase-activated deoxynuclease) which damages DNA and leads to cell death (Barry & Bleackley, 2002).

Fas ligand-mediated killing is initiated by the binding of Fas ligand to Fas receptor (CD95) located on the target cell. This binding induces the oligomerization of caspase-8 through the adaptor molecule FADD. Activated caspase-8, in turn, activates caspase-3 through direct proteolytic events, resulting in downstream caspase activation. Furthermore, Caspase-8 can induce apoptosis through mitochondrial pathways. Here, the BH3-only protein, BID is cleaved. The cleavage of BID promotes the release of BAX/BAK-dependent cytochrome c from mitochondria and the formation of the apoptosome. The apoptosome promotes the activation of caspase-9. Active caspase-9 is responsible for the further caspase processing events by caspase-3 and -7, resulting in final target cell apoptosis. Both intrinsic and extrinsic pathways converge at the activation of caspase (Figure 6) (Cullen & Martin, 2009).

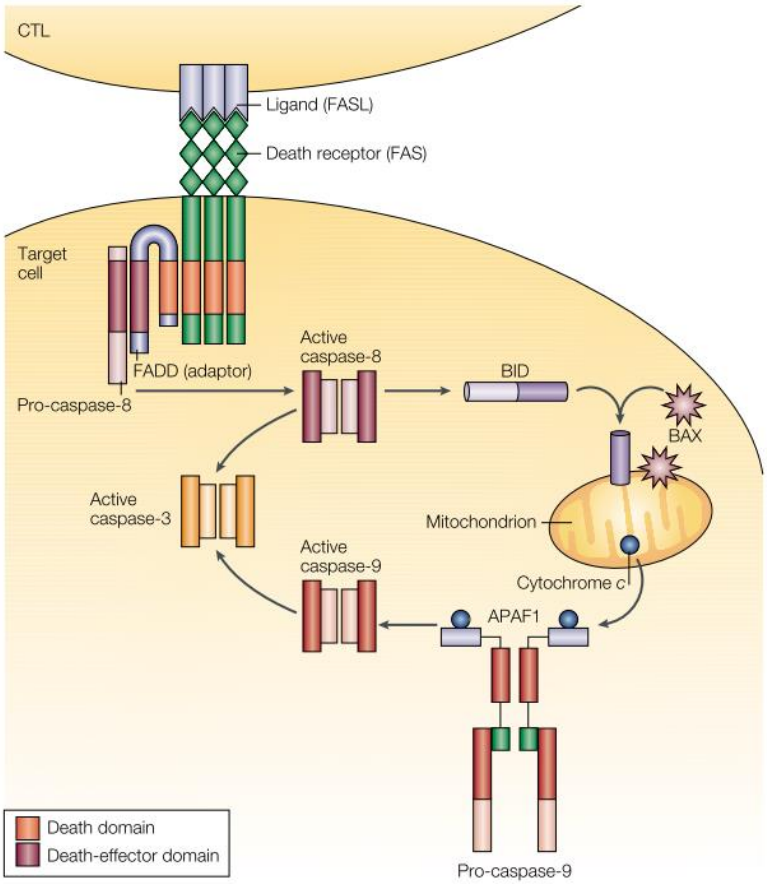

Figure 6: FAS-ligand mediated target cell killing. Apoptotic cell death is mediated by the engagement of FAS (CD95) on a target cell with CTL-expressed FAS ligand (FASL; CD178). The engagement of FAS leads to the recruitment of the initiator caspase, caspase 8, through interaction with the adaptor molecule FAS-associated death domain protein (FADD) by means of death domains and death-effector domains. This results in the activation of caspase-8. Caspase-8 differently affects the different cells of the TYPE I/II SYSTEM. In type I cells, it activates other members of the caspase family, while in type II cells, caspase 8 activation initiates the cleavage of the pro-apoptotic BCL2-family member BID and the subsequent translocation of BID and BAX to the mitochondria. After Insertion into the mitochondrial membrane, BID and BAX promote the release of mitochondrial cytochrome c which in turn leads to the activation of caspase 9 through interaction with the adaptor molecule apoptotic protease-activating factor 1 (APAF1). Finally, caspase 9 is able to activate caspase 3, resulting in final target cell apoptosis. CTL, cytotoxic T lymphocyte. (Barry & Bleackley, 2002).

2.4 Hemibodies

Besides all benefits of current cancer immunotherapies, the rare number of suitable tumor antigens makes the use of high potent T cell activating therapeutic approaches such as BiTE, limited to very few tumor types. To overcome this limitation, a two-part tri-specific T cell-engaging antibody termed hemibody was developed. Hemibodies consist of two complementary polypeptides chains targeting a combination of two distinct antigens. Each hemibody has two specific binding domains. On one end is the single-chain fragment variable domain (scFv) directed against a specific target protein. The scFv is linked via a short 4 amino acid long flexible glycine/serine linker to either a variable heavy chain domain (VH) or a variable light chain domain (VL) of an anti-CD3 antibody. Only if a target cell expresses both target

antigens and the two respective hemibodies bind to the cell, the hemibodies become aligned resulting in the reconstitution of a functional CD3 binding-domain only on the surface of the double antigen-positive target cell. Only now the reconstituted anti-CD3 VH and VL domain can bind and recruit T cells (Figure 7).

For the function of the hemibodies to successfully recruit and activate T cells, the properties of the target antigens, such as their position to each other and their mobility, are critical. The complementation of a functional anti-CD3 scFv domain requires that both target antigens are co-expressed on the same cell and that they can move freely on the cell surface. If this is the case, the distance between the anti-CD3 VH and VL domains is minimized, which enables the alignment of the domains resulting in the engagement of T cells.

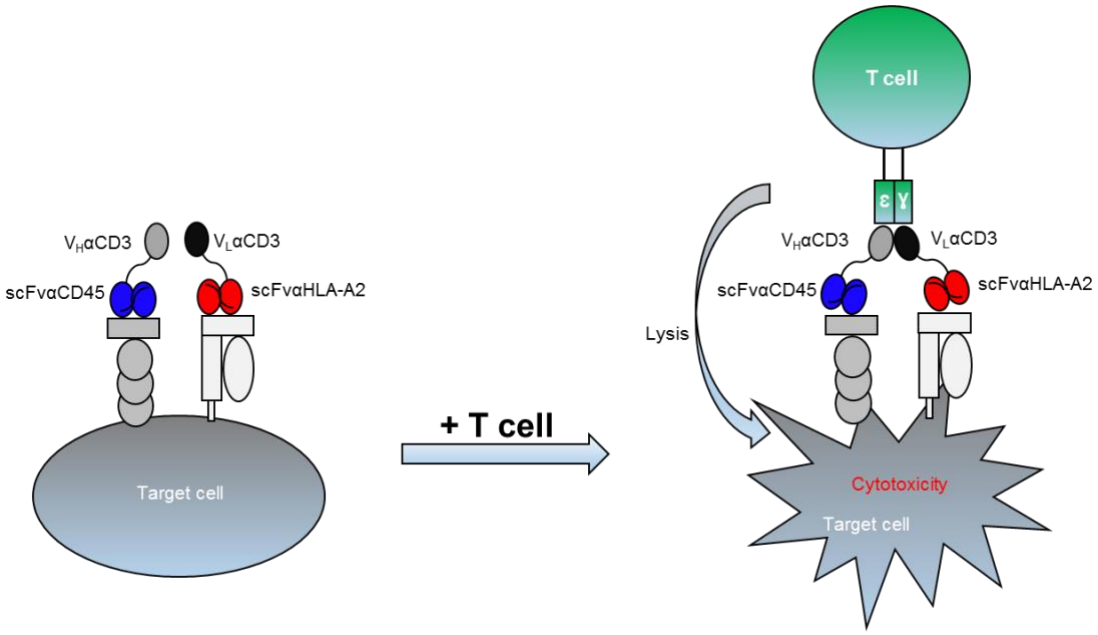

Figure 7: Mode of action of hemibody pair (VHαCD3-scFvαCD45 and VLαCD3-scFvαHLA-A2). Each hemibody consists of a tumor antigen specific single-chain variable fragment (scFv) fused to the variable light (VL) or variable heavy chain domain (VH) of a CD3-specific antibody. Only on double antigen positive target cells, the hemibodies will complement which results in the building of a functional CD3-binding site and engaging of T cells.

2.4.1 Targets of tested hemibodies

2.4.1.1 HLA-A2

T cells and B cells, the most important guardians in adaptive immune response, recognize antigens by two different highly variable receptor molecules; the immunoglobulins that act as antigen receptor on B cells and the antigen-specific receptors of T cells. While B cells are able to recognize extracellular antigens, detection of antigens by T cells is restricted to intracellular peptides presented on MHC molecules. MHC molecules are specialized glycoproteins which are located on the cell surface with a peptide-binding groove that can bind a various number of different peptides. The MHC molecules are encoded within a large cluster of genes that were first identified by their major effects on the immune response to transplanted tissues. This is the reason why the gene complex called the major histocompatibility complex (MHC). The MHC molecule binds to the peptide intracellular and translocate it to the cell surface, where the peptide will be recognized by T cells. MHC molecules are classified into two classes: MHC class I and MHC class II. These two classes differ in intracellular sites to acquire the peptide and their affinity for CD8- and CD4-T cells (Murphy, K. 2011). For this work, hemibody against HLA-A2 antigen which, is a component of MHC class I was used.

Highly polymorphic MHC class I molecules belong to the transmembrane proteins consisting of a single α-chain and β_2-microglobulin. These components enable folding and trafficking to the cell surface. MHC class I molecules are characterized by structural features α1, α2, and α3 domains; these structures build a globular protein. Different protein products encoded by MHC class I genes are termed allomorphs. Since each allomorph contains a unique peptide-binding groove, they bind a distinct subset of peptides (Figure 8). In accordance with the shape, depth, charge of the groove and the binding pockets of the respective MHC molecules, peptide sequences are classified in different groups. In human, genes encoding MHC proteins, are called human leukocytes antigen or HLA genes, because they were first identified through antigenic differences between white blood cells from different individuals. Most individuals express six different MHC class I alleles (two each of HLA-A, HLA-B, and HLA-C). Findings from mass spectroscopy indicated that HLA-A2 could bind thousands of distinct peptides containing a common motif but originate from a plethora of cellular proteins (Bennett, J. 2015).

MHC class I molecules are synthesized in the endoplasmic reticulum and attach their peptide in this location. Peptide bound to MHC class I molecules are originated from proteins degraded in the cytosol by the proteasome (Murphy, K. 2011). The proteasome is a large cytosolic protein complex which degrades peptides. Upon degradation, released peptides will be transferred into the lumen of the endoplasmic reticulum (ER) by a heterodimeric ATP-binding

protein called TAP. In the ER, aminopeptidases such as ERAP1 and ERAP2 will further process the peptides. Peptide loading complex (PLC) mediate the binding of peptides with suitable size and sequence to MHC class I molecules. Subsequently, stable peptide/MHC class I complexes will leave the ER and locate on the cell surface. Most peptide/MHC complexes located on the surface of healthy cells are not recognized by T cells due to self-tolerance. Whereas, a new peptide derived from virus or tumor-associated proteins can give rise to CTL mediated-immune response. CTLs are able to identify small modifications due to their ability to recognize cells presenting as few as 10 peptide/MHC complexes (Vigneron, 2015).

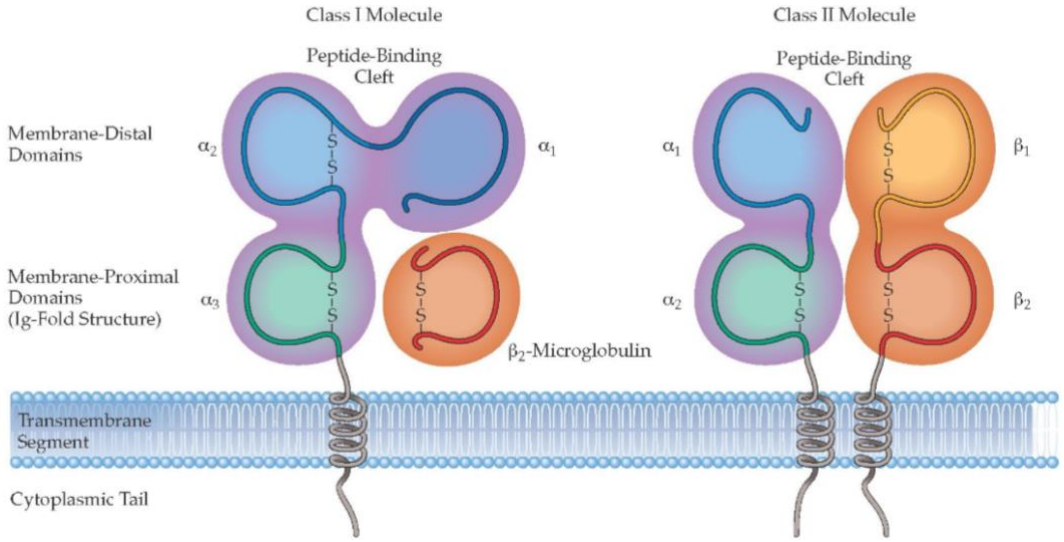

Figure 8: Schematic comparison of the structural features of major histocompatibility complex (MHC) class I and class II molecules. MHC class I molecules are anchored in the membrane by a single transmembrane segment contained a 45-kD α chain and are noncovalently associated with β2-microglobulin (β2m). Three external domains containing intramolecular disulfide bonds are indicated. In contrast, MHC class II molecules involve of noncovalently associated α (32 kD) and β (28 kD) chains. Both chains are anchored within the membrane. However, the overall domain organization of the two molecules are highly similar (https://microbeonline.com/difference-mhc-class-mhc-class-ii-proteins/).

2.4.1.2 CD45

The balance between phosphorylation by protein tyrosine kinase and dephosphorylation by protein tyrosine phosphatase plays a critical role in signal transduction events. CD45 (also known as B220, CD45R, CD45RA, CD45RB, CD45RC, CD45RO, EC 3.1.3.48, LCA, T200, Ly5 and PTPRC) is a receptor phosphatase, which defines the threshold for T cell activation. This receptor was discovered initially as the first prototypic transmembrane protein tyrosine phosphatase. CD45 is a type I transmembrane molecule and is expressed on the surface of all nucleated hematopoietic cells and their precursor except mature erythrocytes and platelets. It has been observed that the cell surface of T and B cells consists of up to 10% of CD45.

Alternative splicing of three different extracellular exons (ABC) pf CD45 results in the expression of multiple CD45 isoforms (Sasaki, Sasaki-Irie, & Penninger, 2001). Six different human isoforms of CD45 mRNAs has been discovered yet, which contain all three extracellular exons (ABC isoform), two of the three exons (AB and BC isoform), only one exon (A isoform or B isoform), or no exons (O isoform) (Hermiston, Xu, & Weiss, 2003).

CD45 has two intracellular protein tyrosine phosphatase homology domains (PTP), a membrane-spanning transmembrane domain, and a large extracellular domain. Interestingly, only the first domain D1 of the PTP unit is catalytically active. The role of the second domain D2 remains unclear. The extracellular domain consists of three membrane-proximal fibronectin type II repeats, a cysteine-rich region, and the variable N-terminal region. Depending on the type of combination of exons used to form the CD45 mRNA, the extracellular CD45 varies in length (Figure 9) (Desai, Sap, Silvennoinen, Schlessinger, & Weiss, 1994).

Genetic findings have indicated that CD45 is a critical regulator of signaling thresholds in T cell function. It could be observed that in mice, loss of CD45 led to the accumulation of immature thymocytes during T cell development. The reason for this observation is that the absence of CD45 causes over-activation of the TCR in CD45-deficient T cells (Courtney et al., 2018).

CD45 both positively and negatively regulates T cell receptor phosphorylation. In T cells, CD45 dephosphorylates the tyrosine kinase LCK, a member of the Src family. In the active form, the terminal tyrosine of LCK is phosphorylated and bound to the SH2 domain and the linker region is bound to the SH3 domain. LCK can be activated when its terminal tyrosine is dephosphorylated by CD45, and its SH3 domain releases the linker region (Murphy, K. 2011). These findings reveal a positive effect for CD45 in activating LCK. The activated LCK, in turn, is necessary for TCR phosphorylation and recruitment of Zap70 kinase. However, CD45 has been reported to act also as phosphatase, which dephosphorylates signaling components such as the TCR complex. Due to this negative regulatory role, CD45 is segregated from the TCR during the formation of the immune synapse (Courtney et al., 2018).

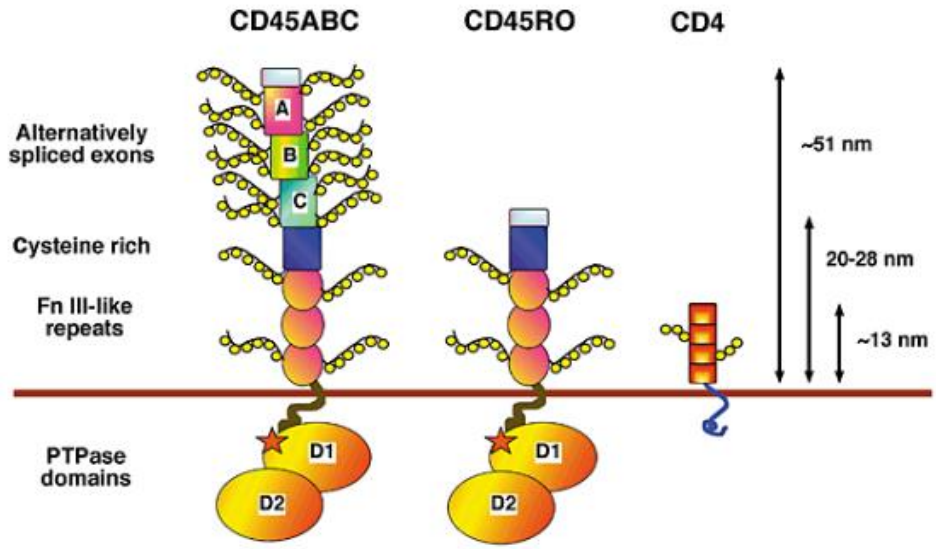

Figure 9: Schematic structure of CD45 molecules. CD45 is expressed in multiple isoforms as a result of alternative splicing of variable CD45 exons. Exons 4/A, 5/B, and 6/C (CD45RABC) contain high molecular weight, whereas CD45RO isoforms have a low molecular weight. Alternative splicing of CD45 variable exons changes the NH2-terminal region of approx. 200 amino acids containing various serine, threonine, and proline residues. All of the O-glycosylation of CD45 occurs in this region resulting in an extensive variation in the glycosylation pattern of different isoforms. The serine-threonine-rich domain is followed by three fibronectin type III (Fn III)-like repeats, a single transmembrane region, and a long intracellular tail. The first membrane-proximal domain of CD45, referred to as the D1 domain contains PTPase activity, while the second domain called D2 domain proves no significant PTPase activity. However, the D2 domain has been shown to have a role in proper folding and/or substrate recruitment. The dimensions of CD45ABC and CD45RO are contrasted to the size of the Ig superfamily molecule CD4 (Penninger, Irie-Sasaki, Sasaki, & Oliveira-dos-Santos, 2001).

2.5 Aims of this study

Our increasing understanding of how the immune system is able to interact with cancer cells, in disease prevention, the early stage of the disease and in disease progression, has led to the rapid growing field of cancer immunotherapy. Immunotherapy exploits the immune system's potential to detect and target tumor cells. The T cells have the highest potential for cytotoxic activity and different therapeutic strategies are using T cells for tumor cell killing, like the CAR T cells or donor lymphocyte infusion after allogeneic stem cell transplantation.

In the last years the development of the bispecific antibodies, the bispecific T cell engagers or BiTEs, have made the way from bench into clinic. Classic BiTE antibodies consist of two antigen binding domains. One is directed against the CD3ε chain of the TCR complex to recruit T cells of the patient. Their second binding domain is directed against an antigen expressed on tumor cells. A great challenge for BiTE therapy is the identification of suitable antigens only expressed on tumor cells. Most tumor antigens are also expressed at low level on healthy tissue, causing severe off-target toxicity of the highly potent T cell therapy. To overcome this limitation, we have developed T cell-engaging antibody derivatives, termed hemibodies. Each Hemibody consist of an antigen binding scFv, directed against an antigen expressed by tumors cells, and either the VH or VL domain of an anti-CD3 epsilon chain binding antibody. When a complementary pair of hemibodies binds their respective antigens on a tumor cell, they become aligned and rebuild the CD3 binding-domain of an anti-CD3 antibody on the surface of the dual antigen positive target cell.

We created a pair of complementary hemibodies against CD45 and HLA-A2 and analyzed their binding to THP1 double positive target cells. In contrast to classic BiTE antibodies, where the mode of action has been reported (Haas et al., 2009), the mechanisms used by hemibodies to kill the target cells are still unknown. The main aim of this thesis was to investigate the mechanisms by which hemibodies activate T cells to eliminate tumor cells. Also, we analyzed the interaction of soluble hemibodies with recombinant soluble CD3 molecules in the solution without target cells.

3 Materials and Methods

3.1 Materials

3.1.1 Instruments

Instruments	Models and Manufacturers
Bench scales	440 - 49N [KERN, DE]
Cell Counter	Countess II FL Automated [Thermo Scientific, DE]
Cell incubator	HERACELL 240i [Thermo scientific, DE]
Centrifuge	Heraeus Multifuge X3R [Thermo Scientific, DE]
FPLC Chromatography System	Äkte start [GE life Science, USA]
FPLC Chromatography System	Äkta pure [GE life Science, USA]
Confocal Microscope	inverted IX81 microscope with an Olympus FV1000 confocal laser scanning system [Olympus, DE]
Cryogenic Storage Tank	LS3000 [Worthington Industries, USA]
Electrophoresis equipment includes cells and power supplies	[BIO-RAD, DE]
ELISA reader	[Tecan Ltd., CHE]
Flow cytometer	FACSCalibur™ Cell Analyzer [BD Biosciences, USA]
Flow cytometer	BD FACSCanto™ II [BD Biosciences, USA]
French Press	EmulsiFlex-C3 Avestin [Atascientific, DE]
Gel Documentation System	UVP GelStudio [Analytik jena, DE]
Imaging system	ChemiDoc™MP Imagelab [BioRAD, USA]
Incubation shaker	Multitron Pro [Infors HT, DE]

Microscope for ca flux measurement	BX51WI upright microscope [Olympus, DE]
Photometer	OD600 DiluPhotometer™ [Implen GmbH, DE]
Plate Reader	Tecan Spark [Tecan Group Ltd. CHE]
Power Supply	PowerPac™ Basic [BIO-RAD, DE]
Safety cabinet	Safe 2020 [Thermo scientific, DE]
Spectrophotometer	NanoDrop™ 2000 Spectrophotometer [Thermo Scientific, DE]
Spectrophotometer	NanoDropTM 2000 [Thermo scientific, DE]
Table Centrifuges	Centrifuge 5424, 5430R [Eppendorf, DE]
Thermal Cycler	C1000 Touch™ [Bio-Rad Laboratories, Inc., USA]
Thermo-Shaker	TS-100C + SC-24NC [BioSan, DE]
Time-lapse microscopy	Leica DMI6000 B [Leica Microsystems, DE]
Transfection system	Neon™ [Invitrogen, DE]
Vortex	Genie2 [Scientific Industries DE]

3.1.2 Equipment and consumables

Equipment and consumables	**Models and Manufacturers**
Äkta Chromatography Columns	HiTrap™ 5 ml TALON crude [GE Life Sciences, DE]
	Hiprep™ 26/10 Desalting [GE Life Sciences, DE]
	HiTrap™ 1 ml Q XL [GE Life Sciences, DE]
	Hiload™ 16/600 superdex™ 200 pg [GE Life Sciences, DE]
	Superdex™ 200 Increase 5/150 GL [GE Life Sciences, DE]
Assay plate with clear flat bottom	96 well, with lid [Costar, DE]

Assay plate with white flat bottom	96 well, with lid [Costar, DE]
Cell culture dishes	10 cellstar [greiner bio one, DE]
Centrifugal filters	Amicon® Ultra – 15, Ultracel® - 30K [Merck, DE]
Centrifuge tubes	100 CellSTAR® tubes [greiner bio-one, DE]
Combitips	advanced® 5 ml [Eppendorf, DE]
Cool Box for freezing of cells	CoolCell [biocision, DE]
Deepwell plates	96/2000 µl [Eppendorf, DE]
ELISA microplates	Clear microplate [R&D Systems, DE]
Flow Cytometry tubes	5 ml [Sarstedt, DE]
Microscopy slides	15 µ-slide 8 well Glass Bottom [Ibidi, DE]
Multi stand Separator for magnetic cell isolation	Quadro [Milteny Biotec, DE]
SafeSeal tubes	1,5 ml [Sarstedt, DE]
Serological pipette	5 ml, 10 ml, 25 ml, 50 ml [CELLSTAR, DE]
Sterile disposable filtration devices with SFCA membrane	Nalgene™ Rapid-Flow™ [Thermo scientific, DE]
Strep-Tactin Chromatography Columns	Econo-Column® [Bio-Rad, DE]
Syringe filters	Minisart® Syringe Filter [Sartorius, DE]
Tips	10/20 µl, 200 µl, 1250 µl Tipone [STARLAB, DE]
Tissue Culture Flasks	25 cm^2, 75 cm^2, 175 cm^2 [TPP, DE]
Tissue culture plate with flat bottom Suspension cells	24 well [Sarstedt, DE]
V-bottom plate	Microplate, 96 well, PS, V-bottom, clear [greiner bio-one, DE]

3.1.3 Software and internet

Software and internet	Website address
A plasmid Editor (ApE)	http://jorgensen.biology.utah.edu/wayned/ape/
Expasy	https://www.expasy.org/
FlOWJO Ver.8.8.6	https://www.flowjo.com/solutions/flowjo/downloads
(Fiji Is Just) ImageJ 2.0.0-rc-68/1.52e; Java 1.8.0_172 [64-bit]; Windows 7 6.1	https://ImageJ.net/Fiji/Downloads
Image Lab 6.0	http://www.bio-rad.com/de-de/product/image-lab-software?ID=KRE6P5E8Z
Imaris x64 9.3.1	https://imaris.oxinst.com/
Leica LAS AF Lite 3.3	https://leica-las-af-lite.software.informer.com/3.3/
Microsoft office	https://www.microsoft.com/de-de/download/office.aspx
Origin Pro 9 f. Windows	https://www.rz.uni-wuerzburg.de/dienste/shop/studierende/software-fuer-studierende/origin/
PubMed	https://www.ncbi.nlm.nih.gov/pubmed/
Snap gene	https://www.snapgene.com/try-snapgene/
Tecan SPARKCONTROL Method Editor V2.2	https://lifesciences.tecan.com/software-magellan?p=tab--1
Unicorn V 6.3	https://www.gelifesciences.com/en/us/shop/unicorn-6-3-p-01118#/order

3.1.4 Reagents

Reagents	Manufacturers and catalog numbers
2-Mercaptoethanol XL-10 Gold	[Agilent Technologies, Cat No 200314-43]
2-Propanol	[Roth, Cat No T910.1]

2x YT Broth, granulated Rot	[Roth, Cat No 6676.3]
3, 3′,5 ,5′-Tetramethylbenzidine Liquid Substrate, Supersensitive, for ELISA (TMB)	[Sigma-Aldrich, Cat No T4444-100ML]
Acetic acid	[Sigma-Aldrich, Cat No 33209]
Acrylamide 30% solution	[Sigma-Aldrich, Cat No A3699]
Agar-Agar	[BioScience Roth, Cat No 5210.2]
Ammonium persulfate	[Roth, Cat No 9592.5]
AmpuwaR sterile water	[Fresenius Kabi AG, Cat No 30-29-256]
Avidin	[IBA Lifesciences, Cat No 2-0204-015]
BioLock Biotin blocking solution	[IBA Lifesciences, Cat No 2-0205-250]
Boric acid	[Roth, Cat No 6943.1]
Bovine Serum Albumin (BSA)	[Sigma-Aldrich, Cat No A7030]
Bromine phenolic blue	[Roth, Cat No T116.1]
Buffer E, Strep-TactinR Elution Buffer	[IBA Lifesciences, Cat No 2-1000-025]
Buffer R, Strep-TactinR Regeneration Buffer	[IBA Lifesciences, Cat No 2-1002-100]
Buffer W, Strep-TactinR Wash Buffer	[IBA Lifesciences, Cat No 2-1003-100]
Carbenicillin	[Hartenstein, Cat No CC56]
Cell culture medium for cell lines	Advanced RPMI (1x) [gibco, Cat No 1640]
Cell culture medium for cultivation of CHO cells	HyClone, ActiSMTM [Health care, Cat No SH31040.02]
Cell culture medium for expansion of CHO cells	HyClone, ActiProTM [Health care, Cat No SH31039.02]
Cell culture medium for primary cells	F-12K Nut Mix (1x) [gibco, Cat No 21127-022]

CellTracker™ Deep Red Dye	[Thermo Fisher Scientific, CatNo C34565]
CellTracker™ Green CMFDA Dye	[Thermo Fisher Scientific, CatNo C7025]
CHO CD EfficientFeed™ A Nutrient Supplement	[Thermo Scientific, Cat No A1023401]
CHO CD EfficientFeed™ B Liquid Nutrient Supplement	[Thermo Scientific, Cat No A1024001]
Cobalt (II) chloride hexahydrate	[Sigma-Aldrich, Cat No C8661]
Co-NTA-Agarose 50% Suspension	[Genaxxon, Cat No S5356.0010]
Coomassie Brilliant Blue G250	[Sigma-Aldrich, Cat No 27815]
CutSmartR Buffer	[New England Biolabs, Cat No B7204S]
Dimethyl sulfoxide (DMSO)	[Sigma-Aldrich, Cat No D4540]
Di-Sodium hydrogen phosphate dihydrate	[Merck, Cat No 1065801000]
D-Luciferin Firefly, potassium salt	[Biosynth Inc., Cat No L-8220]
DNA Gel Loading Dye (6x)	[Thermo Scientific, Cat No R0611]
dNTP Mix	[Thermo Scientific, Cat No R0192]
Dulbecco's Phosphate Buffered Saline (PBS)	[Sigma-Aldrich, Cat No D8537]
E. coli Transformation Kit	[Mix & Go! Zymo Research, Cat No T3001]
EDTA	[AppliChem, Cat No A3145]
Ethanol, absolute	[Th. Geyer, Cat No 11647081]
FastDigestR Green buffer	[Thermo Scientific, Cat No B72]
FBS HI	[Thermo Scientific, Cat No 10082147]
Ficoll-PaqueTMPLUS	[GE Healthcare, Cat No 17-1440-03]
Fluo-3, AM	[Molecular Probes, F1224]
Fura Red, AM	[Molecular Probes, F3021]

Gelatin from bovine skin Type B	[Sigma-Aldrich, Cat No G9391-100G]
Glucose	[Sigma-Aldrich, Cat No G8270]
GlutaMAX™-I CTS (100x)	[Thermo Scientific, Cat No A12860-01]
Glycerol	[Sigma-Aldrich, Cat No G2025]
HBSS, calcium, magnesium, no phenol red	[Gibco, 14025050]
Hygromycin B	[Thermo Scientific, Cat No 10687010]
Imidazole	[AppliChem, Cat No A1073]
IPTG	[Sigma-Aldrich, Cat No I1284]
Kanamycin	[AppliChem, Cat No A1493]
LB Broth (Luria/Miller), granulated	[Roth, Cat No 6673]
L-Glutamine 200 mM (100x)	[Gibco, Cat No 25030-024]
Nancy-520	[Sigma-Aldrich, Cat No 01494]
Oregon Green™ 488 BAPTA-1, AM, cell permeant	[Invitrogen™, Cat No O6807]
Pluronic F-127	[Invitrogen, P3000MP]
Poly-L-Lysine	[ScienCell Research, Cat No 0413]
PSN, Antibiotic mixture (100x)	[gibco, Cat No 15640-055]
Puromycin	[InvivoGen, Cat No ant-pr1]
Q5R High GC Enhancer	[Thermo Scientific, Cat No M0491S]
Q5R Reaction Buffer	[Thermo Scientific, Cat No B9027S]
Red Blood Cell Lysing Buffer Hybri-MaxTM	[Sigma-Aldrich, Cat No R7757-100ML]
Sodium chloride	[AppliChem, Cat No 131659.1214]
Sodium dihydrogen phosphate dehydrate	[Roth, Cat No T879.3]

Sodium hydroxide	[Merck, Cat No 1064621000]
Strep-TactinR SuperflowR	[IBA Lifesciences, Cat No 2-4010-010]
TEMED	[AppliChem, Cat No A1148]
Tris ultrapure	[AppliChem, Cat No A1086]
Tris-HCl (pH 6.8)	[Roth, Cat No 9090]
Trypan Blue solution	[Thermo Scientific, Cat No T8154]
Tryptone BioChemica	[Thermo Scientific, Cat No A1553]
Universal Agarose	[VWR, Cat No 732-2789]
Yeast Extract Bacto™	[BD, Cat No 212730]

3.1.5 Self-made Buffers and Media

Buffers and media	**Recipe**
Buffer E, Strep-TactinR Elution Buffer	Tris-HCl (pH 8.0) 100 mM + NaCl 150 mM + EDTA 1 mM + D-desthiobiotin 2.5 mM
10x SDS Running Buffer	Glycine 1.92 M + Tris 250 mM + SDS 1% w/v
10x TBE Buffer	Tris 890 mM + Boric acid 890 mM + EDTA (pH 8.0) 290mM
2x YT Medium	Tryptone 1.6% w/v + Yeast extract 1% w/v + NaCl 0.5% w/v., pH 7.0, autoclaved
4 x SDS-Loading dye	Tris-HCL (pH 6.8) 25% v/v + SDS 10% w/v + Bromine phenolic blue 0.008% w/v + Glycerol 40% v/v + 2-Mercaptoethanol 20% v/v
Agarose Gels 1%	1x TBE buffer containing: Universal Agarose 1% w/v + Nancy-520 200 ng/ml
ATS buffer	200 mM L-Arginine + 20 mM Tris + 10 mM Succinic acid (pH 7.4 – 8 adjusted with HCl)
Buffer R, Strep-TactinR Regeneration Buffer	Tris-HCl (pH 8.0) 100 mM + NaCl 150 mM + EDTA 1 mM + HABA 1 mM

Buffer W, Strep-TactinR Wash Buffer	Tris-HCl (pH 8.0) 100 mM + NaCl 150 mM + EDTA 1 mM
Calcium Imaging Buffer	135 mM NaCl + 6 mM KCl + 1 mM MgCl2 + 1 mM CaCl2 + 10 mM HEPES + 5.5 mM Glucose ; Adjust the pH with NaOH to 7.4
Co-IMAC Elution Buffer I	Na2HPO4/NaH2PO4 Buffer (pH 7.5) 50 mM + NaCl 300 mM + Imidazole (pH 8.0) 150 mM
Co-IMAC Loading Buffer I	Na2HPO4/NaH2PO4 Buffer (pH 7.5) 50 mM + NaCl 300 mM + Imidazole (pH 8.0) 10 mM
Co-IMAC Regeneration Buffer I	Na2HPO4/NaH2PO4 Buffer (pH 7.5) 50 mM + NaCl 300 mM + Imidazole (pH 8.0) 300 mM
Co-IMAC Wash Buffer I	Na2HPO4/NaH2PO4 Buffer (pH 7.5) 50 mM + NaCl 300 mM + Imidazole (pH 8.0) 5 mM + Triton X-114 0.2% v/v
Coomassie Blue Staining Solution	Methanol 45% v/v + Acetic acid 1% v/v + Coomassie Blue R 250 0.25% w/v
Coomassie Destaining Solution	Methanol 45% v/v + Acetic acid 10% v/v
Desalting & IEX Buffer	Naphosphate (pH 7.5) 50 mM + NaCl 75 mM
Dye loading buffer (for Ca flux)	HBSS/Ca/Mg 2ml + 200 µl FBS + 4 µl pluronic F-127 10% + 2 µl Fluo-3 AM 4 mg/ml + 2 µl Fura Red AM 10 mg/ml
Glycerol buffer	Glycerol 65% + Tris-HCl 25 mM + $MgSO_4$ 0.1 M + ddH_2O
LB Medium	NaCl 1% w/v + Tryptone 1% w/v + Yeast extract 0.5% w/v
PowerCHO™ 2-CD serum-free CHO Medium with Antibiotics	4 mM Glutamine or GlutaMAX™-I CTS + 250 µg/ml Hygromycin B + 1.5 µg/ml Puromycin
Size exclusion buffer	Naphosphate (pH 7.5) 50 mM + 300 mM NaCl

All buffers for use in Äkta-purification, were filter sterilized using a 0.2 µm membrane filter.

SDS Gels 12%

Components	Stacking Gel 3,7%	Running Gel 12%
Acrylamide 30% solution	389 µl	3,2 ml
dH_2O	1,5 ml	2,6 ml
TEMED	23 µl	80 µl
Tris-HCL pH 6,8	288 µl	-
Tris-HCL pH 8,8	-	2,02 ml

3.1.6 Enzymes

Enzymes	Manufacturers and catalog numbers
BamHI FastDigest	[Thermo Scientific, Cat No FD0054]
BmtI HFR	[New England Biolabs, Cat No R0658L]
FastAP™ Thermosensitive Alkaline Phosphatase	[New England Biolabs, Cat No EF0651]
I-SceI HFR	[New England Biolabs, Cat No R06945]
NcoI FastDigest	[Thermo Scientific, Cat No FD0575]
NgoMIV HFR	[New England Biolabs, Cat No R0564S]
Q5R Hot Start High-Fidelity DNA Polymerase	[New England Biolabs, Cat No M0493L]
T4 DNA Ligase	[New England Biolabs, Cat No M0202L]

3.1.7 Markers

Markers	Manufacturers and catalog numbers
GeneRuler™ 1kb Plus DNA Ladder	[Thermo Scientific, Cat No SM1331]

Spectra™ Broad Range Protein Ladder	[Thermo Scientific, Cat No 26634]

3.1.8 Primers for sequencing

The following primers were selected using the software A plasmid Editor (ApE). The primers were purchased from Sigma Aldrich (Germany).

Primer name	Sequence (5´- 3´ orientation)
pCold-Fwd	ACGCCATATCGCCGAAAGG
pCold-Rev	GGCAGGGATCTTAGATTCTG

3.1.9 Recombinant proteins

Recombinant proteins	Manufacturers and catalog numbers
Human CD3ge-hIgG4(KIH)	[ProtTech®, Cat No 03-01-0051]
Human CD3ge	[ProtTech®, Cat No 03-01-0049]

3.1.10 Bacterial Strains

Bacterial strains	Manufacturers and catalog numbers
Mach1 competent E. coli	[Thermo Scientific, Cat No C8620-03]
SHuffleR T7 competent E. coli	[New England Biolabs, Cat No C3029J]

3.1.11 Mammalian cell lines and primary cells

Cell line	Origin	Medium
FreeStyle™ CHO-S K1 Cells	Chinese hamster ovary (CHO) cells are an epithelial cell line derived from the ovary of the Chinese hamster, Source: [Thermo Scientific, Cat No R80007]	HyClone,ActiSM™+ 250 µg/ml Hygromycin + 1,5 µg/ml Puromycin (According to the experiment, without or with antibiotic) + 4 mM L-Glutamine
Jurkat cells	human T-cell leukaemia (acute lymphoblastic) cells; CD3+, CD45+, HLA-A2-	RPMI 1640 + 10 % FBS + 1x GlutaMAX™-I CTS (100x) + 1x PSN (100x)
PBMCs	peripheral blood mononuclear cells of human origin, isolated from blood donor buffy coat by Ficoll density gradient centrifugation; largely monocyte-depleted; CD3+, CD45+, HLA-A2-	RPMI 1640 + 10 % FBS + 1x GlutaMAX™-I CTS (100x) + 1x PSN (100x)
THP-1 cells	human monocytic cell line (acute monocytic leukemia) cells; CD45+, HLA-A2+	RPMI 1640 + 10 % FBS + 1x GlutaMAX™-I CTS (100x) + 1x PSN (100x)

3.1.12 Kits

Kits	Manufacturers and catalog numbers
AlexaFluorTM532Antibody Labeling Kit	[Thermo fisher scientific, Cat No A20182]

AlexaFluorTM546Antibody Labeling Kit	[Thermo fisher scientific, Cat No A20183]
AlexaFluorTM647Antibody Labeling Kit	[Thermo fisher scientific, Cat No A20186]
Human Perforin ELISA set (without plates)	[abcam, Cat No ab83709]
MinElute Gel Extraction Kit	[Qiagen, Cat No 28606]
Mix & Go! E. coli Transformation Kit	[Zymo Research, Cat No T3001]
Neon™ Transfection System 100 µl Kit	[Thermo Scientific, Cat No MPK10096]
NucleoBond®Xtra Maxi	[Macherey-Nagel, Cat No 740414.50]
NucView™ 488 Caspase-3 Assay Kit for Live cells	[Biotium, Cat No 30029]
Pan T cell isolation Kit human	[Milteny Biotec, Cat No 130-096-535]
QIAprep Spin Miniprep Kit	[Qiagen, Cat No 27106]

3.1.13 Antibodies

Antibodies	**Manufacturers and catalog numbers**
APC Mouse IgG2b, κ Isotype Ctrl Antibody	[Biolegend, Cat No 400322]
Biotin anti-human CD3, Clone: OKT3	[Biolegend, Cat No 317320]
Biotin anti-human CD3, Clone: UCHT1	[Biolegend, Cat No 300404]
HLA-A2 Mouse anti-Human, APC, Clone: BB7.2	[eBioscience™, Cat No 17-9876-41]

Mouse anti-Human IgG4 Fc Secondary Antibody, HRP	[Thermo fisher scientific, Cat No A-10654]
PerCP/Cyanine5.5 anti-human CD3 Antibody	[Biolegend, Cat No 344807]
StrepMAB-Immo Chromeo 488 conjugate	[IBA Lifesciences, Cat No 5110007806]

3.1.14 Vectors

Vectors	**Manufacturers and catalog numbers**
pCOLD IV	[Takara Bio Company, Cat No 3364]
pRSF-DUET	[Merck, Cat No 71341)
The UCOER Single Expression Puromycin and Hygromycin Vector Set	[Merck, Cat No UC0E01 and UC0E02]

3.1.14.1 Bacterial vectors

3.1.14.1.1 pCold IV DNA Vector

PCold IV expression Vector (Figure 10) consists of a cold-shock promotor termed Protein A (cspA), making the expression of target proteins in *E. coli* at lower incubation temperatures possible. At low-temperature host protein expression, protein aggregation, and the bacterial protease activity is reduced. This allows expression of difficult proteins, which normally form unwanted protein aggregations and degradation at higher temperatures. Also, this vector contains a lac operator, ampicillin resistance gene (amp), ColE1 origin of replication, M13 IG fragment, and a multiple cloning site (MCS).

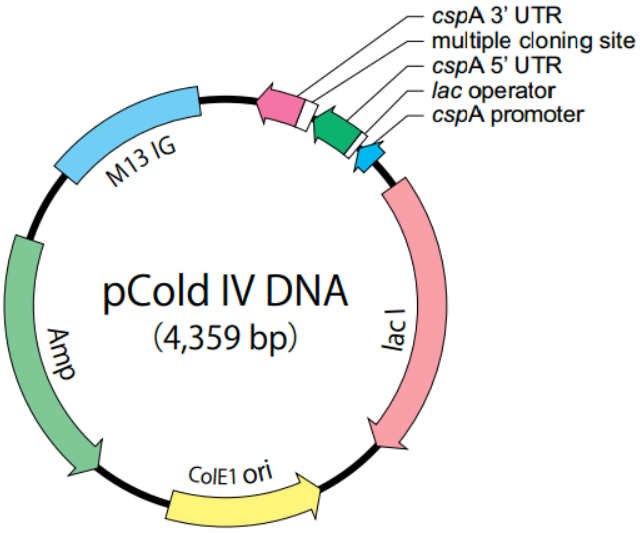

Figure 10: Schematic representation of the expression vector pCold IV DNA. The positions of cold-shock promotor termed Protein A (cspA) promotor, multiple cloning site (MCS), lac operator is indicated. Adapted from the Takara catalog (http://catalog.takara-bio.co.jp/PDFS/3360-3364_j.pdf).

3.1.14.1.2 pRSF-DUET Vector

The pRSF-DUET vector was used to co-express a particular protease to cleave the fusion tag from the N-terminus of the hemibodies after successful production. The recombinant human rhinovirus 3C protease (HRV 3C) is active at 4 °C and recognizes a specific cleavage site from LeuGluValLeuPheGln ↓ GlyPro. The recombinant protein was cloned into the pRSF-DUET vector, which in addition to kanamycin resistance has two multiple cloning sites, each with a T7-Lac promoter.

3.1.14.2 Mammalian Vectors

3.1.14.2.1 CET1019AS-hygro/ CET1019AS-puro

The UCOER Single Expression Puromycin and Hygromycin Vector Set consists of two complementary vectors, CET1019AS-hygro expressing a hygromycin resistance gene and CET1019AS-puro (Figure 11) carrying a puromycin resistance gene. This expression system allows the stable high-level expression of target proteins using the Ubiquitous Chromatin Opening Element (UCOE). UCOE modifies the chromatin structure to inhibit DNA methylation mediated silencing resulting in enhanced protein expression. Moreover, the vectors contain a multiple cloning site with a variety of restriction cleavage sites and a SceI cleavage site for linearization of the vectors. Linearization prevents mammalian cells from randomly cutting the plasmid before incorporation in the host genome. From human and Caviidae (guinea pig)

originated cytomegalovirus (CMV) Promoter-enhancer elements served for a higher protein expression as well.

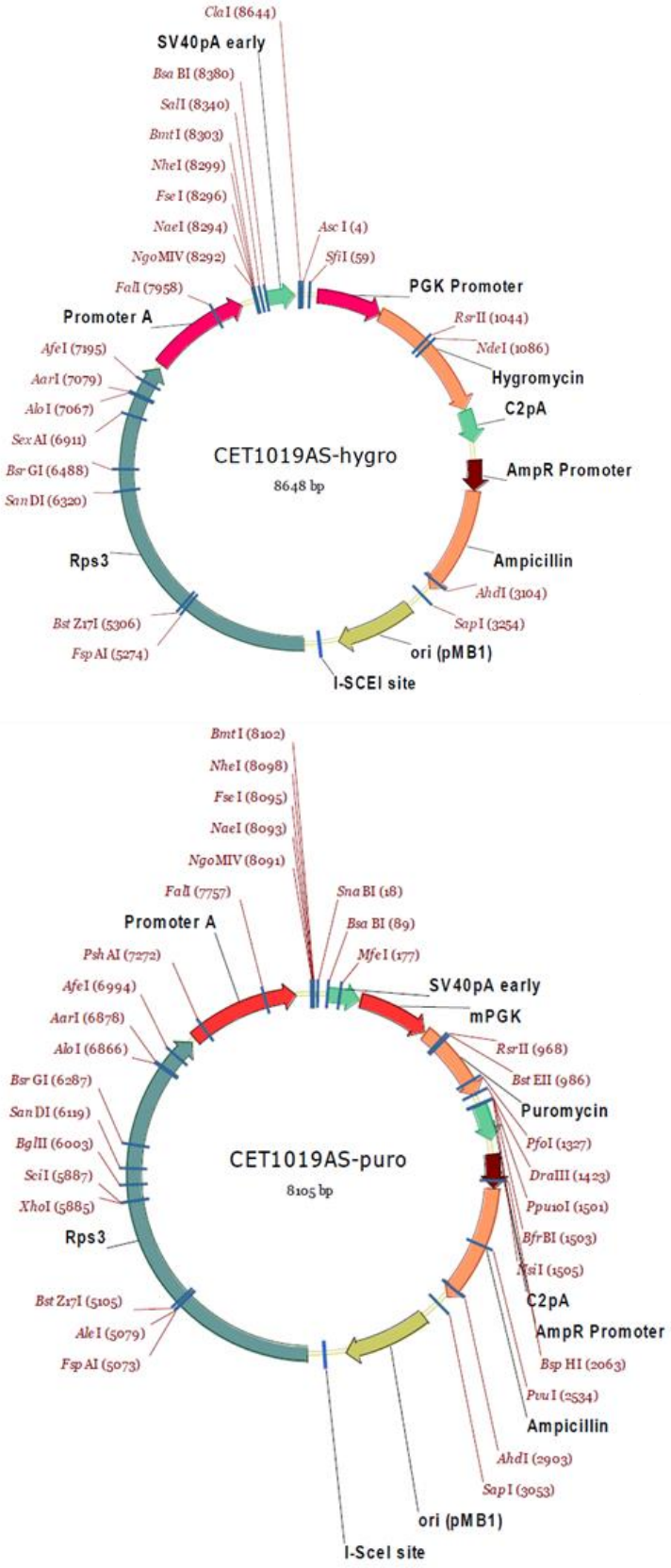

Figure 11: Schematic representation of the expression CET1019AS-hygro vector, and CET1019AS-puro vector. Adapted from the certificate of analysis (batch number: Q2778177) of UCOER Single Expression Hygromycin Vector Set.

3.2 Methods

3.2.1 Production of BiTE scFvαCD3-scFvαHLA-A2 in *E. coli*

3.2.1.1 Construction of BiTE and cloning in pCold IV vector

The cDNA with the BiTE in the pCold Vector already existed in the laboratory before this project started. Briefly, for the construction of BiTE, the cDNA of BiTE with N-terminal Fh8 tag (improves the solubility), GS-(G4S)-linker between scFvCD3 and scFvHLA-A2 and C-terminal His_6 tag (for the later Äkta purification) was cloned in pCold Vector IV.

3.2.1.2 Amplifying of pCold IV Vector containing BiTE

3.2.1.2.1 Preparation of chemically competent Mach1 *E. coli*

To amplifying the pCold vector containing cDNA of BiTE, the mach1 *E. coli* cells were used. To enable the take up of the vector by cells, the cells were made chemically competent according to the protocol of Mix & Go! E. coli Transformation Kit.

3.2.1.2.2 Transformation of chemically competent cells with plasmid DNA

For transformation of Mach1 competent *E. coli*, with a colony-forming unit of about 4*107 cfu/µl, Plasmid DNA was diluted with a maximal concentration of 100 ng/µl.

20 µl of bacteria (stored at -80 °C) were thawed on ice and mixed with 1 µl of the DNA plasmid vector. The mixture was incubated on ice for 30 min, followed by a heat shock at 42 °C for 45 sec. Afterward, the cells were incubated on ice for 5 minutes. Then 120 µl of LB medium was added. After 20 min incubation under shaking at 37°C, the transformation samples were plated on pre-warmed LB agar plates containing 100 µg/ml carbenicillin. The agar plates were incubated overnight at 37 °C. The next day, for mini preparation of plasmid DNA, single colonies were picked with a pipette tip and dropped into tubes containing 3 ml of LB medium

with a final carbenicillin concentration of 100 µg/ml. The inoculated cultures were incubated at 37°C and 170 rpm overnight.

3.2.1.2.3 Isolation of plasmid DNA usind DNA-Mini preparation

For the isolation of plasmid DNA, the overnight cultures (see section 3.2.1.2.2) were harvested by centrifugation for 2 min at 7.000 × g and 4°C. The isolation was carried out using the QIAprepR Spin Miniprep Kit following the manufacturers' instructions. The DNA was eluted in 30 µl of pre-warmed Ampuwa water. After the measurement of the concentration of isolated DNA using Nanodrop, they were stored at 4 °C.

3.2.1.3 Protein Expression of BiTE in *E. coli*

3.2.1.3.1 Transformation of Plasmid DNA to chemically competent shuffle cells and glycerol stock preparation

BiTE construct was expressed in the cytoplasm of Shuffle T7 Express bacteria. For that, in addition to pColdIV-hemibody-plasmid, 3C-protease-PRSFDUET-plasmid was co-transformed. 3C-protease enables the intracellular separation of the Fh8 tag. For long-term storage of the Shuffle cells containing DNA of BiTE, glycerol stock was prepared.

For bacterial transformation with respective constructs, 1 µl of 3C-Protease Plasmid (100 ng) was mixed gently with 50 µl of shuffle cells thawed on ice. In the next step, 30 µl of this mixture was added to 1 µl pColdIV hemibody-plasmid (30-100 ng) and incubated on ice for 30 min. The mixture was heated at 43 °C for 45 sec and was quickly cooled down on ice for 5 min. Afterward, 300 µl LB medium was added to the cells and incubated for 45 min at 37 °C with shaking. After shaking, the cells were mixed with 2 ml 2xYT medium containing 100 µg/ml antibiotics carbenicillin and 50 µg/ml kanamycin and were grown at 30 °C and 125 rpm overnight.

The next day, the optical density of bacteria was measured, and 500 µl from bacteria with OD 0.5-0.8 were mixed with 500 µl Glycerol buffer. The Glycerolsrtocks were stored at - 80 °C.

3.2.1.3.2 Expression of BiTE in shuffle cells

The cytoplasm of bacteria contains different chaperons for expression of correctly folded proteins. However, the formation of disulfide bonds is not possible in the cytoplasm of *E. coli* cells. The chemically competent *E. coli* K12 cells termed shuffle cells promote disulfide bond formation in the cytoplasm using expression of a chromosomal copy of the disulfide bond isomerase DsbC. For the expression of pColdIV vector containing BiTE, 1000 µl glycerol stock was added to the preculture of 500 ml 2x YT Medium which contained 0.2 % w/v Glucose and 100 µg/ml antibiotics carbenicillin and 50 µg/ml kanamycin. The mixture was grown at 30 °C and 125 rpm overnight. The next day, the optical density of bacteria was measured by spectrophotometry. In the next step, a defined volume of preculture to achieve an OD 600 of 0.1 was added to each 1 L of fresh expression medium, and the reaction was cultured at 30°C and 125rpm till the medium reached an optical density between 1.0 – 1.5. When the culture reached this OD, the temperature was cooled down to 10 °C for 2 h to adjust the *E. coli* cells to the low temperature. After two hours the temperature was raised to 14°C and protein expression was started by addition IPTG (Isopropyl β-D-thiogalactopyranoside) to a final concentration of 0.1 mM. IPTG activates the lac operon. The culture was grown at 14 °C and 125 rpm for 18 – 20 h.

3.2.1.3.3 Harvest of *E. coli* cells

The cell density of the overnight culture was measured using a spectrophotometer. Afterward, the cells were centrifuged for 30 min at 4800 x g and 4 °C. After centrifugation, the cell pellet was resuspended in Co-IMAC Loading Buffer I. For every measured OD of cell culture medium, a fixed volume of Co-IMAC Loading Buffer I was used to resuspend the cell pellet (10ml buffer for every OD 1.0 measured). To disrupt the cell pellet, the cells were loaded three times onto an EmulsiFlex-C3 (Avestin) homogenizer. After homogenization, the cell lysate was centrifuged two times at 15.000 x g and 4 °C for 15 min to remove all remaining cell debris. Finally, the lysate was filtered using syringe filters with diameters of 5.0 and 1.2 µm. In all steps, the cell pellets and lysates were kept on ice to prevent degradation by protease.

3.2.1.4 Purification of BiTE from *E. coli*

3.2.1.4.1 Selection of his-tagged BiTE using Cobalt Immobilized Metal Affinity Chromatography (Co-IMAC)

In the first step, before loading the cleared lysate supernatant, the column was equilibrated with 5 Column Values (CV) of demineralized water followed by 10 CV of Co-IMAC loading buffer. Then, the lysate was loaded onto the column. The column was washed with 5 CV of Co-IMAC loading buffer followed by 50 CV of Co-IMAC wash buffer. Before elution, the column was washed with 10 CV of Co-IMAC loading buffer. Elution was performed with 5-10 CV of Co-IMAC elution buffer. Until further processing, the eluates were stored at 4°C. To regenerate the column, 5 CV of Co-IMAC regeneration buffer was used. For final storage, the column was washed with 5 CV of distilled water and 5 CV of a 20% ethanol solution. All steps of the purification were performed at 4°C.

System settings were set as follows:

Equilibration flow rate	5.0 mL/min
Sample loading flow rate	5.0 mL/min
Wash flow rate	5.0 mL/min
Elution flow rate	3.0 mL/min

The elution fractions were started to collect at 50 milli-Absorption-Unit (mAU), and the collection was stopped at 50 mAU. A sample of the IMAC-purified construct was stored for the later analysis by SDS-Gel.

3.2.1.4.2 Further purification of BiTE including anion exchange chromatography (AIEX) and size exclusion chromatography (SEC)

For further purification of the BiTE construct, the buffer was exchanged to Desalting & IEX Buffer (50 mM Na phosphate pH 7.5, 75 mM NaCl) using a HiPrep 26/10 desalting column and then purified by MonoQ anion exchange chromatography (AIEX) using a 1 ml HiTrap Q FF column. Finally, the eluted proteins were purified by size exclusion chromatography (SEC) by a HiLoad 16/600 Superdex 200 pg column. In brief, the Co-IMAC elution fraction(s) with an end volume of approx. 10-25 ml were filtered using a 0.2 µm membrane filter. Each time, a

maximal volume of 10 ml was loaded onto the desalting column. Before the run, the columns were washed with demineralized water to remove all remaining ethanol. Afterward, the column was equilibrated with Desalting & IEX Buffer. Subsequently, elution fractions were loaded on the column using a 10 ml loop. The elution was performed in Desalting & IEX Buffer. In the next step, the purified construct was loaded onto the AIEX column. From the column, the constructs were eluted using the Desalting & IEX Buffer. Directly after elution, the buffer was exchanged with buffer containing 50 mM Na phosphate pH 7.5 and 300 mM NaCl. After IEX purification, the constructs were purified using SEC chromatography. For this purpose, the IEX eluents were loaded onto an SEC column. The elution was performed in SEC buffer (Naphosphate pH 7.5, 50 mM + 300 mM NaCl). The complete purification process was performed at RT.

3.2.1.4.3 SDS-Polyacrylamide Gel Electrophoresis

To control the quantity and purity of the column extracted proteins, SDS-Polyacrylamide Gel Electrophoresis (SDS-PAGE) was used. Protein samples were mixed with 4x SDS loading buffer and were incubated at 98 °C for 5 min. Afterward, the samples were loaded onto an SDS-PAGE gel and run at 90 V to 120 V for approximately 60-90 minutes. The staining of the SDS-PAGE gel was performed with Coomassie blue staining solution for 15 minutes on an orbital shaker, followed by destaining for approximately 1h using Coomassie destaining Solution. The SDS-PAGE gel was stored in dH2O overnight. The next day, a digital image was taken by Gel Doc™ Gel Documentation System (Bio-Rad).

3.2.2 Production of hemibody constructs in CHO-S cells

3.2.2.1 Cultivation of CHO-S cells

For a higher growth and transfection efficiency, CHO-S cells which are adapted to serum-free suspension culture were used. These cells are clonal isolated from Chinese hamster ovary (CHO K1) cells (Lattenmayer et al., 2007).

CHO-S cells were cultivated in 250 ml Erlenmeyer cell culture flasks in 30 ml of HyClone, ActiSM™ CHO Medium in a humidified (80% rel. humidity) incubation shaker (INFORS HT) at 37°C and 125 rpm with 5% CO2 atmosphere. Cells were split every 3-4 days at a density of $5*10_6$ cells/ml. For antibiotic selection, cells were seeded at less density. Countess II FL Automated Cell Counter and trypan blue solution for live/dead discrimination was performed

for counting the cells. For long-term storage, $15*10_6$ cells were resuspended in 800 µl freezing medium consisting of 90% v/v conditions HyClone, ActiSM™ medium and 10% v/v DMSO. After freezing the cells in a cryobox at -80°C, the cells were transferred into liquid nitrogen storage container.

3.2.2.2 Construction of VLαCD3-scFvαHLA-A2 and VHαCD3-scFvαCD45 hemibodies and cloning in hygro/puro vectors

Hemibody cDNA was designed using the GeneArt Gene Synthesis Tool (Thermo Scientific). To possible the glycosylation of the sequence, an N-glycosylation site was inserted into the GS linker between VH and VL of the antigen-specific scFv domain. The hemibody had an N-terminal signal peptide for extracellular secretion into solution. A Twin-strep-tag II was added to the C-terminal end for binding and purification of the construct. To optimize translation, codon optimization for Cricetulus griseus (chinese hamster) was performed. The designed DNA construct was manufactured by BioCat GmbH.

3.2.2.3 Amplifying of plasmid DNA

To transform the lyophilized pUC57 vector containing hemibody insert into MachT1 cells, 5 µg of vector were reconstituted in 50 µl of dH_2O to the final concentration of 100 ng/µl. 10 ng/µl of vector was transformed in Mach1cells (ca. $4*10_7$ cfu/µl). Transformation and following colony picking and inoculation was carried out as described in section 3.2.1.2.2. To gain sufficient amounts of plasmid DNA containing the designed gene, the extraction of plasmid DNA was achieved by the NucleoBond®Xtra Maxi kit according to the manufacturer protocol.

3.2.2.4 Cloning of hemibodies into the puro and hygro vectors

To clone the hemibody gene from the pUC57 vector into the final CHO-expression vector CET1019AS-puro andCET1019AS-hygro, both hemibody inserts were cut out of the pUC57 vector using restriction enzymes NgoMIV and BmtI, and finally, the inserts were ligated into CET1019AS-puro/ CET1019AS-hygro CHO-expression vector. Digestion reaction was done as follows:

3 µl	CutSmartR Buffer (10x)
X µl	Backbone DNA (~3 µg)
1 µl	NgoMIV HFR

1 µl	BmtI HFR
Ad 30 µl	ddH2O (Ampuwa)

Samples were incubated for 1.5 h at 37°C.

The digested inserts and linearized CHO-expression vector were ligated as follows:

2 µl	T4 DNA Ligase Buffer
1 µl	T4 DNA Ligase
50 ng	Dephosphorylated vector
X ng	Digested insert
Ad 20 µl	ddH2O (Ampuwa)

Subsequently, the ligated CHO-expression vector was transformed into MachT1 cells and isolated using a maxi preparation kit.

The ligated CHO-expression vector was sequenced at LGC Genomics (Berlin) for correct inserts.

3.2.2.5 Amplifying of CHO-expression vector

For amplifying of Plasmid DNA, MachI competent cells were transformed as described in section 3.2.1.2.2. MachI cells carrying the CHO-expression vector were grown in Erlenmeyer culture flasks with 400 ml LB-medium containing 100 µg/ml carbenicillin. The cultures were incubated overnight at 37 °C and 125 rpm. The next day, DNA was prepared using the NucleoBondR Xtra Maxi Plasmid DNA Purification Kit. Finally, DNA was eluted in 200 µl of pre-warmed Ampuwa water. For further procedure, DNA was diluted to a final concentration of 5 µg/µl.

3.2.2.6 Linearization of Mammalian Expression Constructs

To allow the integration of the vector into the CHO-S genome, the plasmid DNA has to be linearized. The linearization was performed as follows:

60-80 µg	DNA

5 µl	10x CutSmartR Buffer
5 µl	I-SceI
Ad 50 µl	ddH2O (Ampuwa)

The reaction mixture was incubated at 37°C overnight. On the next day, the enzyme was heat-inactivated at 80°C for 1 h. To test, whether the linearization was successful, a mixture of 500 ng of Plasmid DNA and 6xDNA gel loading dye with a final volume of 12 µl was loaded on a 1% w/v agarose gel. The gel was run at 110-130 V for approx. 1 h. The nucleotide products were visualized and documented by the fluorescence activity of the DNA-intercalating dye Nancy-520 on a UV transilluminator.

3.2.2.7 Transfection of CHO-expression vector into CHO-S Cells by electroporation

For transfection, parental CHO-S cells were split at $0.5x10_6$ cells/ml one day before transfection. The next day, cells were centrifuged at 250 xg for 6 min and the vector was transfected into the CHO cells by electroporation using Neon™ Transfection System 100 µl Kit. For each vector construct, six electroporations with $1.5x10_6$ - $2.0x10_6$ cells and 12 - 16 µg of DNA was used. The electroporation settings of the transfection system were as follows:

Pulse voltage	1620 V
Pulse width	10 ms
Pulse number	3

After electroporation, the cells were seeded into 6-well culture plates containing 2 ml of pre-warmed PowerCHO™ 2-CD serum-free CHO medium without antibiotics. The plates were incubated on a shaker in the cell incubator. The next day, cells were electroporated again with the second vector carrying the same gene but another antibiotic resistance gene. After electroporation, the cells were put back into the incubator with fresh medium without antibiotics.

3.2.2.8 Generation of stable CHO Cell Line

To select a stable CHO cell line after transfection with vector DNA, cells were cultivated for two days without antibiotics. After two days, the cells were subjected to selection pressure by

adding 2 ml of HyClone, ActiSM™ with antibiotics into each well of the 6-well plates containing 2 ml of cell suspension (final concentration 0.75 µg/ml puromycin, 125 µg/ml hygromycin). When cells started to grow, antibiotic concentration was increased. The cells surviving the highest antibiotic pressure were transferred into 250 ml Erlenmeyer cell culture flasks containing 30 ml of HyClone, ActiSM™ medium with antibiotics. Stable cultures under full antibiotic selection were split twice weekly and inoculated at $0.3x10_6$ cells/ml.

3.2.2.9 Expansion and Purification of VH and VL variants in CHO-S Cells

CHO cells expressing hemibody constructs were set in 1L Erlenmeyer culture flasks containing 300-500 ml of HyClone, ActiPro™ medium with supplementations (see section 3.1.11). The cells were seeded at a density of $0.3x10_6$cells/ml. The cell growth was documented every day by measurement of cell density. Once the cell growth reached $5x10_6$ – $6x10_6$ cells/ml, fresh CHOFeed™A supplemented with a volume of 2% and CHOFeed™B with a volume of 0.2% of the total cell media was added. The cells were fed so long until the percentage of dead cells exceed 10%. At this point, the cells were centrifuged at 4200 rpm for 1 h at 6 °C with Heraeus Multifuge X3R centrifuged, and supernatant was filtered using a 0.2 µm bottle top filter. For subsequent purification of the twin-strep-tagged hemibodies by affinity-chromatography (AFC), biotin in the CHO supernatant had to be blocked. For this purpose, 1 ml of BioLock biotin blocking solution was added to 300 ml volume of cell supernatant. The supernatant was stored at 4 °C.

3.2.2.9.1 Purification using Strep-Tactin chromatography

The purification of twin-strep-tagged hemibodies was done as follows: The cell supernatant was loaded on an equilibrated Strep-Tactin column with a CV of 1 ml. Afterward the column was washed with 5 wash fractions, each 1 CV with buffer W. The fractions were collected and named as wash fraction for later analysis using SDS Gel. Protein was eluted in 6 elution fractions with a volume of 1 CV with elution buffer.

3.2.2.9.2 Analytical size exclusion chromatography

To test, whether the AFC-purified hemibodies will aggregate after concentration, the purified proteins with Strep-tag were concentrated in different steps using the Centrifugal filters (Amicon® Ultra – 15, Ultracel® - 30K). From each concentration step 50 µl volume was analyzed at a flow rate of 0.3 ml/min by gel filtration chromatography using a Superdex 200

5/150 GL column installed in an Äkta Pure system. The running buffer, ATS (200 mM L-Arginine + 20 mM Tris + 10 mM Succinic acid; pH 7.4 – 8) was used.

3.2.2.9.3 Preparative size exclusion chromatography

To separate the monomer AFC-purified proteins from the aggregated proteins, 5 ml constructs were loaded on a HiLoad 16/600 Superdex 200 pg column and separated in fraction of 2 ml using a deep-well plate. The constructs were eluted in ATS buffer (200 mM L-Arginine + 20 mM Tris + 10 mM Succinic acid; pH 7.4 – 8). The purification procedure was done according to bacterial SEC purification (see section 3.2.1.4.2) with the exception that purification of CHO constructs was performed at 4 °C.

3.2.3 Functional and biochemical characterization of hemibodies

3.2.3.1 Cell cultivation

Mammalian cells were cultured in suitable tissue culture flasks in the respective volume of the complete RPMI culture medium in a humidified (60% rel. humidity) incubator at 37°C with 5 % CO_2 atmosphere. Cells were split every 2-3 days at a density of 1 x 10_6 cells/ml. Counting of cells was performed using the vital stain trypan blue. For freezing, cells of 60 – 80 % confluence were harvested by centrifugation for 4 min at 1200 rpm using Heraeus Multifuge X3R. The pellet was resuspended in 80% complete RPMI medium (see 3.1.11) and 20% DMSO. Per vial, approx. 2x10_6 cells were aliquoted in cryovials. To slowly freeze the cells, they were stored in CoolCell at -80°C for 2-3 days. Finally, the frozen cells were placed to LS3000 Cryogenic Storage Tank. Cells were thawed quickly at 37°C in a water bath, washed once with PBS at 1200 rpm for 5 minutes and were transferred into respective tissue culture flask filled with complete RPMI medium.

3.2.3.2 Peripheral blood mononuclear cells (PBMCs) isolation from blood

To isolate PBMCs consisting of lymphocytes and monocytes from the whole blood received from a healthy donor, density-gradient centrifugation using the Ficoll-based lymphocyte separation was performed. The blood was mixed with PBS at 1:1 ratio, and the mixture was slowly pipetted onto a Pancoll/Ficoll layer. To separate whole blood from ficoll, the falcon tubes were centrifuged at 3400 rpm for 25 min, without brake. After centrifugation, the interlayer consisting of PBMCs is transferred into another falcon and washed twice with PBS. Afterward,

for removing residual erythrocytes, the cells were mixed with 15 ml Erythrocytes Lysis Buffer and incubated at RT for 15 min. Afterward, the cells were washed with PBS twice and finally, the cells were transferred to a cell culture flask containing 70 ml of F12-K medium and incubated in a cell incubator. For all of the experiments in this thesis, HLA-A2-negative PBMCs were used.

To test the surface expression of the molecule HLA-A2, $2x10_5$ cells were washed with 2 ml PBS at 1200 rpm for 5 minutes. The resuspended cell pellet in 150 µl PBS was transferred into FACS tube and incubated with 0.5 µg antibodies targeting HLA-A2 or the appropriate isotype control for 40 min at 4 °C in the dark. Finally, cells were washed twice with 2 ml PBS and resuspended in 300 µl of PBS. The analysis was performed by flow cytometry using BD FACSCalibur.

3.2.3.3 $CD3_+$ T Lymphocytes Isolation from PBMCs

For further analysis, $CD3_+$ T lymphocytes were isolated from PBMCs using the Pan T Cell Isolation Kit based on the negative selection of T cells. In short, non CD3 positive cells from the PMBC cell pool were depleted using biotin-conjugated monoclonal antibodies against the cell surface markers CD14, CD15, CD16, CD19, CD34, CD56, CD123 and CD235a. By the second step, non-target cells were then labeled with microbeads conjugated to monoclonal anti-biotin antibody (isotype: mouse IgG1) and depleted by holding them within a MACS column in the magnetic field of a MACS separator, while the unlabeled T cells consisting of only CD3 positive cells run through the column.

3.2.3.4 Flow cytometry assays

All flow cytometry experiments except Calcium flux assay was performed using FACSCalibur™ Cell Analyzer, and the data were evaluated using FlowJo version 8.8.6 Program. Calcium flux was measured using BD FACSCanto™ II.

3.2.3.4.1 Caspase assay

To measure the intracellular caspase-3 activity in THP-1 target cells after redirecting of T cells with hemibodies, a substrate consisting of a fluorogenic DNA dye and DEVD substrate specific for caspase-3 (NucView™ 488 Caspase-3 Assay Kit for Live cells) was used. After cleavage of the non-fluorescent and non-functional substrate by caspase-3 in the cytoplasm, the

substrate forms a high-affinity DNA dye that labels the nucleus bright green. For the killing assay, the isolated PBMCs containing only $CD3_+$ T lymphocytes were counted and incubated with THP-1 target cells at ration (5 effector cell:1 target cell). For this purpose, per well, $0.5x10_6$ PBMCs in 50 µl of pre-warmed RPMI medium were mixed with $0.1x10_6$ THP-1 target cells with a volume of 50 µl. In the second plate, hemibodies were diluted with RPMI medium in 5 steps with the highest concentration of 120 nM. To get the final concentration of hemibodies, 20 µl of RPMI medium containing hemibodies was added to the 100 µl cell mixture per well. The mixture of THP-1 cells with PBMCs without hemibodies was used as negative control. As positive control bi-specific T-cell engager targeting HLA-A2 was used. To measure cell killing after 30 minutes of incubation with constructs, 2 µl caspase substrate was added to each well. After 30 min incubation at 37°C and 5 % CO_2, the cells were transferred from wells to FACS falcons, and their caspase activity was measured by FACS. The 16 h time point cells were incubated in the Plate at 37°C and 5% CO2 for 16 h. On the next day, the cells were treated equal to time point 30 min, and the caspase activity was measured by FACS.

For FACS analysis, a gating strategy was used to separate cells with caspase activity. For calculation of caspase activity, the Caspase positive cells in the absence of hemibodies and BiTE (R1), and the cells in the presence of them (R2) were measured.

Caspase activity was normalized as shown in the below formula. Percent of cells with caspase activity in the absence of stimulator (R1) was subtracted from the percent of cells in the presence of stimulator (R2), resulting in the final percentage of caspase activity.

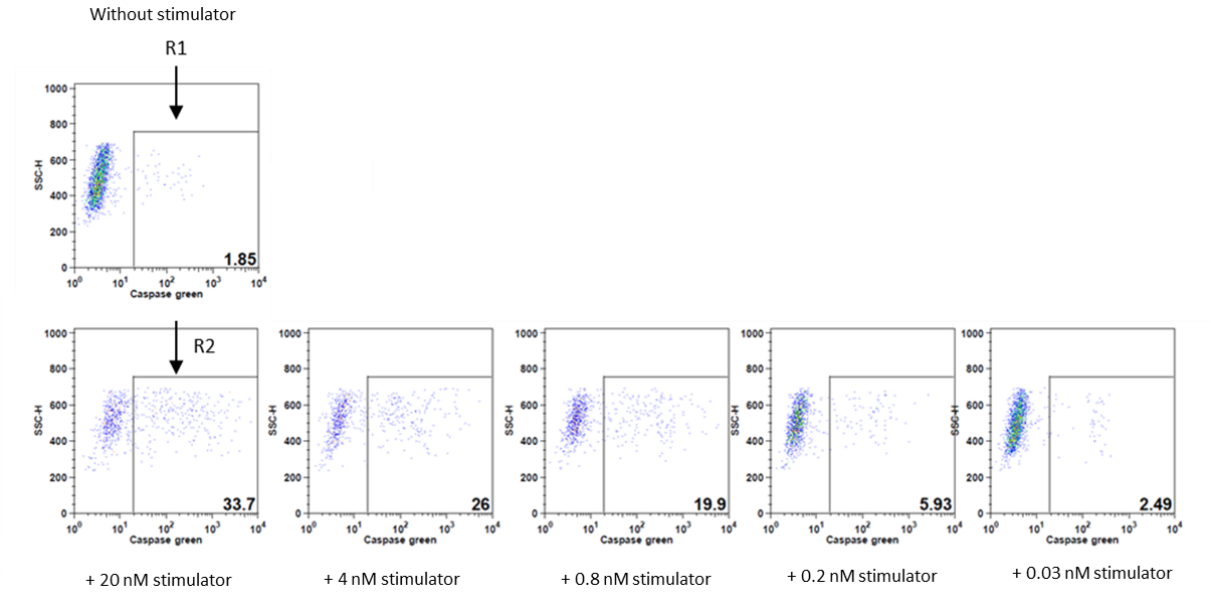

(R2 - R1) = (% of apoptotic cells with stimulator - % of apoptotic cells without stimulator) = caspase activity (%).

3.2.3.4.2 Conjugation assay

To study the target cell (THP-1) - T cell (Jurkat) conjugation in the presence of hemibodies or BiTE antibody, we used a conjugation assay. In this assay, THP-1 cells were labeled with CellTracker™ Deep Red Dye, while Jurkat cells were stained with CellTracker™ Green CMFDA Dye according to the staining protocol of the manufacturer. After staining of 50000 THP-1 cells and 250000 Jurkat cells, the cells were incubated with hemibodies or BiTE antibody as described in section 3.2.3.4.1. The conjugate formation was measured after different time points using FACS analysis.

The double-stained cells represent the conjugates between THP-1 target cell and Jurkat T cell. R1 displays the percent of conjugates in the absence of stimulator, while R2 presents the percent of conjugates in the presence of stimulator at the indicated titrated concentrations.

The normalization was achieved by the subtraction of % double-positive cells with stimulator (R2) from % of double-positive cells without stimulator (R1) resulted in the percentage of stimulator mediated THP-1-Jurkat cell conjugates.

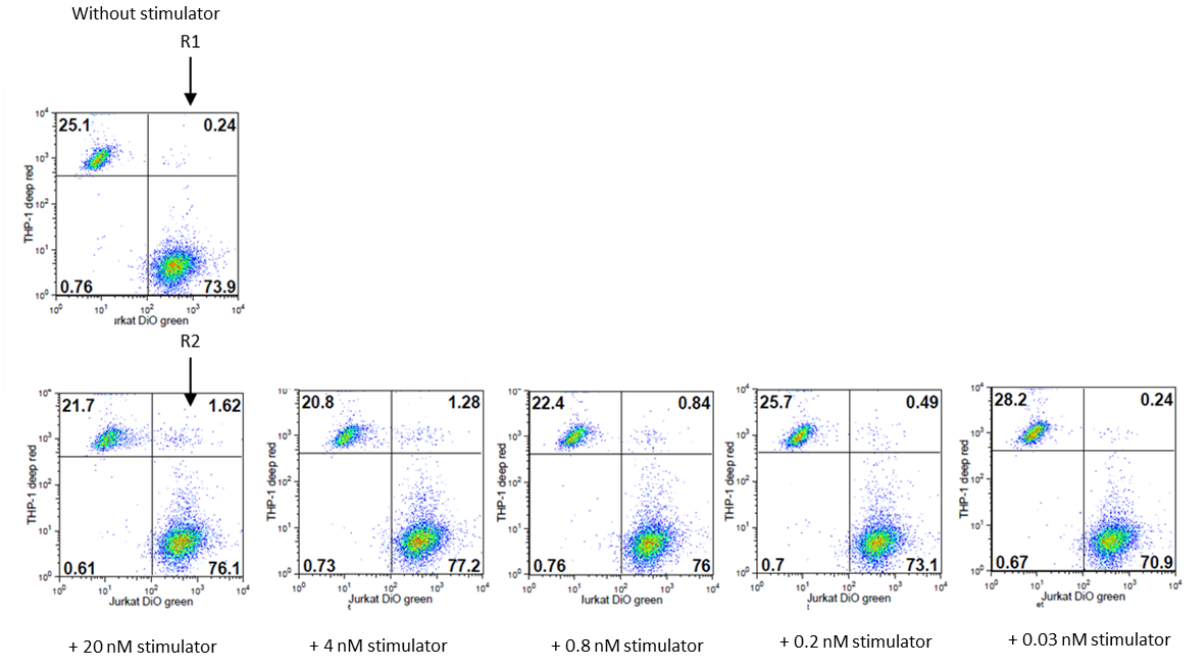

R2 – R1 = % of double-positive cells with stimulator - % of double-positive cells without stimulator = % of normalized stimulator mediated THP-1-Jurkat cell conjugates.

3.2.3.4.3 CD3 downregulation

To test, whether CD3 molecule on $CD3_+$ HLA-A2- PBMCs will be downregulated in the presence of hemibodies or BiTE, a FACS assay was established. The incubation of PBMCs with hemibodies or BiTE was performed like in the caspase assay (see section 3.2.3.4.1). After 16 h incubation of cell mixture under standard cell culture conditions (at 37°C and 5% CO_2), the cells were labeled with PerCP/Cyanine5.5 anti-human CD3 Antibody at 4 °C for 1h. After incubation, they were transferred to V-bottom plate and centrifuged at 1300 rpm for 5 min. Finally, the cells were resuspended in 100 µl PBS and transferred to a FACS tube. The measurement was done by the flow cytometer.

The stained cells demonstrate the $CD3_+$ T cells. The percent of $CD3_+$ T cells were separated into two gates R1 and R2. R1 indicates the proportion of $CD3_+$ T cells in the absence of stimulator, whereas R2 displays the amount of $CD3_+$ T cells in the presence of stimulator.

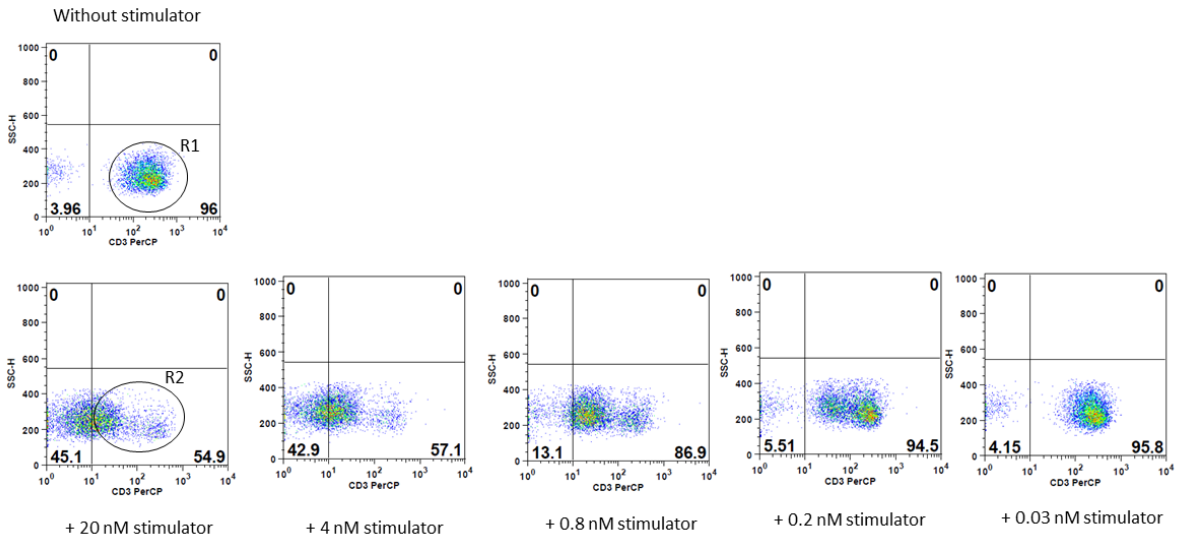

The percentage of normalized $CD3_+$ T cells was calculated by dividing of % of $CD3_+$T cells with stimulator (R2) by % of $CD3_+$T cells without stimulator (R1).

R2/R1 = % of $CD3_+$T cells with stimulator / % of $CD3_+$T cells without stimulator = normalized $CD3_+$ T cells (%).

3.2.3.4.4 Analysis of transient intracellular calcium flux in T cells

This assay uses non-radiometric dyes, in combination with flow cytometry to monitor TCR-triggered calcium changes over time. For this purpose, the Jurkat T cells were stained with dye-loading-buffer. Cells at 1x10_6 cells/ml in 1ml dye-loading-buffer were incubated for 30 min at 37 °C. After incubation, cells were washed with PBS for 5 min, centrifuged at 1000 rpm and resuspended in 1ml HBSS/Ca/Mg/FBS and stored on ice in the dark. For calcium mobilization, the samples were warmed up at 37 °C for 5-10 min and directly analyzed with flow cytometer for calcium baseline measurement. Afterward, stimulators were added (in the case of hemibodies and BiTE, preincubated with THP-1 target cells) mixed well and the measurement was immediately continued for further 6 minutes (Figure 12).

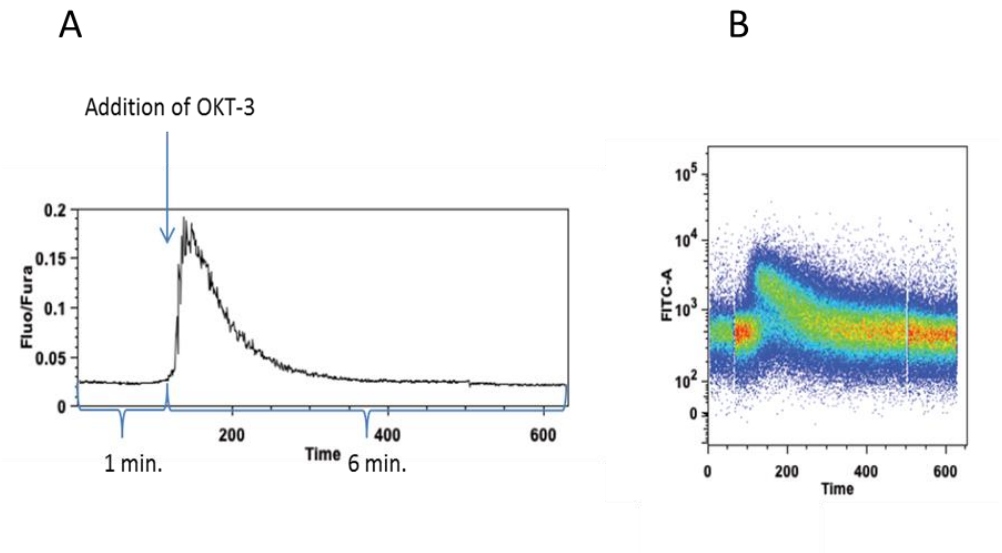

Figure 12: Analysis of transient intracellular calcium flux. A) Histogram of calcium binding dye-loaded Jurkat cells treated with OKT-3 was created using FlOWJO Ver.8.8.6 software. **B)** Baseline fluorescence of calcium binding dye-loaded Jurkat cells was measured for 1 min. Measurement was stopped, OKT-3 was added, shortly mixed and measurement was continued immediately for further 6 min (right pic).

3.2.3.5 ELISA assays

3.2.3.5.1 Luciferase-based killing assay

To measure the constructs mediated cytotoxicity, the T cells were stimulated according to the caspase assay (see section 3.2.3.4.1). In contrast to the caspase assay, here the number of dead cells was used for evaluation of the cytotoxicity. In this assay 10000 THP-1 target cells, expressing the firefly luciferase transgene were incubated with the 50000 $CD3^+HLA\text{-}A2^-$

PBMCs (5: 1, E: T ratio) in the presence of respective constructs for 16 h at 37°C and 5 % CO_2.To determine the killing of the target cells, the intracellular luciferase activity of target cells was measured using the reaction with D-Luciferin. After 16 h, D-Luciferin was added to a final concentration of 0.5 mM and incubated at 37°C for 30 min. Subsequently, light emission was quantified with an infinite M200 pro ELISA reader. As positive control for cytotoxicity, 10% DMSO was used. As negative control, the viability of cells without constructs was measured.

3.2.3.5.2 Measurement of released Perforin

The amount of released perforin from construct stimulated $CD3_+$ PBMCs was measured by Human Perforin ELISA set. The incubation of PBMCs with hemibodies or BiTE was performed like in the caspase assay (see section 3.2.3.4.1). The cells were incubated for 16 hours with constructs at regular cell culture conditions (37 °C and 5% CO_2). Afterward, the cells were transferred to V-bottom plates and centrifuged at 1300 rpm for 5 min. 100 µl of supernatant per well was transferred to a flat-bottom 96 well plate and stored at 4°C for further measurements by ELISA. The ELISA assay was performed in accordance with the Human Perforin ELISA set protocol.

3.2.3.5.3 Binding studies of constructs and soluble CD3 epsilon/gamma by ELISA

To analyze the interaction between hemibodies and recombinant CD3 Epsilon and gamma protein bound to human IgG4 (CD3ge-hIgG4), an ELISA assay was developed. VLαCD3-scFvαHLA-A2 (K33) was used at 1000 nM in PBS and coated onto an ELISA plate for 2h at RT. Afterward, the wells were blocked using pre-warmed 0.2% bovine gelatin (in PBS, pH 7.4) for 2 h. In the meantime, a mixture of 1000 nM VHαCD3-scFvαCD45 (K35) and titrated CD3ge-hIgG4 (100 – 0.05 nM) (1: 2 dilution steps) in blocking buffer was incubated at RT for 30 min. After blocking, the wells were washed three times with PBS containing 0.05% Tween20; pH 7.4. The mixture of K35 with CD3 was added to the wells and incubated for 1 hour. Afterward, the wells were washed three times with wash buffer, and for detection, an HRP linked anti-Human IgG4 antibody (1: 1000) in blocking buffer was added to each well and incubated for 1h. Then the wells were washed again three times with washing buffer and subsequently 100 µl of TMB substrate was added per well to induce the color reaction. As stopping solution, 100 µl of 1M H2SO4 was used per well. Finally, the plate was read using a Spark multimode microplate reader (Tecan).

As controls, the binding of 311 nM of BiTE antibody with 100 – 0.05 nM of CD3ge-hIgG4 protein was measured. Furthermore, the interaction of 17 nM of OKT3 antibody with 100 – 0.8 nM of CD3ge-hIgG4 protein was analyzed. In these assays, the BiTE or OKT3 constructs were immobilized on the 96-well plate, and the titrated CD3ge-hIgG4 molecule was added to the wells.

3.2.3.6 Microscopy experiments

3.2.3.6.1 Analysis of caspase activity in target cells using time-lapse microscopy

For imaging, the process of caspase activity in the THP-1 target cells, 250.000 $CD3^+$ PBMCs were mixed with 50.000 THP-1 target cells and 20 nM construct. For visualization of caspase activity, 2 µl of caspase substrate (see section 3.2.3.4.1) was added. After 30 min incubation time at RT, the cells were filmed with a time-lapse fluorescence microscope for 16 h. The microscope used an HCX PL APO 63x UV objective with a numerical aperture of 1.30. The imaging system was controlled by Leica LAS AF Lite 3.3 software. Emission was detected with an EMB cube using a TL-BF contrast filter and a YFP cube with an FLUO contrast filter. For the live imaging, the Leica-DFC9000GTC-VSC05760 camera used a binning of 2x2. The imaging climate was set as follows: 37 °C, 2% CO_2, 25% O_2. For the generation of movies, ImageJ software was used. The Imaris x64 9.3.1 software was used to quantify the caspase activity.

3.2.3.6.2 Fluorescence staining of constructs

To visualization the location of hemibodies and the BiTE antibody on the cells, they were labeled with different Alexa Fluor dyes according to the imaging experiment. For this purpose, the concentrated constructs in PBS were labeled using the AlexaFluor Antibody Kit. For staining, 100 µl of the prepared constructs at 1 µg/µl was dissolved in the 1/10 volume of 1 M sodium bicarbonate buffer to reach the pH 8-9. Then the solution was incubated with amine-reactive dye. Subsequently, to remove the unbound dye, the fluorescent conjugates were purified using a size-exclusion spin column with a molecular weight cut-off of 30,000 dalton, optimized for proteins with molecular weight greater than 40,000 daltons. The final labeled constructs were resuspended in PBS, pH 7, 2, and 2 mM sodium azide. The labeling steps were performed in the dark to avoid the possible photobleaching.

3.2.3.6.3 Transfection of T cells with ZAP70-GFP

For transfection of Jurkat T cells with the ZAP70-GFP gene, a lentiviral method was used. Lentivirus based on the epHIV7 vector with EF-1alpha promotor was produced in the Hudecek lab using LentiX cells. For transduction, 250.000 Jurkat cells in 200 µl RPMI medium with supplementation (see 3.1.11) were mixed with Polyibrin to a final concentration of 5 µg/ml. The cells were plated into a 48 well plate and subsequently 1-3 µl Lentivirus supernatant with an infection rate of 240.800 TU/µl was added. After 2 hours of incubation under standard cell culture conditions (at 37°C and 5% CO_2), 900 µl fresh RPMI medium was added. The cells were incubated at 37 °C for 2 days. Two days after the viral transfection, the cells were analyzed by FACS analysis for expression of the recombinant protein.

All materials used for the transfection of the Jurkat cells were kindly provided by Julian Rydzek from the Hudecek group, University Hospital Würzburg.

3.2.3.6.4 Analysis of immunological synapse (IS) and ZAP70 recruitment using confocal laser scanning microscopy

In order to analyze IS formation and ZAP70 recruitment to the CD3 receptor complex, 25.000 THP-1 cells were incubated with respective constructs (hemibodies or BiTE antibody) at 3 µg/ml in 100 µl PBS for 30 min on ice and in the dark. To remove the unbound construct from the cells, the mixture was washed one time with cold PBS, centrifuged at 200 g for 5 min and stored on ice until microscopy. Shortly before imaging, the cells were hand warmed and pipetted to 25.000 Jurkat cells or ZAP70-GFP expressing cells (in PBS). Images were acquired using an inverted IX81 microscope equipped with an Olympus FV1000 confocal laser scanning system, an FVD10 SPD spectral detector and diode lasers of 405, 473, 559, and 635 nm. The presentative images were acquired with an Olympus UPLSAPO60x (oil, numerical aperture: 1.35) or Olympus UPLFLN 40x (oil, numerical aperture: 1.30) objectives. For a high-resolution confocal scanning, an automatic pinhole setting was used. The resolution was set with at least 2 pixels per micron in x-y direction. Z-stack images were processed by maximum intensity projection, and the noise was reduced using despeckle function and then cropped to focus on the cell of interest. Images are shown as RGB (32 bits per pixel). The image processing was performed using ImageJ software.

3.2.3.6.5 Imaging of intracellular calcium flux

To measure the intracellular cytoplasmic calcium flux in Jurkat T cells, 80.000 suspension Jurkat cells were incubated for 2 h on poly-L-lysine coated cover glasses and were loaded prior to calcium imaging with the Kindly provided by Corinna Martin from the Robert Blum group University Hospital Würzburg). The dye was stored as 5 mM stock solution of 20% Pluronic F-127 and DMSO (both life tech.) and for imaging was dissolved in calcium imaging buffer to a final concentration of 5 µM. The THP-1 cells were prepared in the same way as for IS microscopy. To induce the calcium flux, 40.000 THP-1 cells preincubated with hemibody or BiTE antibody were directly pipetted to the Jurkat cells during calcium imaging. The imaging setup consisted of a BX51WI upright microscope (Olympus) equipped with a 20× water-immersion objective (Olympus UMPLanFL N; NA 0.5), a coolLED epifluorescent light source for 470 nm (Visitron Systems), equipped with a Rolera XR Mono fast 1394 CCD camera (Qimaging). Image sequences were acquired at 10 Hz using the streaming software Streampix.

4 Results

4.1 Production of constructs in *E. coli* and CHO-S cells

The hemibodies and BiTE constructs were designed and cloned by Agnes Banaszek (Banaszek, A., 2013). In Brief: for the hemibodies the scFv domains specific for CD45 or HLA-A2 were linked to the VH or VL domain of a CD3-specific antibody. The resulting constructs are termed as VHαCD3-scFvαCD45 and VLαCD3-scFvαHLA-A2 (Figure 13 B, C). For the BiTE antibody as positive control, the scFv domain against HLA-A2 was linked to the scFv domain of the CD3-specific antibody. The constructed BiTE is termed scFvαCD3-scFvαHLA-A2 (Figure 13 A). The DNA plasmid for BiTE antibody was synthesized by GeneArt™. DNA sequences of hemibodies for production in CHO-S cells were ordered from BioCat GmbH.

The sequence encoding for scFv targeting CD3ε is derived from diL2K antibody (Brischwein et al., 2006), which is a de-immunized version of the mouse monoclonal antibody L2K (Dreier et al., 2002). For the construction of HLA-A2 constructs, the human HLA-A2-specific antibody fragment 3PF12 was isolated from an alloimmunised patient by phage display and kindly provided by Nicholas A. Watkins, University of Cambridge, UK. This construct has a nanomolar affinity for its target HLA-A2 and no cross-reactivity with HLA-A2-negative platelets (Watkins, Brown, Hurd, Navarrete, & Ouwehand, 2000). The scFv domain against human CD45 is derived from the murine IgG1 antibody clone BC8. This clone recognizes all human CD45 isoforms (Lin et al., 2006).

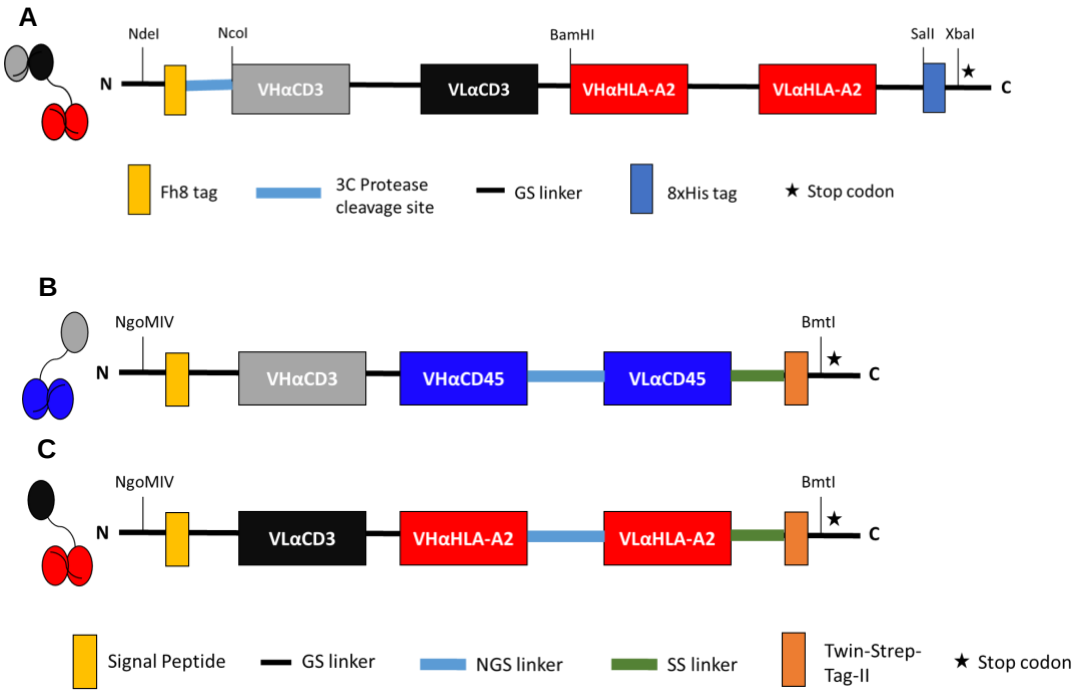

Figure 13: Schematic structure of BiTE antibody and hemibodies. For the production of BiTE, E. coli was used, whereas hemibodies were produced in CHO-S cells. **A)** BiTE consists of two scFvs domains, one against CD3ε and another one against a tumor antigen. scFv fragments of BiTE are linked via flexible GS linkers. They also have an N-terminal fusion site (Fh8), which improves the solubility and is cut off after production via a 3C protease. C-terminal, BiTE contains an 8x His-tag for the later purification. **B)** and **C)** Hemibody contains a VH or VL chain of an αCD3ε scFv and a tumor antigen scFv. An N glycosylation site was added to the GS linker between VH and VL of antigen specific scFv domain, and for secretion of the recombinant protein out of the cell, a signal peptide was added to the N-terminus of the construct. The addition of a Twin-strep-tag II to the C-terminus of the gene sequences enables the purification of construct. N: N-terminus, C = C-terminus.

4.1.1 Expression of scFvαCD3-scFvαHLA-A2 (BiTE) in *E. coli*

The BiTE antibody was expressed in cytoplasm of shuffle cells and purified using its histidine-tag by Co-IMAC. To remove the protein aggregates which can interfere with the effectiveness of the therapy, or activate immune responses and thus cause side effects, the Co-IMAC eluted proteins were further loaded on the size exclusion chromatography (SEC) column. The resulted peak of SEC-purified BiTE was monomeric and could be detected at approx. 70 ml (Figure 14 A).

To determine the degree of purity and amount of produced protein, the final protein extract was loaded onto an SDS-PAGE Gel and then the protein was visualized using the Coomassie Blue stain. The initial IMAC-purified sample contains many unspecific bands, while the monomeric fractions resulted from SEC purification, consist of only one specific band (Figure

14 B). This result confirms that the final purification improved the purity of the BiTE protein significantly.

To further functional and biochemical characterization of BiTE construct, a high amount of monomeric protein was needed. For that, marked bands (red cycles) (Figure 14 B) were pulled together, and the concentration of the protein was calculated using BSA standards. The final concentration of the mixed samples amounted to approx. 0.03 µg/µl in an end volume of 4 ml. To reach a final concentration of 1 µg/µl, the mixture was concentrated using Centrifugal Filters (Amicon®Ultra-15) to 1 µg/µl. Parallel to that, the protein was transferred from SEC buffer to PBS buffer.

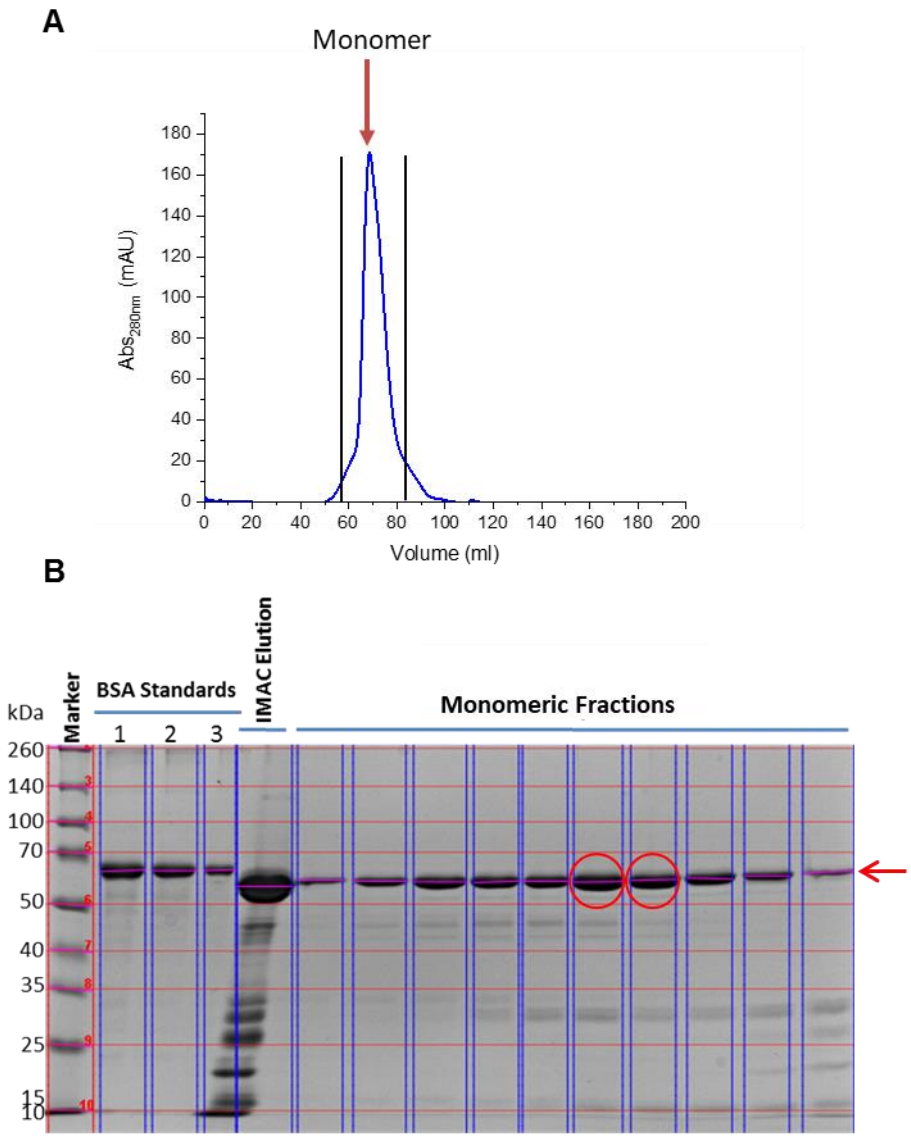

Figure 14: Preparative size exclusion chromatography (SEC) and corresponding SDS-PAGE analysis of BiTE construct scFvαCD3-scFvαHLA-A2 produced in E. coli. A) Gel filtration chromatogram of BiTE scFvαCD3-scFvαHLA-A2 (construct 71) (V_e = ~ 70 ml). Gel filtration purification was performed using a HiLoad 16/600 Superdex 200 pg column (GE Healthcare©). The constructs were eluted in 50 mM Na-phosphate pH 7.5, 300 mM NaCl buffer at a flow rate of 1 ml/min. Each fraction was collected in a volume of 2ml. Eluted constructs were detected by their absorbance at 280 nm. The monomeric peak is shown with an red arrow and two black lines marked the selected fractions for SDS-gel analysis **B)** SDS-gel from AFC-purified BiTE construct expressed in E.coli. Shown are a protein ladder with 10 standard proteins of 10, 15, 25, 35, 40, 50, 70, 100, 140, 260 kDa. The concentration of eluted AFC-fractions was determined by BSA standards 1-5, their concentrations are as followed: 1: 0.5 µg/ml, 2: 0.25 µg/ml, 3: 0.125 µg/ml. IMAC elution indicates the fraction eluted from IMAC purification and monomeric fractions indicate the selected SEC-purified protein form the marked region (two black lines in A). The arrow shows the theoretical size of construct 71, which amounted to approx. 64 kDa and the red cycles marked two SEC-fractions which were pooled and concentrate for further analysis assays.

4.1.2 Expression of VLαCD3-scFvαHLA-A2 (construct 33) and VHαCD3-scFvαCD45 (construct 35) in CHO-S cells

For the imaging experiments, constructs have to be labeled, and for this purpose, big amounts of constructs would be needed. Therefore, the tested hemibodies were expressed in Chinese hamster ovary (CHO) cells with an inserted N glycosylation site in their GS linker region. CHO cells have been shown to express therapeutic proteins in substantially better purity and higher expression yield in comparison to the prokaryotic expression system. CHO cells have been reported to regulate posttranslational modifications, including glycosylation improved solubility, bioactivity, and additionally decrease the immunogenicity of produced therapeutic proteins (Butler & Spearman, 2014).

To evaluate the purification process and the final hemibody purity, protein samples of all fractions of each chromatography step were loadet onto a 12% SDS-PAGE gel. After electrophoresis the gel was stained using Coomassie Blue stain for visualization of proteins. Figure 15 A,B shows Strep-Tactin purified constructs stained for protein visualization. The elution fractions E2 and E3 have the highest protein amount. Construct 35 has a calculated molecular weight of approx. 44 kDa and the molecular Wight of construct 33 is aprox. 42 kDa. The protein bands at higher molecular weight, as the calculated hemibodies weight, are most likely from constructs with posttranslational modifications (e.g., N-glycosylation). The bands below the calculated molecular weight are most likely from protein degradation and/or unspecific bound cellular proteins. The majority of the unspecific proteins can eliminated with additional washing steps, as seen in elute 4 to 6.

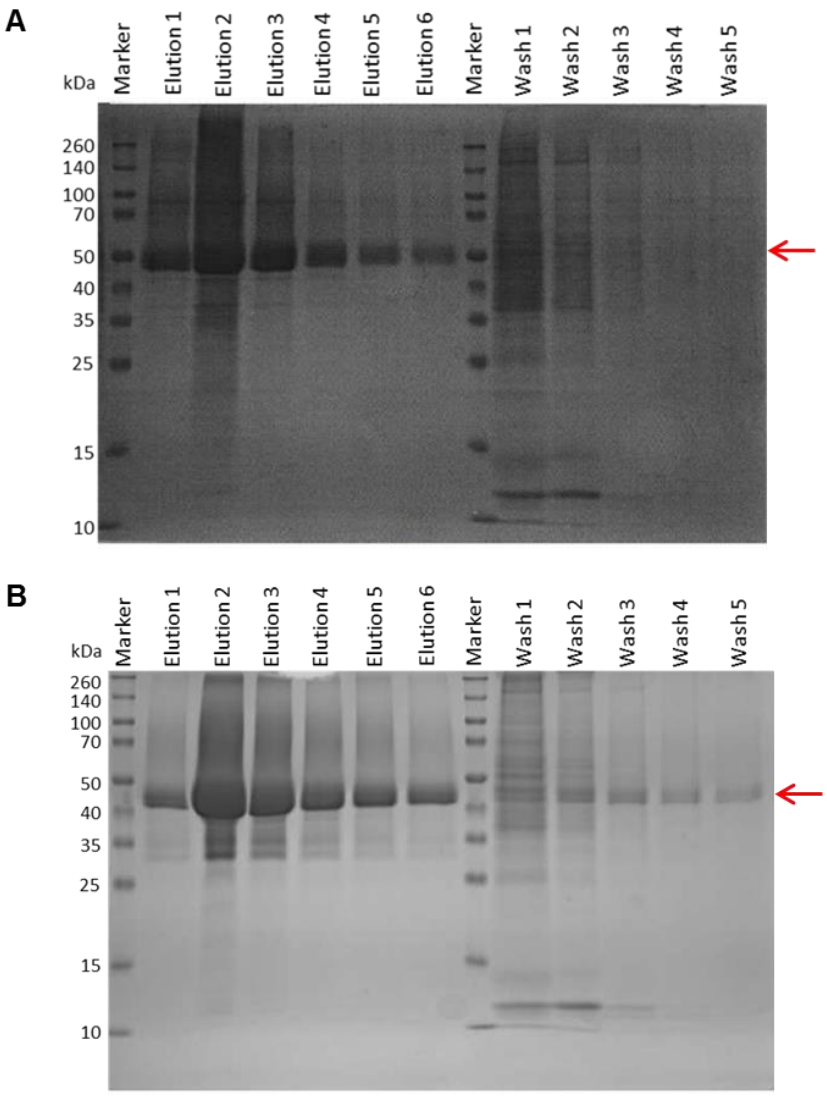

Figure 15: SDS-PAGE analysis of purified hemibody constructs expressed in CHO cells. A) Hemibody VHαCD3-scFvαCD45 (construct 35) and B) VLαCD3-scFvαHLA-A2 (construct 33). The Strep-Tactin-purified hemibody constructs were separated by 12% SDS-PAGE under reducing conditions and visualized by Coomassie Blue staining. Prior to loading of probes on the gel, they were mixed with 1xloading dye followed by heating 95 °C for 5 min. Finally, 20 µl per sample was loaded on the gel. The loaded fractions are lettered in the picture. Arrowhead points to the calculated size of the constructs (A), which amounted to approx.44 kDa and construct 33 (B) to approx.42 kDa. The concentration of eluted fractions for both constructs were determined by NanoDrop spectrophotometer.

The concentration of eluted proteins was determined by a NanoDrop spectrophotometer. The calculation is achieved using extinction coefficient and molecular weights, which is based on the law of Lambert-Beer, where the absorption is measured at 280nm. Extinction coefficient and the molecular weights were calculated for each construct using the protein analysis software tool ExPASy. The extinction coefficients and the molecular weights for constructs 35 and 33 are as followes; C35: Ext.coef. 94115 L*mol-1*cm-1, MW 43,78kD. C33: Ext-coef. 83685 L*mol-1*cm-1, MW 41.75kD. Table 1 indicates the calculated concentrations of Strep-Tactin-purified constructs.

Table 1: Determination of the protein concentrations of C35 and C33 hemibodies expressed in CHO-S cells.

Elution Fraction	Volume (ml)	Concentration (mg/ml)		Protein amount (mg)	
		Construct 35	**Construct 33**	**Construct 35**	**Construct 33**
1	5	0.265	0.247	1.32	1.235
2	5	2.315	3.486	11.57	17.34
3	5	0.346	1.709	1.5	8.545
4	5	0.097	1.111	0.48	5.555
5	5	0.059	0.339	0.29	1.695
6	5	0.052	0.2	0.26	1

To analyse protein aggregation of the purified hemibodies we used size exclusion chormatographie (SEC). The elution fractions E1-E3 from hemibody VHαCD3-scFvαCD45 and E1-E6 form hemibody VLαCD3-scFvαHLA-A2, each were polled, and further polished through size exclusion chromatography (SEC) on a HiLoad 16-600 superdex 200pg column. To define the apparent molecule weight of the SEC-purified constructs, the column was calibrated with Cytochrome C (12.4 kDa), Carbonic Anhydrase (29 kDa), Albumin (66 kDa), Alcohol Dehydrogenase (150 kDa) and beta-Amylase (200 kDa) as standard proteins. The SEC purification was performed at 4°C.

As can be seen in the Figure 16 in the case of construct 35 (Figure 16 A), the peak at 80-90 ml (Monomer) is the expected peak of monomeric hemibody construct. The peak at 40-60 ml (Aggregate) is likely from multimeric aggregates of the hemibody. For the second hemibody construct 33 (Figure 16 B), the monomeric peak is running at 70-80ml and the multimeric aggregate peak is running at 50-70ml. For further hemibody experiments, the monomeric peak of each construct was collected in 2 ml fractions in ATS running buffer.

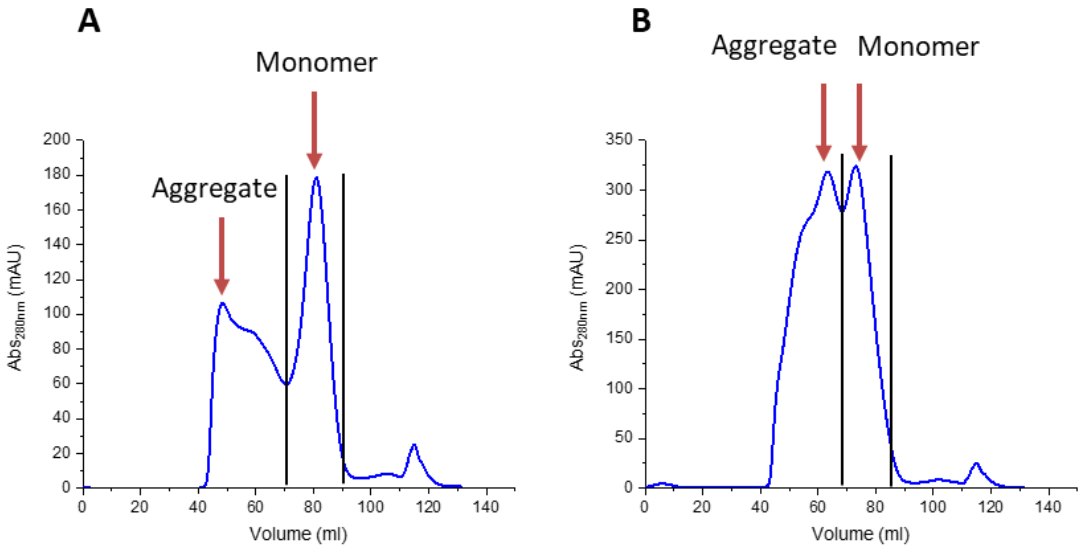

Figure 16: Preparative size exclusion chromatography (SEC) of hemibody constructs produced in CHO-S cells. A) Hemibody VHαCD3-scFvαCD45 (construct 35) (V_e = ~ < 80 ml) **B)** VLαCD3-scFvαHLA-A2 (construct 33) (Ve = ~ 80 ml). Gel filtration was performed using a HiLoad 16/600 Superdex 200 pg column (GE Healthcare©). The constructs were eluted in ATS buffer at a flow rate of 1 ml/min. Each fraction was collected in a volume of 2ml. ATS buffer was used as an elution buffer. 5 ml sample of each hemibody was loaded on the column. Eluted constructs were detected by their absorbance at 280 nm. **A)** and **B)** The red arrows indicate aggregate and monomer peaks. The two black lines in each graph show the selected and pooled monomeric fractions.

For further characterization of the SEC purified hemibodies elution fractions from the monomeric peak and from the aggregate peak as control were loaded onto a SDS-PAGE (Figure 17). The SDS-PAGE analysis is showing clear bands for construct 35 (A) and some unspecific lower bands for construct 33 (B).

For further experiments only the samples marked with a red cycle were used. These expected monomeric hemibody fractions of construct 35 had a concentration of 0.38 µg/µl, and of construct 33 a concentration of 0.72 µg/µl, each in a final volume of 2 ml. The final hemibody fractions were rebuffered in PBS and concentrated via Centrifugal Filters (Amicon®Ultra-15) to 1µg/µl for the further experiments.

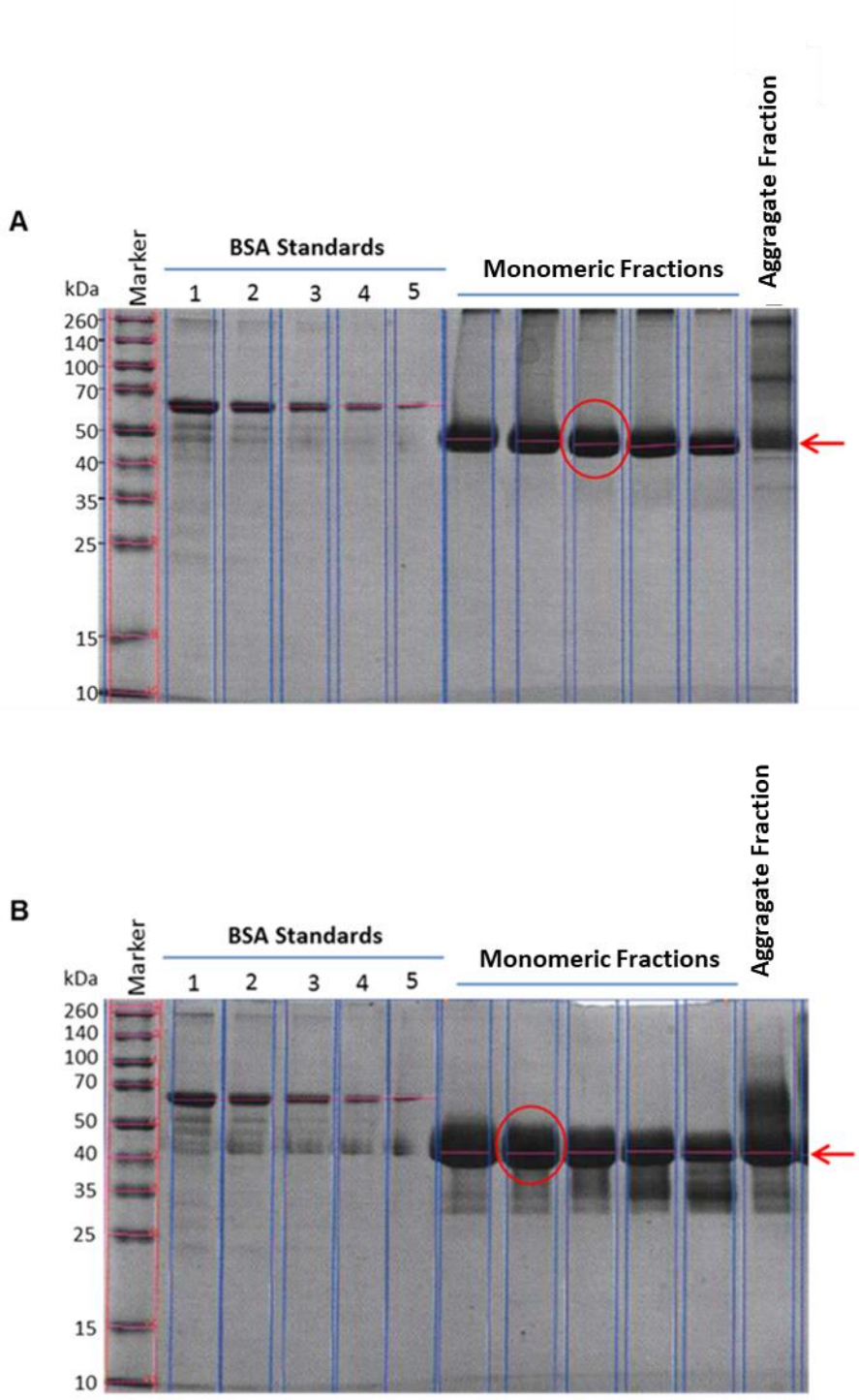

Figure 17: SDS-PAGE analysis of SEC-purified hemibody constructs expressed in CHO-S cells. A) Hemibody VHαCD3-scFvαCD45 (construct 35) **B)** VLαCD3-scFvαHLA-A2 (construct 33). The hemibodies were purified using gel filtration chromatography. The indicated fractions were separated by 12% SDS-PAGE under reducing conditions and visualized by Coomassie Blue staining. Prior to loading of probes on the gel, they were mixed with 1xloading dye followed by heating. Finally, 20 µl per sample was loaded on the gel. Arrowhead points to the calculated size of the hemibody constructs 35 (A), which amounted to approx.44 kDa and construct 33 (B) to approx.42 kDa. The concentration of constructs was determined with Nanodrop and additionally with the loaded BSA standards in lane 1-5, their concentrations is as follows: 1: 0.5 µg/ml, 2: 0.25 µg/ml, 3: 0.125 µg/ml, 4: 0.062 µg/ml, 5: 0.031 µg/ml. **A)** and **B)** Species1: indicates aggregate peak. Species2: indicates the monomeric peak. The red cycles marked SEC-fractions which were selected and concentrated for further analysis assays.

4.2 Aggregation analysis of concentrated hemibodies produced in CHO-S cells over time

To test, whether hemibodies will aggregate after concentrating and over time, VHαCD3-scFvαCD45 (C35) hemibody was concentrated in titrated steps. After concentrating, to analyze for possible protein aggregation, they were loaded on an analytical 5-150 superdex 200pg column and analyzed. The same experiment was performed after incubation of the concentrated hemibody for 24 h at 4 °C (Figure 18 A). After gel filtration chromatography the samples were loaded onto an SDS-PAGE-gel (Figure 18 B).

To compare the amount of aggregation proportion between differently concentrated hemibodies, peak A, containing the aggregated proteins, was selected and its percentage was determined. It can be exposed, that the % area of selected peak A is very similar between all tested concentrations in the time point 0 and time point 24 h. The profiles of visualized bands on the SDS-Gel are very similar as well, confirming the results from the chromatography analysis.

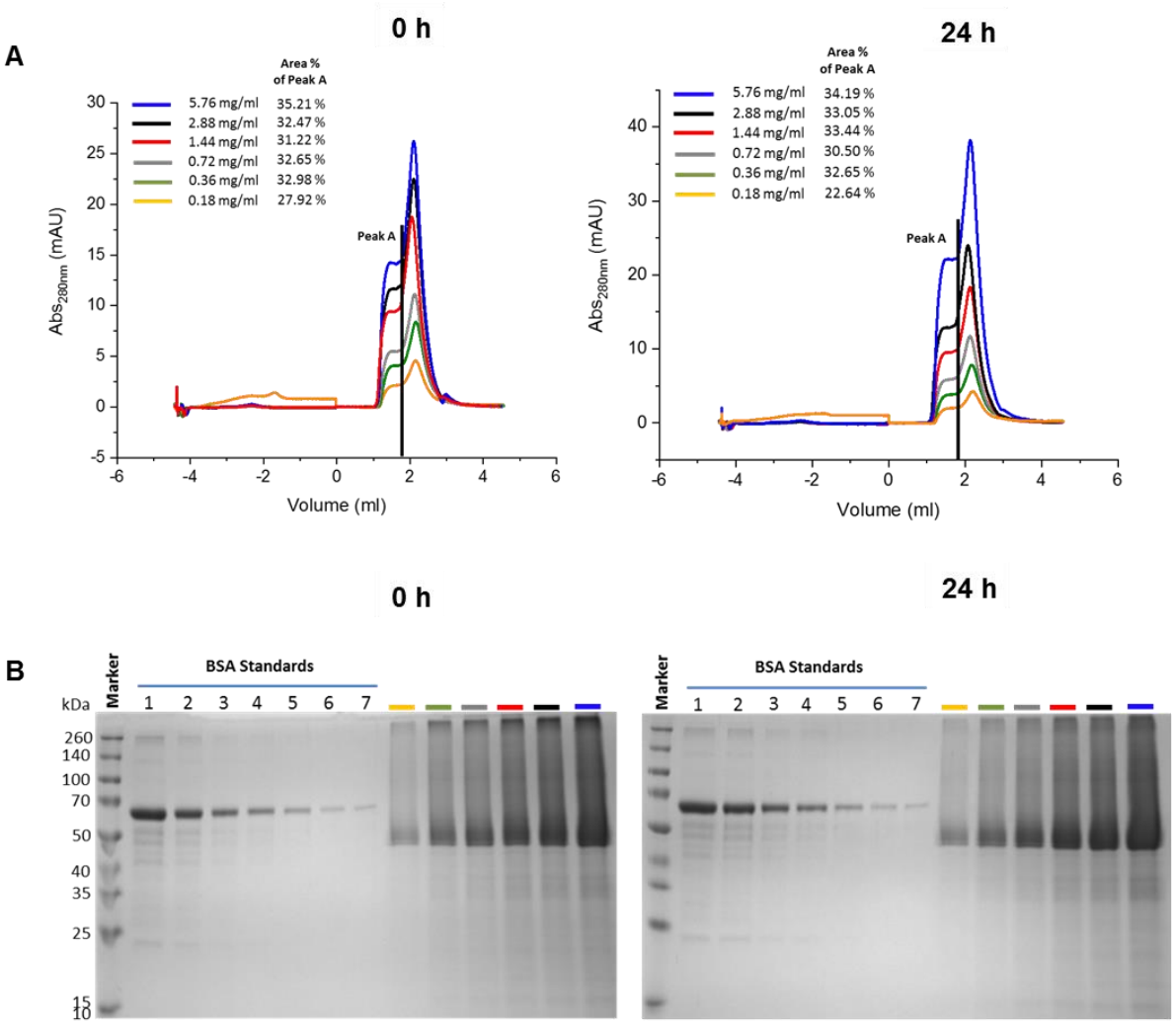

Figure 18: A) Analytical gel filtration chromatography (SEC) and B) the respective SDS-PAGE analysis of different concentrated hemibody construct VHαCD3-scFvαCD45 (c35) produced in CHO-S cells. Measurement was performed at time point 0 after concentrating and after 24 h. Gel filtration was performed using a 5/150 Superdex 200 pg column (GE Healthcare©). ATS buffer was used as the running buffer. The chromatogram is indicated for a 50 µl sample of the different concentrated samples shown with different color codes. Eluted constructs were detected by their absorbance at 280 nm. Area % of peak A presents the proportion of aggregate. Parallel to the AFC-analysed construct, the same concentrated probes were loaded on SDS-gel. All of the bands run at approx.44 kDa, which corresponds to the molecular weight of construct 35. For determination of concentrations, BSA standards in the following concentrations were used: 1: 0.5 µg/ml, 2: 0.25 µg/ml, 3: 0.125 µg/ml, 4: 0.062 µg/ml, 5: 0.031 µg/ml, 6: 0.015 µg/ml, 7: 0.007 µg/ml.

4.3 T cell activation events in response to stimulation with the VHαCD3-scFvαCD45 x VLαCD3-scFvαHLA-A2 hemibodies and scFvαCD3-scFvαHLA-A2 BiTE

4.3.1 Cell lines

In all experiments, the monocytic cell line THP-1 is used as target cells in the context of acute myeloid leukemia (AML). Since THP-1 overexpresses CD45 and HLA-A2, it was used for analysis of effector cell activation of hemibodies VHαCD3-scFvαCD45 and VLαCD3-scFvαHLA-A2, as well as BiTE scFvαCD3-scFvαHLA-A2. As T cells, either T cell leukemia cell line Jurkat or HLA-A2$^-$ CD3$^+$PBMCs were used. In all cytotoxicity assays, unless otherwise stated, the cells were used in an Effector cell (E): Target cell (T) ratio of 5: 1. This ratio has been established based on the preliminary works in our group.

4.3.2 Determination of Immunological synapse

4.3.2.1 Analysis of florescence-labeled constructs for their functionality in the term of killing potency

To visualization the binding of constructs on the cells, they were labeled with Alexa Fluor dye (see 3.2.3.6.2).

To test, whether the labeled constructs differ in the functionality activity from unlabeled constructs, we used our established luciferase dye based killing assay. In this assay the luciferase-positive THP-1 cells were used. The luciferase activity correlates with the amount of the viable firefly luciferase-expressing THP-1 tumor cells. To measure the luciferase positive cells, D-Luciferin was added to the reaction followed by quantification with Elisa reader (see 3.2.3.5.1).

To analyze the T cell activation potential of the individual labeled and unlabeled form, complementary hemibodies VHαCD3-scFvαCD45 and VLαCD3-scFvαHLA-A2 and BiTE scFvαCD3-scFvαHLA-A2 were tested. The constructs were used at a final concentration from 20 to 0.04 nM. As a control, only PBMCs with target cells in the absence of constructs was used, and this luciferase activity was as 100% viability control. As positive control for cell killing, cells were incubated with DMSO.

BiTE and complementary hemibodies show a similar target cell killing activities in a concentration-dependent fashion, which is similar between labeled and unlabeled form. Unexpected, the single hemibodies also stimulate the cells but only at the highest concentration of 20 nM (Figure 19).

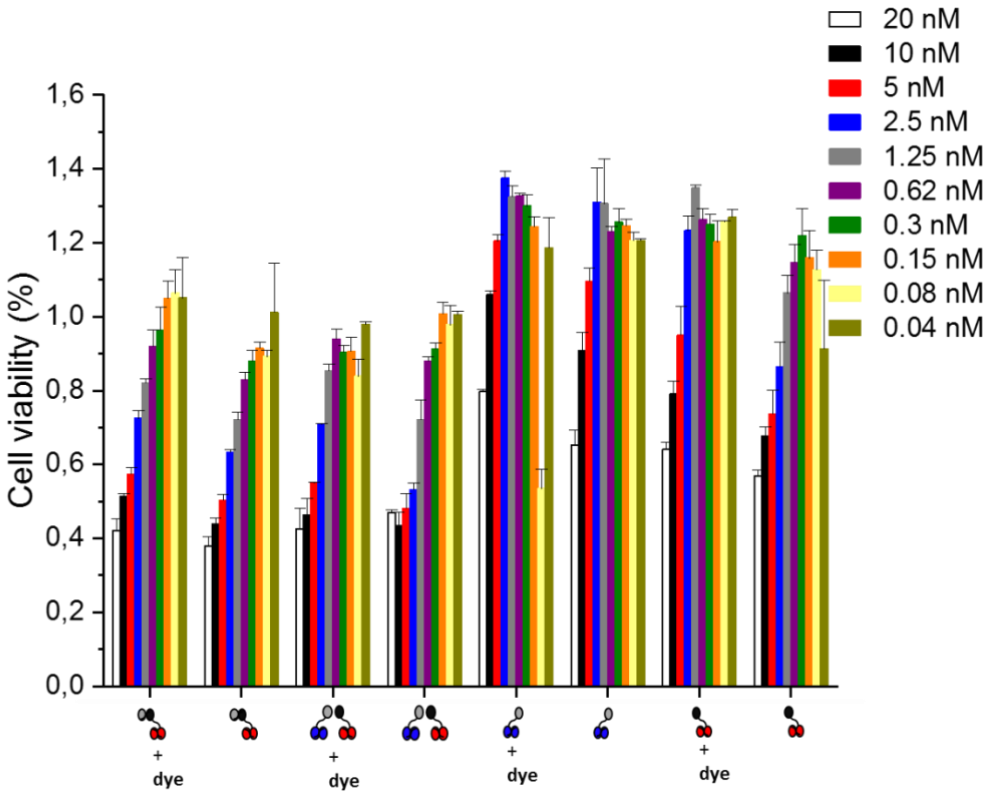

Figure 19: Cytotoxicity mediated by labeled and unlabeled complementary hemibodies VHαCD3-scFvαCD45 x VLαCD3-scFvαHLA-A2, BiTE scFvαCD3-scFvαHLA-A2 (positive control) and single hemibodies. A mixture of HLA-A2- and CD45-expressing fluc-positive THP-1 and HLA-A2-negative PBMCs were incubated with titrated constructs (20 – 0.04 nM) with two-fold dilution steps, (E: T ratio of 5:1). After 16 h, the specific substrate D-Luciferin was added to the cells. The cell viability was measured with Elisa reader after 16 h. Data are mean + SEM over 2 experiments.

4.3.2.2 The localization of hemibodies within the synaptic cleft

The tight binding of a T cell with an antigen-presenting cell (APC) is leading to the formation of an immunological synapse (IS), which consists of a central supramolecular activation cluster (cSMAC). It is the place where TCR binds to HLA-A2. Additionally, the downregulation of CD3 has been reported to occur in this region of the IS. cSMAC is surrounded by the peripheral cluster (pSMAC), and it is enclosed in turn by a further ring termed distal cluster (dSMAC). Proteins with a long extracellular domain such as CD45 phosphatase are observed to be located in dSMAC far away from cSMAC (Alarcon et al., 2011).

Our aim in this experiment was to study the immunological synapse mediated by hemibodies between T cells and target cells. Parallel to hemibodies, a BiTE antibody was used as positive control. The IS formation in the presence of BiTE has already been studied by Offner et al. (Offner, Hofmeister, Romaniuk, Kufer, & Baeuerle, 2006).

For the analysis of IS, hemibodies and BiTE were labeled with corresponding Alexa Fluor and incubated with THP-1 target cells to allow the binding of constructs to cells. Just before the microscopy, the preincubated mixture of target cells and labeled constructs were added to the Jurkat T cells, which have already been placed to the ibidi plate. The imaging was performed by laser scanning microscopy at RT without CO_2.

Given the observation, that CD45 is normally excluded from the cSMAC, in which HLA-A2 are located, our findings are very surprising. We found that complementary hemibodies against CD45 and HLA-A2 are collocated in the target cell-T cell interface. This colocalization was not in the cSMAC where CD3 triggering is happening, but in the periphery of the cell-cell interface (Figure 20 B). In contrast to the hemibody observation, in the synapse driven by the BiTE antibody, the HLA-A2 protein was localized in the middle of the cell-cell interface, as seen in typical synapse formation (Figure 20 A). To measure the colocalization of complementary hemibodies, a line was defined across the cell-cell interface and a plot profile was created using the ImageJ calculation program. The Plot profile presents a two-dimensional graph of the intensities of pixels along the selected line (Figure 20 A, B).

Furthermore, the target cell-T cell synapse was analyzed by confocal microscopy over 30 min period (Figure 20 C).

The target cell-T cell conjugates were grouped into two groups: stable and dynamic, based on the stability of the synapse. The resulted synapse in the presence of complementary hemibodies is dynamic, and target cell-T cell contact is not as tight as cell-cell contact promoted by BiTEs, although BiTEs induce a stable synapse between the cells. This observation is represented as a graph in Figure 20 C, which indicates the percentage of stable and dynamic rings in the contact zone in the presence of corresponding constructs.

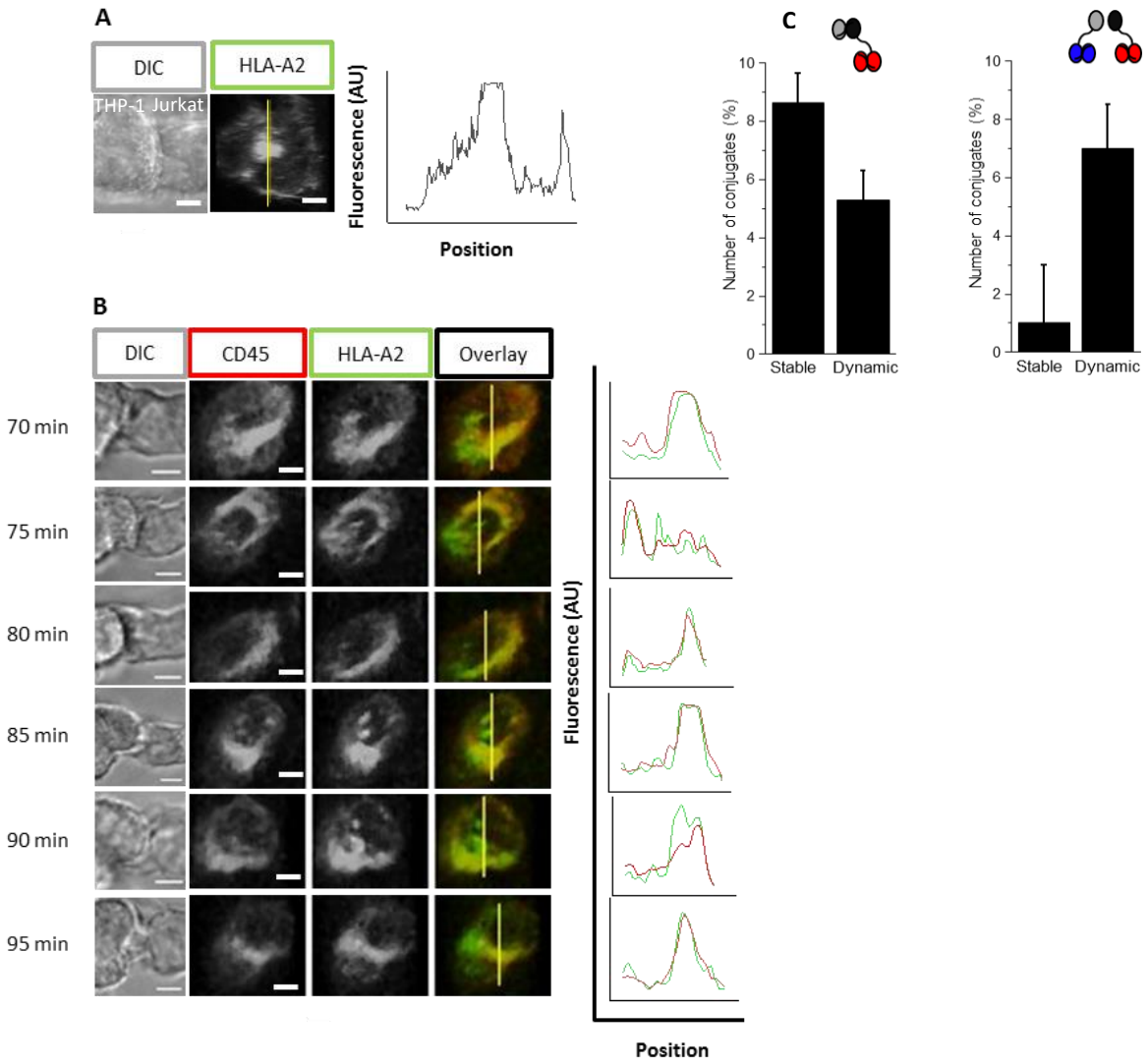

Figure 20: Representative confocal pictures of the interface between a THP-1 target cell and Jurkat T cell, in the presence of the indicated fluorescently labeled A) DIC; gray, scFvαCD3-scFvαHLA-A2; green (BiTE); and B) complementary hemibodies, DIC; gray VHαCD3-scFvαCD45; red, VLαCD3-scFvαHLA-A2b; green; The preincubated THP-1 target cells with 3 µg/ml Alexa Fluor labeled constructs were added to the Jurkat T cells, and the localization of labeled hemibodies in the cell-cell interface of the conjugates was analyzed using confocal microscopy. **A)** Clustering of HLA-A2 molecule bound to scFvαCD3-scFvαHLA-A2 in the middle of the cell-cell contact zone. The line profile across the cell-cell interface is shown on the right side**. B)** The images from one target cell-T cell conjugate over time (from 70 min. after initiation of cell-cell interaction for 95 min.) using hemibodies against CD45 and HLA-A2. The graphs show the relative fluorescence intensity of the complementary hemibodies VLαCD3-scFvαHLA-A2 (green) and VHαCD3-scFvαCD45 (red) at the yellow line in the cell-cell interface. For 3D projection, 8-bit Z-stack images were processed by maximum intensity projection. Images are shown as RGB images (8-bit per color channel). Scale bars, 5 µm in length. **C)** Characterization of conjugate type over 30 min by confocal microscopy. The data are calculated from three individual experiments + SEM.

4.3.2.3 ZAP70-GFP translocation to the cell membrane in response to stimulation

To confirm that hemibodies can trigger T-cell receptor signaling in stimulated T cells, we analyzed the translocation of labeled ZAP70 in Jurkat T cells by microscopy.

ZAP70 is a non-recptor phosphotyrosine kinase playing an essential role in the initiation of TCR signaling. Upon T cell receptor activation with peptide on HLA-A2 on APCs, the phosphorylated CD3ζ chain recruits ZAP70 from cytoplasm to the cell membrane. Upon association of ZAP70 to ITAM motif of CD3, ZAP70 changes its conformation and is finally phosphorylated by LCK. This step led to increased kinase activity of ZAP70. Activated ZAP70, in turn, induces the activation of many downstream signals (Wang et al., 2010).

For detection of ZAP70 with microscopy, THP-1 target cells were incubated with 3 µg/ml labeled complementary hemibodies, or BiTE or single hemibodies and just before microscopy; they were added to transfected Jurkat cells expressing a ZAP70-GFP fusion protein. Interestingly, in the cells stimulated with hemibodies, ZAP70 did not translocate completely to the cell-cell interface. In contrast in cells treated with BiTE, the ZAP70 translocation can be seen in the middle of the cell-cell interface (Figure 21 A, B).

The Figure 21 C indicates normalized fluorescence mean intensity of the ZAP70 GFP recruited to the cell-cell interface over 33 min. For this measurement, the cell-cell interface was defined by a line. The fluorescence intensity across the selected line was measured using the function, time Series Analyzer V2.0 over 33 min with the ImageJ program. For normalization, the average fluorescence intensity of the background was subtracted from the average fluorescence intensity of the ZAP70 GFP positive cells. The intensity of ZAP70 increased over time in the presence of BiTE until the time point 29 minutes. After reaching a plateau, the signal decreased. In the cells stimulated with complementary hemibodies, the signal shows an unstable course. In the presence of individual hemibodies, no clear ZAP70 signal could be detected. These observations are in agreement with the results from IS microscopy. In summary, we were able to show that in contrast to expected translocation of ZAP70 from cytoplasm to the cell membrane in the presence of BiTE, complementary hemibodies induce an impaired translocation.

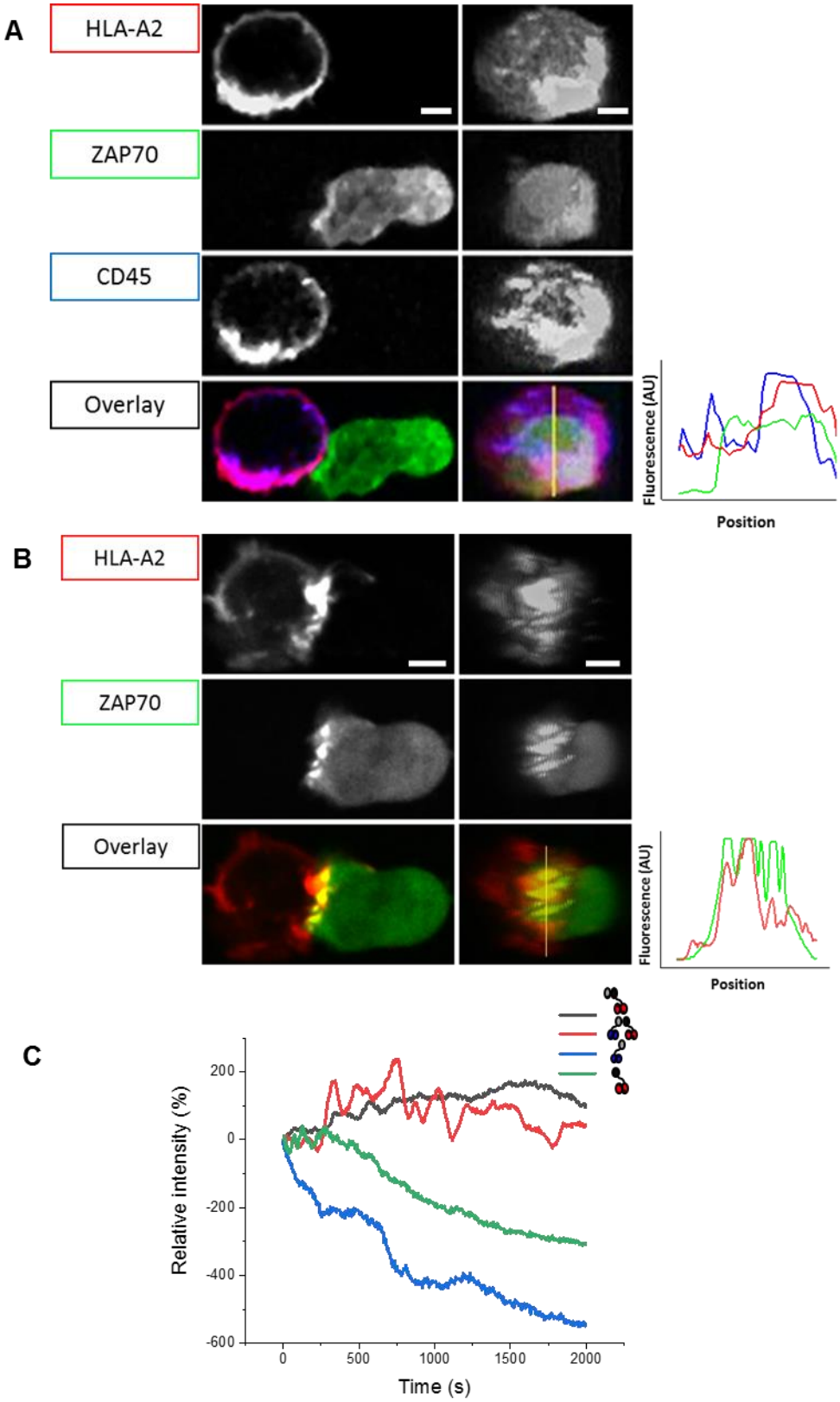
A
HLA-A2
ZAP70
CD45
Overlay
Fluorescence (AU)
Position
B
HLA-A2
ZAP70
Overlay
Fluorescence (AU)
Position
C
Relative intensity (%)
200
0
-200
-400
-600
0
500
1000
1500
2000
Time (s)

Figure 21: Representative confocal images of ZAP70-GFP (green) recruitment at the THP-1 target cell-Jurkat T cell interface mediated by A) fluorescently labeled complementary hemibodies, VHαCD3-scFvαCD45; blue, VLαCD3-scFvαHLA-A2; red and B) scFvαCD3-scFvαHLA-A2; red (BiTE). The expressing CD45 and HLA-A2 THP-1 target cells were incubated with 3 µg/ml of each respective constructs and directly before microscopy were added to the ZAP70-GFP positive Jurkat cells. **A)** The left pics present the recruitment of ZAP70 (green) at the THP-1-ZAP70GFP positive Jurkat cell conjugate interface mediated by complementary hemibodies CD45 (blue) and HLA-A2 (red). The two different pictures show two different views of the same cell cell conjugates. The overlay image shows the cell-cell interface at which the intensities of labeled CD45, HLA-A2, and ZAP70 proteins were measured. A line was used to measure the cell-cell interface (yellow line). **B)** The translocation of ZAP70 to the cell membrane of Jurkat T cells stimulated with the scFvαCD3-scFvαHLA-A2; red (BiTE). 3D projection was created by the maximum intensity projection of 8-bit Z-stack images. Images are shown as RGB images (8-bit per color channel). Box color indicates the overlay image. Scale bars, 5 µm in length. **C)** Quantification of ZAP70 intensity across a selected line (not shown here) in the conjugate interface over 2000 sec (s). Data are presented as the normalized mean over three experiments, with two cells each.

4.3.3 The transient increase of intracellular Calcium in response to stimulation

Oscillations of cytosolic Ca^{2+} concentration is important for T cell activation. Repetitive exchanges of Ca^{2+} between the endoplasmic reticulum (ER) and the cytosol led to the oscillatory spikes (Wacquier, Combettes, Van Nhieu, & Dupont, 2016). The fluctuating cytosolic Ca^{2+} levels after T cell activation is referred to as Ca^{2+} signals. These signals have a critical impact on a variety of intracellular T cell processes (Scharenberg, Humphries, & Rawlings, 2007).

Due to the important role of Ca^{2+}in the downstream signaling process of TCR, we measured Ca^{2+} alterations over time in the stimulated cells with complementary hembodies, BiTE as positive control and single hemibodies serving as negative control (Figure 22).

The quantification of intra cellular Ca^{2+} was performed with different methods, including flow cytometry (not shown in this work) and Fluorescence microscopy.

For microscopy, the measurement was done as follows: The attached Jurkat T cells on cover glass were loaded prior to calcium imaging with the cytoplasmic calcium indicator Oregon Green 488 BAPTA-1 solution. For the induction of calcium flux, the preincubated THP-1 cells with constructs were directly added to labeled Jurkat cells during imaging. The changes in Ca^{2+}signal was evaluated by time Series Analyzer from ImageJ program and Calculated by this formula: ΔF (F-F0)/F0 where F is the subtraction of every Ca^{2+}signal from the background signal. F0 is the average of all the signals started from the time point 0, until the beginning of the stimulation. The final calculation concentration was normalized by subtraction of the calculated Ca^{2+}signal of the control (THP-1 cells without stimulator) from the THP-1 cells with stimulator.

After the addition of stimulator at the time point 30 s, a clear rise of the signal in the presence of BiTE could be measured. We were able to detect 20 s before adding the stimulators, a small fluctuation of the cytoplasmic calcium levels. This may be due to the unspecific activation of Jurkat cells by contact with the tip of the pipette. In contrast to BiTE, in the presence of both hemibodies only a minimal increase in cytoplasmic calcium could be detected (Figure 22). Taken together, BiTE construct induces the highest intracellular calcium flux in Jurkat T cells, while complementary hemibodies promote more or less an impaired calcium flux in the cytoplasm. Single hemibodies cause even a decrease in the amount of intracellular calcium, which might be more an experimental artifact based on the observation that the addition of THP-1 cells without any stimulator induces a decrease in intracellular calcium amount as well.

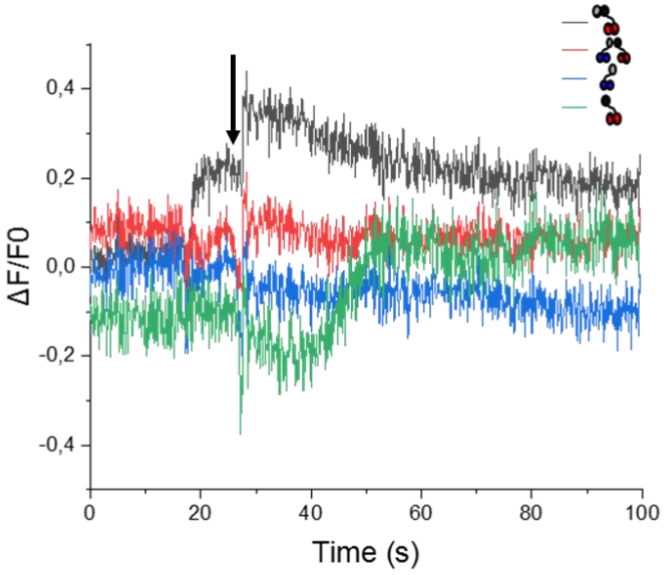

Figure 22: Response of Jurkat T cell calcium signal to combination of hemibodies, VHαCD3-scFvαCD45 x VLαCD3-scFvαHLA-A2; red compared to BiTE scFvαCD3-scFvαHLA-A2 black (positive control) and single hemibodies VHαCD3-scFvαCD45; blue and VLαCD3-scFvαHLA-A2; green. The preincubated THP-1 cells with 20 nM of each respective constructs were given to the stained Jurkat cells with cytoplasmic calcium indicator Oregon Green, and the increase of intracellular calcium was measured by microscopy. The arrow points to the time point of the stimulator addition. Represented are the relative changes in Ca^{2+} evoked by the addition of constructs expressed as ΔF/F0 as a function of time. Data are generated as a mean + SEM from three experiments, each experiment 20 cells.

4.3.4 CD3 epsilon/gamma down regulation as a termination signal

Central supramolecular activation cluster (cSMAC) has been reported to be important for termination of TCR signaling, where CD3 will be degraded, resulting in its downregulation (Varma, Campi, Yokosuka, Saito, & Dustin, 2006). Therefore, we wanted to analyze the CD3 downregulation after construct activation of T cells.

For this purpose, a mixture of HLA-A2$^-$ CD3$^+$PBMCs and THP-1 target cells were stimulated with hemibody according to the caspase assay (see section 3.2.3.4.1) and the quantification of CD3 downregulation was performed by flow cytometry (Figure 23 A). To ensure that the CD3 downregulation is a consequence of construct stimulation and is not due to the covering of CD3 molecules by constructs, the same experiment was performed in the presence and absence of BiTE antibody side by side (Figure 23 B).

The highest CD3 downregulation could be observed at the highest concentration of BiTE antibody or combination of hemibodies used. At this concentration more than half of the CD3 molecules were downregulated. As expected, single hemibodies did not cause CD3 downregulation. Only for the single hemibody against CD45, we observed at the highest concentration a small effect on CD3 expression (Figure 23 A).

In summary, the T cells stimulated with BiTE at 20 nM, showed the highest CD3 downregulation followed by stimulation with BiTE at 4 nM and complementary hemibodies at 20 nM. The individual hemibodies are not able to induce significant CD3 downregulation.

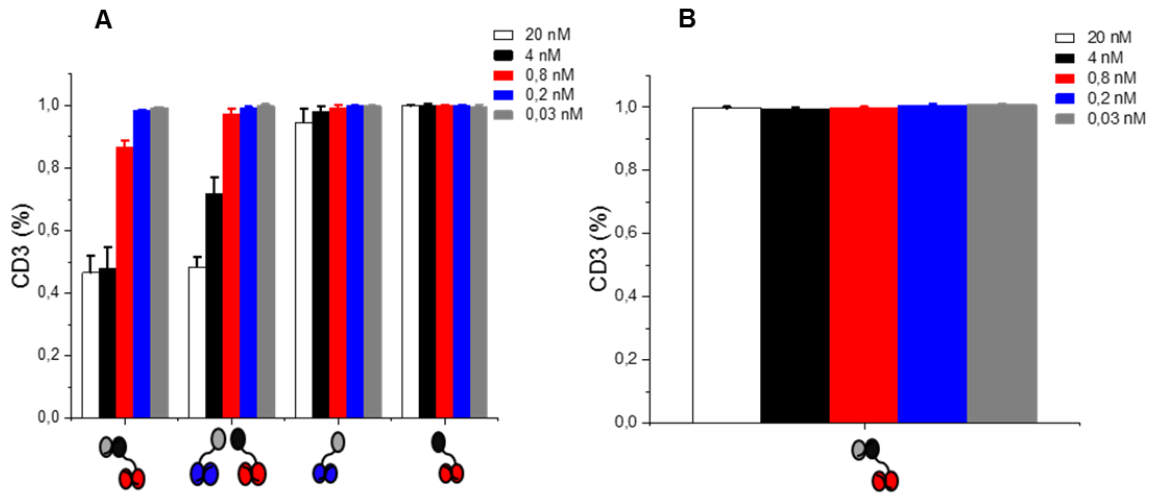

Figure 23: Downregulation of CD3 epsilon molecule of CD3+ HLA-A2-negative PBMCs upon stimulation by hemibodies VHαCD3-scFvαCD45 x VLαCD3-scFvαHLA-A2, scFvαCD3-scFvαHLA-A2 BiTE, and single hemibodies. A) Titrated constructs (20 – 0,03 nM) with 5 dilution steps were added to a mixture of HLA-A2 and CD45-expressing THP-1 target cells and CD3+ HLA-A2-negative PBMCs (E: T ratio of 5: 1). The amount of CD3 epsilon was quantified after 16 h using a flow cytometer. **B)** Equivalent to A) only with the difference that the measurement was performed in the absence of THP-1 target cells. Data are normalized mean + SEM over three experiments.

4.3.5 Release of Perforin in the synapse cleft

Perforin is a cytolytic protein from lytic granules released in the cell-cell interface. Perforin is taken up by target cells and is polymerizing the target cell membrane to form ring-like structures with a central pore (Millard, Henkart, Reynolds, & Henkart, 1984).

To measure the amount of released perforin in synapse cleft between THP-1 target cells and HLA-A2- CD3+ PBMCs treated with BiTE or hemibodies, we used an ELISA kit according to the manufacturers protocol.

The experimental setup was done as described in the caspase assay (see 3.2.3.4.1). After a 16-hour incubation of cells with stimulators, the supernatant was collected to measure the perforin concentration using the ELISA Kit. For normalization, the amount of released perforin in the unstimulated cells was subtracted from that of construct-stimulated cells.

Surprisingly, in contrast to higher caspase activity promoted by hemibodies compared to BiTE (Figure 25), released perforin from hemibody stimulation is much lower compared to BiTE antibody stimulation. While BiTE induces a perforin secretion of approximately 600 pg/ml at 20 nM at the highest concentration, complementary hemibodies led to secretion of only 200 pg/ml at the same concentration. The BiTEs and hemibody induced perforin release was concentration-dependent. There was no detectable perforin release at low hemibody concentration of 0.8 nM and 0.2 nM. Single hemibodies were not able to induce perforin release in the cell-cell interface (Figure 24).

In conclusion, BiTE induced the highest perforin release in the synapse cleft compared to complementary hemibodies.

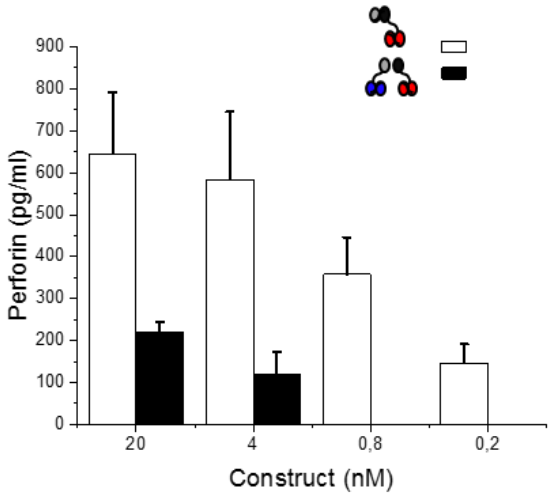

Figure 24: Perforin release induced by hemibodies VHαCD3-scFvαCD45 x VLαCD3-scFvαHLA-A2, scFvαCD3-scFvαHLA-A2 BiTE. A mixture of HLA-A2 and CD45 expressing THP-1 target cells and CD3+ HLA-A2-negative PBMCs were incubated with titrated constructs (20 – 0,03 nM) with dilution steps of 5 and an E: T ratio of 5: 1. After 16 h, the supernatant was tested for released perforin concentration by ELISA according to the manufacturer's protocol. The experiment was performed in triplicate. Data are presented in mean + SEM.

4.3.6 Activation of caspases 3/7 in target cells

To analyze if hemibody mediated target cell killing is mediated via the caspase pathway, we used a fluorescent based caspase assay. In this assay a caspase-3 specific substrate with fluorogenic DNA dye and a DEVD substrate was used. After cleavage of the non-fluorescent and non-functional substrate by caspase-3 in the cytoplasm, the substrate forms a high-affinity DNA dye that labels the nucleus bright green. The caspase activity was evaluated by quantification of bright green apoptotic cells by flow cytometry. Caspases are a member of the protease family and play an essential role in the breakdown of the cytoskeleton and the nuclear membrane as well as fragmentation of DNA during the apoptosis process (Russell & Ley, 2002).

For analysis of caspase activity in target cells, complementary hemibodies or BiTE were titrated from 0.03-20 nM and added to a mixture of CD45 and HLA-A2 expressing THP-1 target cells with HLA-A2- CD3+PBMCs at an E: T ratio of 5: 1. Single hemibodies were used as negative control and BiTE HLA-A2 as positive control. The mixture of cells and stimulators were incubated for 16 h under cell culture conditions. The caspase activity was measured after 30 min and 16 h.

BiTEs and complementary homebodies showed similar caspase activity on PBMCs in a concentration-dependent manner (Figure 25). Stimulation of HLA-A2- CD3+PBMCs with the highest concentration of BiTEs and hemibodies led to significant caspase activation in target

cells after 16h. Already after 30 minutes, a low caspase activity could be detected in stimulated cells with BiTE. The highest caspase activity was detected with complementary hemibodies at 20 nM. As expected, single hemibodies, used as negative control, indicate nearly no stimulatory effect on T cells (Figure 25 A).

To analyze if the caspase activity was influenced by the ratio of the two complementary hemibodies, we analyzed the caspase activity under conditions were one hemibody was kept constant, and the concentration of complementary hemibody was reduced in a concentration-dependent manner (Figure 25 B,C). In this assay the concentration of the constant hemibody stayed at 20 nM, and the concentration of the complementary hemibody was decreased in a titration series from 20 nM to 0.03 nM. BiTE with the same titration manner as the experiment A was served as a positive control. Surprisingly, after 16 h, in the setting were the concentration of the VHαCD3-scFvαCD45 hemibody remained constant and the VLαCD3-scFvαHLA-A2 hemibody was titrated in a concentration-dependent manner, the decline of caspase activity from 20 nM to 4 nM was very small (Figure 25 B). Interestingly, when the hemibody VLαCD3-scFvαHLA-A2 was kept constant, and the hemibody VHαCD3-scFvαCD45 was titrated, the caspase activity was still higher compared to BiTE (Figure 25 C).

In summary, the highest concentration of complementary hemibodies mediated the highest caspase activity. As expected, single hemibodies were not able to induce caspase activity.

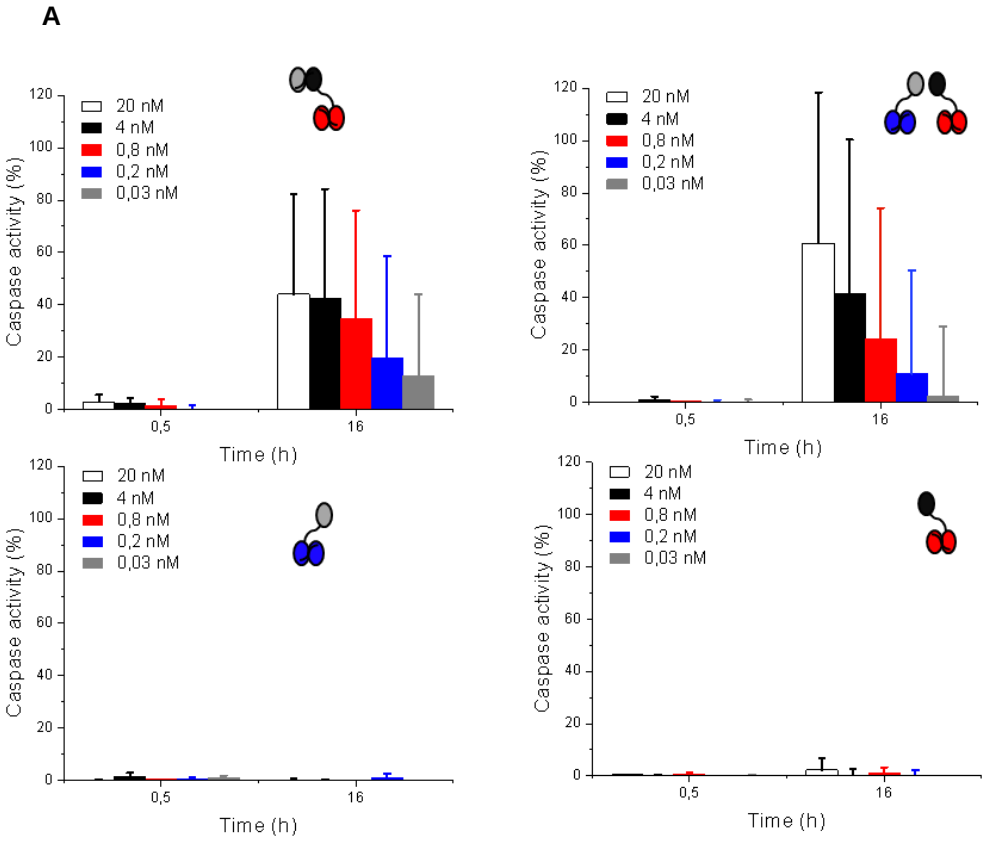

B

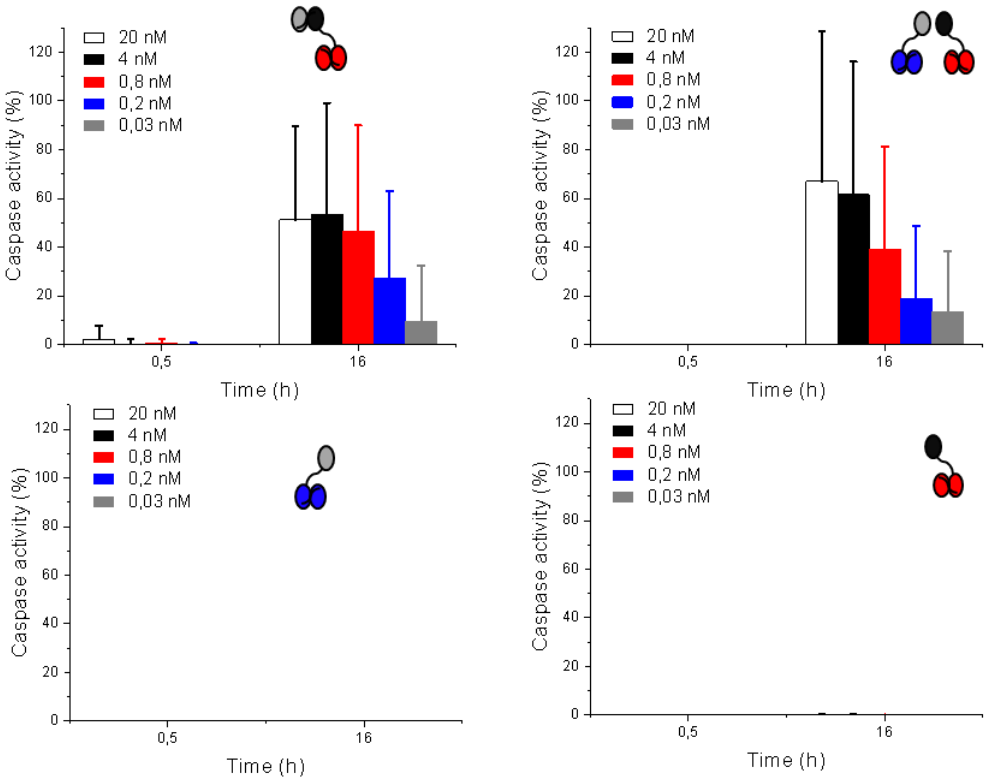
20 nM
4 nM
0,8 nM
0,2 nM
0,03 nM
Caspase activity (%)
Time (h)
0,5
16

C

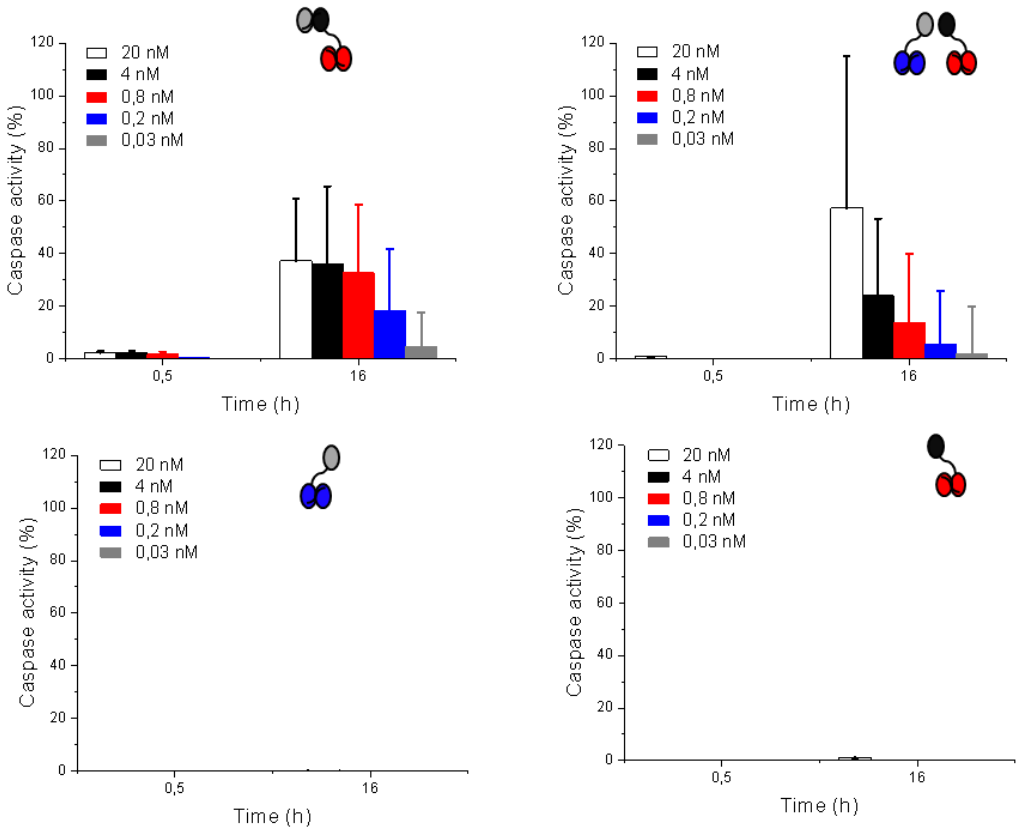
20 nM
4 nM
0,8 nM
0,2 nM
0,03 nM
Caspase activity (%)
Time (h)
0,5
16

Figure 25: Caspase 3/7 activity mediated by CD3+ HLA-A2- PBMCs stimulated with hemibodies VHαCD3-scFvαCD45 x VLαCD3-scFvαHLA-A2, scFvαCD3-scFvαHLA-A2 BiTE as positive control and individual hemibodies. The preincubated PBMCs with HLA-A2 and CD45 expressing THP-1 target cells in an E: T, 5: 1 ratio was added to the titrated respective constructs. After 0,5 h or 16 h, a caspase specific substrate was given to the mixture, and the reaction was measured by flow cytometer**. A)** To induce the caspase activity by complementary hemibodies, both of single hemibodies were titrated. **B)** In this experiment, the concentration of VHαCD3-scFvαCD45 hemibody was kept constant, and the concentration of VLαCD3-scFvαHLA-A2 hemibody was titrated. **C)** Concentration of hemibodies was opposite to B. Each experiment A), B), C) was performed three times. The data are presented as mean + SEM.

The same caspase specific substrate used in Figure 25 was used in time-lapse imaging of the caspase activity in target cells. In this experiment the preincubated target cells with hembodies or BiTE or single hemibodies, were mixed with HLA-A2- CD3+ PBMCs. For 30 min before time-lapse microscopy, a caspase substrate was added to the cell mixture. The experiment was repeated 3 times. However, due to the strong clustering of the cells, only one experiment could be evaluated for caspase activity. Caspase activity was detected by the presence of DNA-GFP in the nucleus resulted from the cleavage of caspase specific substrate by caspase enzyme. The caspase activity was measured using the Imaris program. The calculated sum of all of fluorescence signal intensities were divided by the sum of voxel numbers at each time point. Selected frames from a movie with a total length of 16 hours, are shown in Figure 26 A. In the presence of complementary hemibodies, the initiation of the caspase activity in THP-1 cells was detected after 130 min. The highest signal was observed at 150 minutes. At this time point, the cells swell the most. Afterward the cells shrank, and DNA degrade resulting in lesser fluorescence signal. Stimulation with BiTE induced caspase activity already after 105 minutes. However, the cell shrinkage occurred after 255 minutes. The Figure 26 B presents the course of caspase activity intensity over 16 hours., At the later time point, BiTE treated cells showed the highest caspase activity, whereas complementary hemibodies showed higher caspase activity at earlier time points . As expected, the single hemibodies showed no significant caspase activity.

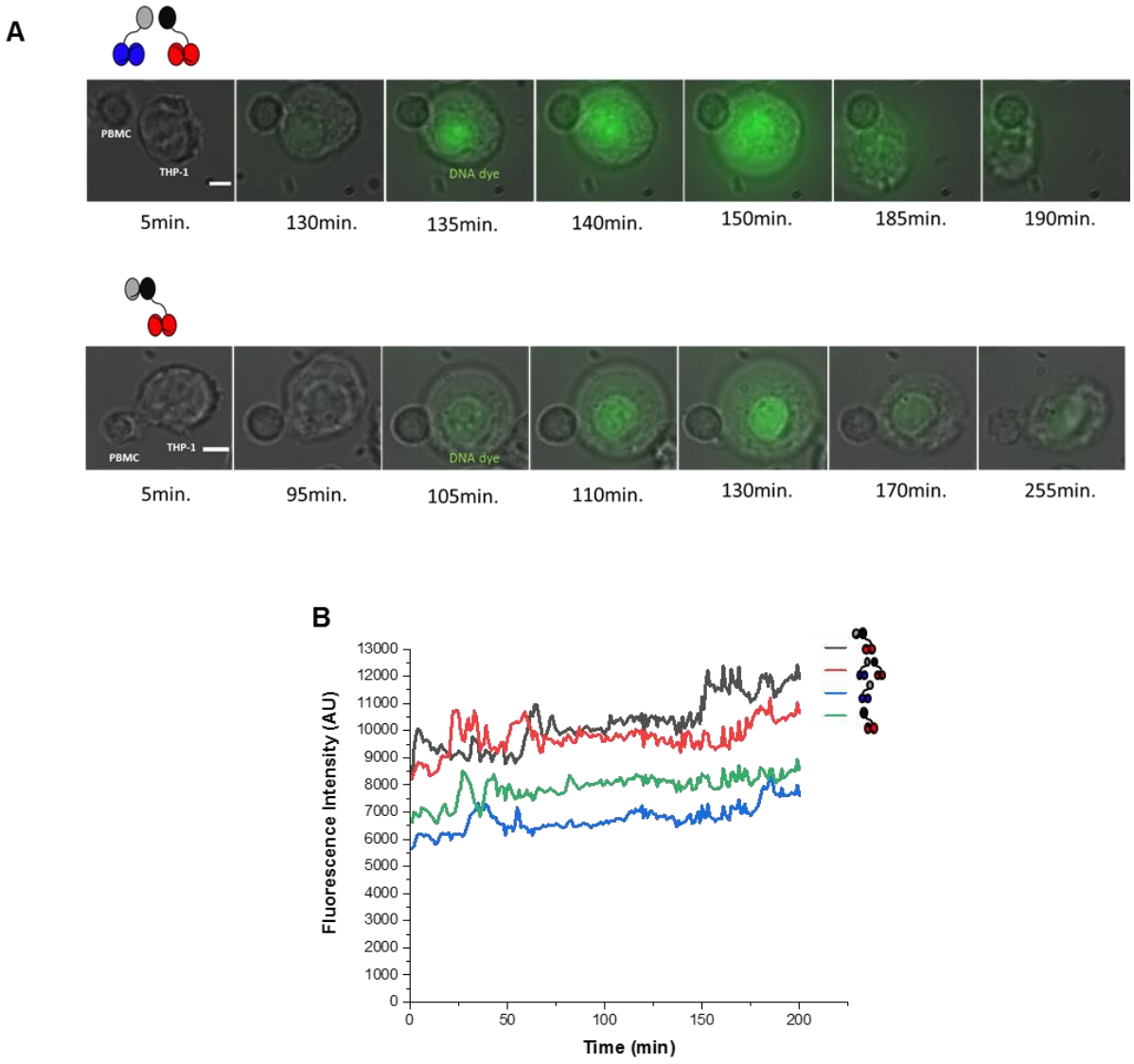

Figure 26: Representative frames from time-lapse movie tracking the Caspase 3/7 activity in the THP_1 target cell in the presence of construct activated-CD3+ HLA-A2-negtive PBMCs. T cell stimulation was achieved with hemibodies VHαCD3-scFvαCD45 x VLαCD3-scFvαHLA-A2, scFvαCD3-scFvαHLA-A2 BiTE as positive control and individual hemibodies. To stimulate the PBMCs just before microscopy, the preincubated THP_1 target cell with respective hemibodies were added to the PBMCs. To visualize the caspase activity process, the caspase specific substrate bound to a GFP DNA dye was added to the mixture. The cells were filmed for 16 h. **A)** Selected frames from the Caspase activity detected by the presence of GFP in the nucleus (green). Times are indicated in minutes **B)** Quantification of the fluorescence intensity in the term of caspase activity over 16 h. Data are calculated from one experiment. Scale bars, 5 µm in length.

4.3.7 Construct-mediated conjugation of target cells with T cells

To quantify, how many target cells and T cells are attached together by constructs, a conjugation assay was developed. For that, both THP-1 target- and Jurkat T cells were stained with fluorescent membrane dyes in green and red, respectively according to the kit. The stimulation procedure of the target cells was done as the same as the caspase assay. Finally, after different timepoints, ranging from 0.5 to 24 h, the amount of stimulator driven cell-cell conjugates identified as double-positive events, were measured using a flow cytometer. BiTE was served as a positive control and single hemibodies as negative control.

As demonstrated in the Figure 27, hemibodies induce the most conjugates in a concentration-dependent manner, with an increase over time. The highest percent of cell-cell conjugates in the presence of BiTE reached only 5%. Single hemibodies were not able to form cell-cell conjugates.

In summary complementary hemibodies are the most effective stimulator in the context of the number of conjugates after the first 30 min of the initiation of target cell-T cell contacts. The increase of complementary hemibody driven cell-cell conjugates was time and concentration dependent.

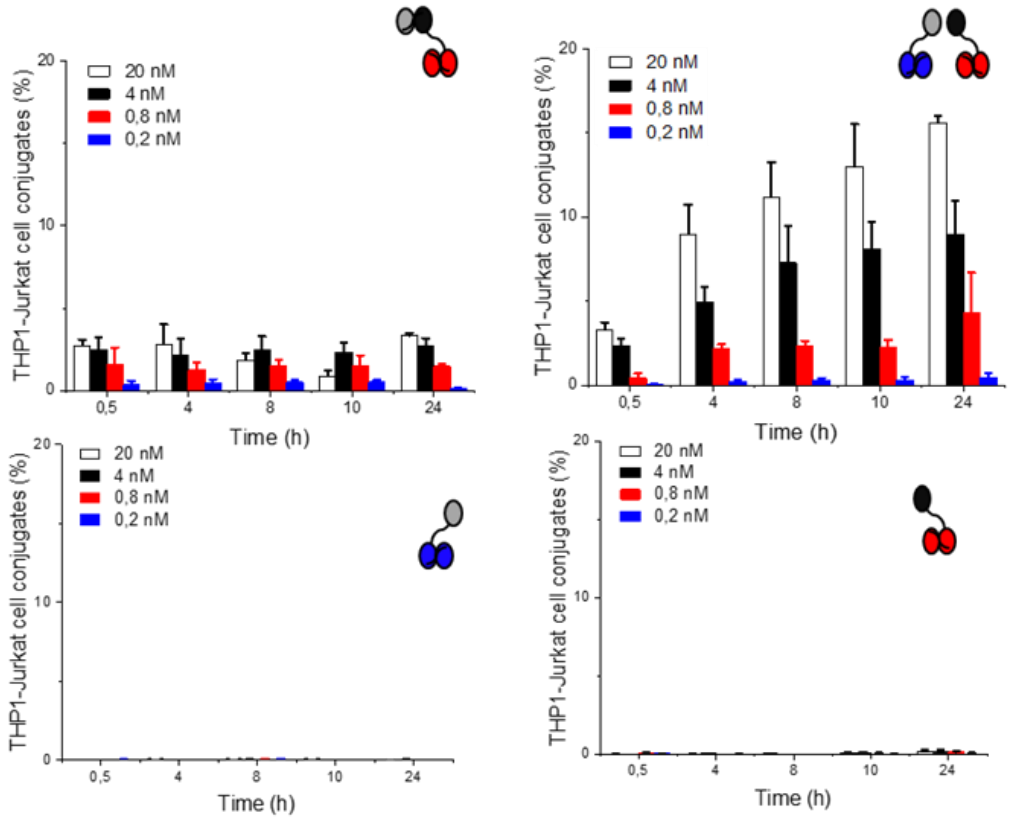

Figure 27: The hemibody-mediated conjugate formation between THP-1 target cell and Jurkat T cell. The quantification of conjugates driven by constructs over different time points. Constructs used were hemibodies VHαCD3-scFvαCD45 x VLαCD3-scFvαHLA-A2, scFvαCD3-scFvαHLA-A2 BiTE as positive control and individual hemibodies. Prior to the stimulation, THP-1 cells and Jurkat cells were stained with different dyes. The stained cells were mixed at a ratio of E: T, 5: 1. Titrated constructs (20 nM-0.2 nM) were added to the mixture. After each indicated time point, 0.5, 4, 8, 10, and 24 h, the percentage of cell conjugates was measured by flow cytometry. The data are presented as normalized mean of three experiments + SEM.

4.4 Binding Studies of recombinant Human CD3ge-hIgG4 protein and hemibodies

4.4.1 Interaction analysis between VHαCD3 and VLαCD3 domains of the hemibodies in the presence of recombinant CD3 molecule

To test whether soluble complementary hemibodies are able to bind the CD3 molecule in the absence of target cells, we developed an Elisa assay, which is an adaption of Ueda Elisa (Ueda et al., 1996). For this purpose, VLαCD3-scFvαHLA-A2 was coated on the plate, and after incubation, a preincubated mixture of VHαCD3-scFvαCD45 with recombinant CDeg, which was coupled additionally with a hIgG4 was added to the plate. As control, the CD3

molecule alone without a second complementary hemibody VHαCD3-scFvαCD45 was added to the VLαCD3-scFvαHLA-A2 on the plate. For analysis of scFvαCD3-scFvαHLA-A2 interaction with soluble CD3 molecule, BiTE was incubated on the plate, and subsequently CD3 molecule was added. The detection of CD3 molecule in all experiments was performed by the addition of HRP labeled anti hIgG4 to the plate. If the CD3 is bound to an interaction partner on the plate, it will not be removed by washing and will be detected.

To calculate the K_D-value (Dissociation constant), the parameters of recorded absorbance in 450 nm as y and increasing concentration of CD3 eg molecule as x were fitted using an analytical model: y = X / (P1 + X). P1 is equal to the K_D-value.

The binding curve of complementary hemibodies and CD3 molecule reached the saturation at about 40 nM of CD3 (Figure 28 A), while the binding curve of BiTE to CD3 molecule reaches at a higher CD3 concentration the saturation (Figure 28 B), pointing out to a higher Kd value and more pure binding in the absence of the cells. As expected, in the killing specific concentration range, no binding of soluble reaction partner with CD3 molecule could be measured.

In conclusion, only at high concentration out of therapeutic range, the complementary hemibodies are able to bind the CD3 molecule in solution. The single hemibody VLαCD3-scFvαHLA-A2 is not able to bind to CD3 alone (Figure 28 C).

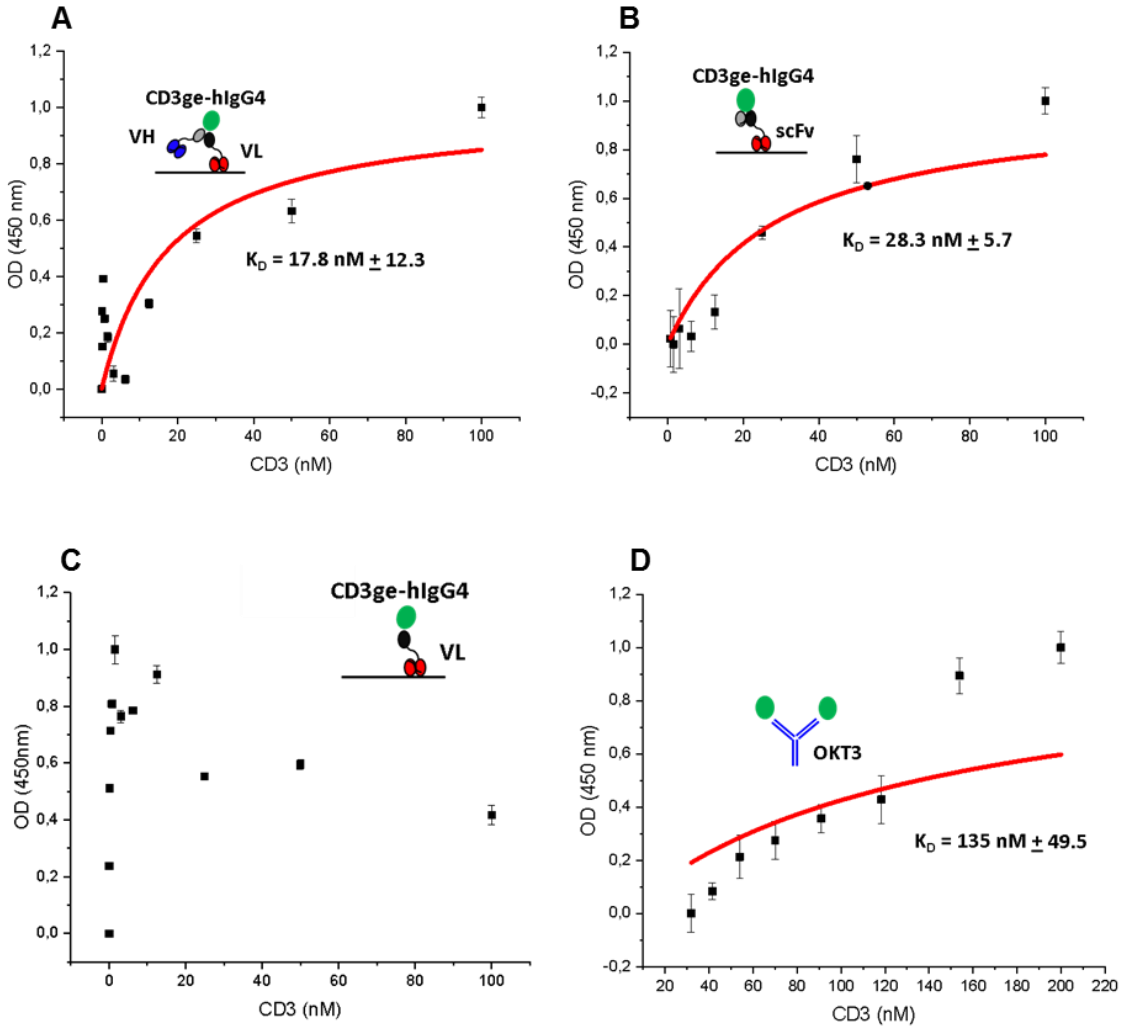

Figure 28: Study of the interaction of hemibodies with the Human CD3ge-hIgG4 molecule. A) The interaction of approx. 1000 nM immobilized hemibody VLαCD3-scFvαHLA-A2 on the plate with a soluble mixture of approx. 1000 nM VHαCD3-scFvαCD45 and titrated CD3 eghIgG4 (100 - 0.05 nM) (1 : 2 dilution steps) was detected. The measurement of interaction was achieved by the detection of hIgG4 using a dye reaction of HRP conjugated anti hIgG4 antibody with TMB substrate. **B)** The binding of approx. 311 nM immobilized scFvαCD3-scFvαHLA-A2 BiTE to the CD3 eg hIgG4 (100 – 0.8 nM) (1 : 2 dilution steps). **C)** To control whether a single hemibody is able to interact with CD3 molecule, equal to A) the same concentration of VLαCD3-scFvαHLA-A2 was immobilized on the plate, but soluble CD3 eghIgG4 alone was added to the plate. **D)** As positive control, the binding of approx. 17 nM immobilized OKT3 to the soluble titrated CD3eghIgG4 (200 – 32 nM) (1: 1.3 dilution steps) was measured. In B), C) and D), the detection was performed equal to that of A)**.** The data are presented as normalized mean of three experiments + SEM.

5 Discussion

This work presents the biochemical and functional characterization of a new format of dual antigen restricted T cell engaging antibodies. The so-called hemibody technology was originally investigated in the context of an HLA-mismatched allogeneic stem cell transplantation model for acute myeloid leukemia (AML). The hemibody format consist of two single-chain polypeptides, each composed of an antigen binding single chain variable fragment (scFv1 or scFv2) fused to either the variable heavy (VH) or the variable light chain (VL) domain of a T-cell activating anti-CD3 antibody.

Each of these polypeptides is a hemibody. Once the individual hemibodies bind to their respective target antigen, the V_H and V_L domains become aligned and re-associate subsequently to reconstitute the original CD3-binding site. This way, CD3-positive T lymphocytes become activated and retargeted for target cell destruction. The complementation of the hemibodies brings the target cell and T cell into close proximity resulting in initiation of an immunological synapse (IS) in the cell-cell interface. The T cell activation is initiating specific downstream signaling events in the T cell including calcium flux in the T cell cytoplasm and secretion of cytolytic effector molecules, as well as specific signaling events in the target cell including caspase activation.

In this work hemibodies were used directed against the pan-hematopoietic lineage marker CD45 and the human leukocyte antigen-serotype HLA-A2. The dual hemibody strategy was evaluated by comparing it to classic bispecific BiTE antibody targeting HLA-A2. Since the hemibody mediated T cell activation is mediated by complementation of two individual hemibodies, we used single hemibodies as controls.

Different bispecific antibody (bsAbs) formats are currently in clinical trials or are already approved for therapy. Among the different formats, the bispecific antibodies retargeting CD3 positive T cells for target cell destruction gained attention in 2018 due to the accelerated United states Food and Drug Administration approval of blinatumomab (Blincyto, Amgen Inc.) for the treatment of adult and pediatric patients with B-cell precursor acute lymphoblastic leukemia (Gokbuget et al., 2018). In contrast to regular IgG antibodies, containing a fragment crystallizable region (Fc) and thus having a long serum half-life of days to weeks, BiTE molecules lack the Fc region. Without the Fc region their molecular weight is small around 55 kDa. The small size improves their capability to infiltrate solid tumors (Kontermann & Brinkmann, 2015). In contrast to classic IgG antibodies, which induce target cell destruction via complement activation or activation of NK cells, the CD3 directed BiTE antibodies use the potential of T cells as effector cells (Loffler et al., 2000). Despite the first success of BiTE

antibodies in clinic, their use is restricted. One of the major limitations of bispecific antibodies is the lack of tumor-specific antigens. To overcome this limitation, hemibodies were developed. Hemibodies are able to retarget T cell mediated effector function towards a dual antigen signature in contrast to a single antigen. This dual antigen restriction gives the hemibodies an advantage over classic bispecific antibodies.

In this present study we investigated the dual antigen restriction of the hemibody technology by using hemibodies targeting CD45 and HLA-A2. The hemibody function depends on their ability to dimerize correctly with spatial organization of all three antigen-binding sites, and on the distribution of target antigens on the cell surface of the target cell (Banaszek A., 2013). The presence of both target antigens presented on the surface of the target cell is obligatory for the hemibody mediated T cell activation. To investigate the homebody activity against double antigen positive target cells in detail, VHαCD3-scFvαCD45 and VLαCD3-scFvαHLA-A2 hemibodies were produced. The antibody sequences from the anti-CD3 antibody diL2K was used (Brischwein et al., 2006), from a human anti HLA-A2 antibody (Watkins et al., 2000) and a murine anti CD45 antibody (Matthews et al., 1991).

Bluemel et al. has suggested that the potency of BiTE-mediated target cell lysis is influenced by epitope distance and antigen size. After testing a total of five BiTE antibodies and using a total of 14 different CHO target cell lines expressing distinct recombinant versions of MCSP and EpCAM antigens, they concluded that the more distant a BiTE antibody binds to the target cell membrane, the less is the stimulatory effect on the T cells (Bluemel et al., 2010).

According to these findings, the large size of the CD45 molecule makes it a challenging target in combination with the much smaller HLA-A2 molecule. The parental monoclonal antibody of scFvCD45, BC8 clon, can bind all CD45 isoforms and is most likely recognizing an epitope in the C-terminal part of the extracellular domain, expressed by all CD45 isoforms (McCall, Shotton, & Barclay, 1992). The size of the extracellular domain of the wild type CD45 protein is approximately 28 nm (McCall et al., 1992). In contrast to the CD45 molecule, the extracellular dimension of HLA-A2 molecule is only about 7 nm (Bjorkman et al., 1987). The anti scFvHLA-A2 clone used for the hemibodies recognizes the amino acid residues 142 and 145 located on the α2 domain of the heavy chain of the HLA class I molecule close to the peptide-binding cleft (Watkins et al., 2000). Not only the size of the target antigens is crucial, also the size of the activated T cell receptor complex (TCR) is important. The length of CD3ε is approx. 4 nm (Sun, Kim, Wagner, & Reinherz, 2001) and the entire TCR-peptide-MHC complex is approximately 14 nm in size (Garboczi et al., 1996). Based on the observation of Blumel et al, the size difference between two target antigens and the binding side of the targeting antibodies is crucial for the optimal cell-to-cell contact for T cell stimulation.

Therefore, to improve the linker between the antigen binding domain and the effector binding domain of the hemibodies, a flexible 7 amino acid long glycine-serine linker was inserted between the variable domains of anti-CD3 and the antigen binding scFv fragments (Figure 13) (Banaszek A. 2013).

Another important aspect for targeting large extracellular molecules such as CD45 with T cell activating antibodies concerns the kinetic segregation model (KS) (Davis & van der Merwe, 2006). The KS model postulates that steric effects derive the passive size-dependent exclusion of the large proteins such as CD45 working as an inhibitory phosphatase, from the contact area. This event is causing an increase of kinase activity, which in turn promotes the phosphorylation of pMHC-bound TCRs within the contact zone. These events subsequently lead to the initiation of receptor triggering and following downstream T cell receptor signaling (Davis & van der Merwe, 2006).

In summary the size of the target molecule is playing an essential role in the efficiency of synapse formation. Therefore we were interested in the formation of synapse promoted by VHαCD3-scFvαCD45 and VLαCD3-scFvαHLA-A2 hemibodies. For this study we analyzed the binding of labeled hemibodies to the target and effector cell. We also analyzed the translocation of ZAP70 from the cell cytoplasm to the cell membrane as a signal for the initiation of IS formation. We compared the IS formation driven by complementary hemibodies in contrast to a BiTE antibody mediated IS formation.

As described previously, important for the IS formation is the movement of receptors in the plasma membrane; the net charge of their intra cellular domains, mainly caused by phosphorylation and dephosphorylation of TCR domains, decides the further fate of the T cell activation. CD45 exclusion as inhibitory phosphatase from the middle of the IS contact zone, where TCR is located, to the periphery is one of these critical movements. Surprisingly, we observed that the binding of hemibodies to CD45 and HLA-A2 on the target cell led to their colocalization out of the cell-cell interface with the formation of a ring-shaped structure (Figure 20 B).

Based on the mechanistic concept of the hemibody technology, it is clear that the two fragments have to come into close proximity in order to reconstitute a functional CD3 binding site. In this context, the observation of the ring-shaped structure allows two assumptions: (i) the interaction strength of the VH and VL interface is strong enough to drag out and to relocate the HLA antigens from the center into the periphery of the synapse to pair with its partner, (ii) that CD3 molecules are activated in the pSMAC as evident by the atypically located recruitment of ZAP70. Surprisingly in this respect: it works even in the presence of the phosphatase CD45, which in many experimental setups exerts TCR/CD3 inhibitor functions (Furlan, Minowa, Hanagata, Kataoka-Hamai, & Kaizuka, 2014).

According to published data (Li et al., 2017) (James & Vale, 2012), the hemibodies are forming a suboptimal IS between the T cell and the target cell, which we referred to as an atypical synapse.

The co-localisation of the two molecules in the periphery may be explained by the size of the CD45 molecules, which is about 147 kD and spans over 50 nm. Given that the synapses averages 13 nm in the center, it appears consequent to re-locate the reconstituted complex into periphery, where sufficient space is prevalent.

In contrast to the atypical synapse formed by complementary hemibodies, we detected a typical synapse formed by the BiTE antibody scFvαCD3-scFvαHLA-A2 (Figure 20 A). As expected, labeled BiTE against HLA-A2 was detected in the middle of the cell-cell interface, forming a classical “bull’s eye” IS (Offner et al., 2006).

To confirm the BITE and hemibody induced recruitment of ZAP70 to the immunological synapse we used fluorescent tagged ZAP70 and microscopy (Figure 21).

Stimulation by complementary hemibodies, promoted a weak translocation of ZAP70 to the cell membrane. We observed ZAP70 to associate opposite to CD45 and HLA-A2 at the peripheral/distal SMAC after hemibody treatment, mirroring the ring shaped IS structure (Figure 21 A).

In contrast to hemibodies, BiTE induced synapses recruit ZAP70 mainly to the middle of the synapse (cSMAC). As can be seen in Figure 21 B, ZAP70 signal is mostly located in the cell-cell interface.

Measuring the ZAP70 signal across the contact zone of the cell-cell conjugates for the complementary VHαCD3-scFvαCD45 x VLαCD3-scFvαHLA-A2 hemibodies, the BiTE scFvαCD3-scFvαHLA-A2 and single hemibodies demonstrated a remarkable stable ZAP70 recruitment for BITEs and hemibody combinations. A high-level fluorescence intensity was detected for about 30 min (Figure 21 C).

These observations confirm again that ZAP70 recruitment to the cell-cell membrane in the presence of BiTE differs from that by complementary hemibodies.

To look closer for cell activation, we analyzed cytosolic calcium flux in the scFvαCD45 x VLαCD3-scFvαHLA-A2 hemibodies-activated T cells, compared to scFvαCD3-scFvαHLA-A2 BiTE and single hemibodies (Figure 22). During T cell activation, the interaction of a T cell with an antigen-presenting cell (APC) leads to recruitment and activation of ZAP70 and following activation of PLCγ1, which in turn, allows the release of intracellular calcium from the endoplasmatic reticulum (ER) store (Joseph, Reicher, & Barda-Saad, 2014). This transient cytosolic calcium increase occurs within the first seconds after engagement of the TCR. The

transient increase promotes rapid MTOC reorientation and F-actin rearrangement. These downstream events allow the formation of an IS within minutes. Furthermore, the rapid release of calcium from intracellular ER stores mediates the opening of calcium release-activated calcium (CRAC) channels, located in the plasma membrane. These channels allow a sustained influx of extracellular calcium across the plasma membrane in a process called store-operated calcium entry (SOCE). The SOCE is important for cellular calcium signaling and maintaining the cellular calcium balance. These events control TCR-dependent calcium signaling, which is crucial for correct T cell response (Joseph et al., 2014).

Interestingly, the BiTE antibody induced T cell activation showed a significant calcium flux increase. Whereas the complementary hemibodies showed an insufficient increase of cytosolic calcium. The single hemibodies had no significant change cytoplasmic calcium levels. In accordance with published data, that the rapid transient intracellular calcium increase is an indirect result from the engagement of ZAP70, it is most likely that the low transient calcium flux observed by complementary hemibodies T cell stimulation is caused from the impaired ZAP70 translocation. However, the low transient calcium flux under hemibody stimulation is enough for T cell activation (Figure 22), CD3 internalization (Figure 23 A), perforin secretion (Figure 24), and caspase activity in target cell (Figure 25).

When we looked at T-cell and target cell conjugates, formed by BiTE or hemibodies, we observed differences. It was surprising that complementary hemibodies induces a higher number of stable conjugates compared to BiTE antibody (Figure 27). Although it has to be noted that the measurement of conjugates was performed only in the first 30 min. after T cell activation, it is possible that cell cell conjugate formation is different at later time points.

The reason why hemibodies, with their atypical immunologic synapse, are building more cell conjugates is not clear. As described previously, F-actin regulation depends on intracellular calcium. It is possible that under hemibody induced low cytoplasmic calcium levels, the movement of ICAM-1 across the cell-cell interface is impaired, causing a decrease in cell conjugate disruption .

The downregulation of the CD3 epsilon/gamma chain is important for termination of T cell activation. Therefore, we investigated the effect of Hemibodies and BiTE antibody on the CD3 expression of effector cell (Figure 23). TCR downregulation happens in response to various stimuli like recognizing antigenic peptides displayed by MHC molecules, anti-TCR Antibody binding, or treatment of T cells with activators or protein kinase C (PKC). The regulation of TCR expression fulfills different functions at different stages of T cell ontogeny, including tolerance induction or T cell activation (Lauritsen et al., 1998).

The stimulation of $CD3_+$ T cells with complementary hemibodies at 20 nM led to CD3 downregulation, similar to BiTE antibody induced CD3 downregulation (Figure 23 A). However, at lower concentration the hemibody induced CD3 down regulatory is lower compared to the BiTE antibody. As expected, individual hemibodies could not induce CD3 downregulation, which is in line with the observation that single hemibodies alone are not able to activate T cells.

To measure hemibody-mediated cytotoxicity, we measured intracellular caspase-3/7 activation in target cells (Figure 25).

Caspases are proteases that cleave their target proteins at specific aspartate residues, resulting in the breakdown of the cytoskeleton and the nuclear membrane as well as fragmentation of DNA (Russell & Ley, 2002). We measured the caspase 3/7 activity by using a fluorogenic DNA dye bound to DEVD substrate specific for caspase-3. In line with hemibody induced formation of immunological synapse, ZAP70 translocation and intracellular transient calcium influx, the complementary hemibodies induced dose dependent caspase activity in the target cells, similar to the BiTE antibody group.

To look more in detail how hemibody activated T cells cause target cell killing, we analyzed the production of perforin after T cell activation. Hauff et al. (Hauff C., 2009) reported that Granzyme B is is important for BiTE-mediated killing of tumor cells. The penetration of granule proteases (granzyme B) into the target cell, requires pores in the membrane of the target cell. These pores are formed by the membrane-disruptive protein perforin (Voskoboinik et al., 2006). Therefore, we measured the amount of released perforin in the synapse cleft (Figure 24). The complementary hemibodies induced perforin production in a concentration-dependent manner. The perforin production was higher in the BiTE antibody group. Why BiTE antibody is inducing a higher perforin secretion is not clear.

A possible explanation for this observation is that the amount of released perforin does not correlate directly with caspase activity. We have data (Kouhestani et al., work in progress), using CD107a as a degranulation marker, indicating that hemibody induced T cell activation induce similar production of cytotoxic granules compared to BiTE. This observation is in line with Dustin & long et al, who reported that FasL is present in the granules of CTL that co-express perforin and granzymes and will be exocyted into the synaptic cleft in response to TCR triggering (Dustin & Long, 2010).

Also, it has been suggested that the formation of a tight contact area is critical for the cytoskeletal polarity and following the release of the cytotoxic agents such as perforin at the cell-cell interface. From our observation it is possible that a suboptimal cell-cell conjugation

characterized by loose contact zone, in the presence of complementary hemibodies is not suitable for the optimal release of perforin (Dustin et al., 1998).

As TCR/pMHC interactions mediate essential downstream signaling events for activation and differentiation of T cells, the understanding of the correlation between these molecular interactions plays an essential role in the characterization of hemibodies.

To quantify the interaction between THP-1 target cells and Jurkat T cells, we used a conjugation assay, measuring the cell-cell conjugates induced by complementary hemibodies or BiTE antibody at different time points (Figure 27). Complementary hembodies induce the highest percentage of cell conjugates. While the percentage of cell conjugates in the BiTE group was at all time points less than 5%, the percent of cell-cell conjugates formed by Complementary hemibodies constantly increase over 24 hours in a concentration-dependent manner with the highest value of approx.15%.

A prolonged or a very short TCR/pMHC interaction has been reported to correlate negatively with the T cell function, whereas intermediate TCR/pMHC interaction results in the most effective T cell function (Riquelme, Carreno, Gonzalez, & Kalergis, 2009). In contrast to these reports, our data show that complementary hemibodies despite a prolonged and time-dependent increase in cell conjugates, are able to mediate even a higher caspase activity at the highest concentration in comparison to BiTE antibody. A possible reason for these differences is the difference of their kinetic. Since the kinetic of BiTE-mediated TCR triggering is much faster than that of complementary hemibodies, the CD3 downregulation and thus termination of the TCR signaling is much faster in the presence of BiTE resulting in dissociation of cells after a short time. On the contrary, in the presence of hemibodies, the T cell activation events, including IS formation, ZAP70 activation, and calcium influx occurs substantially slower. Therefore, it is possible that more cell conjugates and thus more engaged T cells are causing higher cytotoxicity by hemibodies. Another possible explanation for the described observation is provided by the study from Hoffman et al. who showed that a bispecific antibody of the BiTE class can sustain multiple rounds of target cell lysis by T cells and that T cells in the presence of BiTE remain highly motile avoiding clusters of T and target cells (Hoffmann et al., 2005).

Another explanation is coming from the concept of kinetic proofreading, which plays a role for T cell receptor signaling that can distinguish between agonist and endogenous ligands. Important here is the duration of engagement of TCR to the pMHC. The ligand that stays bound longer is more likely to complete the T cell activation cascade (Chakraborty & Weiss, 2014). According to this model, it is possible that in the presence of complementary hemibodies with slower kinetic compared to BiTE, the two cell populations stay longer bound together and have more time to complete the downstream signaling cascade.

For the complementary nature of the hemibodies it is important that first both respective hemibodies have to bind to their target antigens on the same target cell and in a second step the split anti CD3 domains reconstitute the functional anti-CD3 binding site for redirecting T cells.

If a cell expresses only one target antigen, only one hemibody will bind and the complementary hemibody will be free in the solution. In this situation, one hemibody bound and one not bound, hemibodies lack high enough avidity to reconstitute the split anti CD3 domains. To test this, we developed an Elisa assay based on the open sandwich ELISA from Ueda et al. Ueda developed a specific ELISA to determine whether the stability of the VL-VH association can be enhanced by antigen (Ueda et al., 1996).

In our assay, we analyzed the binding of a hemibody pair to recombinant CD3 eg/ IgG4 under condition, by which one hemibody was attached to the plate served as an artificial surface and the other hemibody was in the solution (Figure 28 A). For this purpose, VLαCD3-scFvαHLA-A2 was immobilized on the plate, and a mixture of VHαCD3-scFvαCD45 with CD3 eg/ IgG4 was added to the plate. The binding of the CD3 eg/ IgG4 to the immobilized hemibody was measured using an anti-IgG4HRP labeled secondary antibody. The control reaction was set up that to the immobilized VLαCD3-scFvαHLA-A2, only CD3 eg/ IgG4 alone was added. The interaction of an immobilized BiTE with CD3 eg/ IgG4 in the solution was performed as the positive control. We found that split anti CD3 from complementary hemibodies binds CD3 eg/ IgG4 molecule at a Kd value of 17.8 nM while BiTE binds the CD3 molecule at a higher Kd value of 28.3 nM. The affinity of hemibody constructs to CD3 molecule could only be detected at a very high concentration of constructs (1000 nM for hemibodies and 311 nM for BiTE). This finding demonstrates that the immobilized hemibody is able to bind its complementary hemibody and CD3 molecule only in a high concentration out of the therapeutic range.

.

5.1 Outlook for future research

Following experiments should focus on the receptor patterning on the T cells in response to the immunological synapse. Unanswered questions are: Where will the CD3 unit especially CD3 epsilon domain localize upon hemibody mediated IS formation?

What happens to the localization of the CD45 phosphatase and LCK kinase after hemibody stimulation? Answering these questions will provide more insight into the function of the observed atypical IS derived by complementary hemibodies.

As noted before, the size of the target protein is important for the function of the BiTE antibody (Bluemel et al., 2010). For the future hemibody studies, different hemibodies targeting different epitopes/ regions of a large target antigen should be investigated. Also, for different hemibody pairs, the synapse formation and killing activity has to be determined.

The apoptosis pathway mediated by hemibodies has to be analyzed more in detail. Further experiments should be conducted to get more detail about the role of perforin in hemibody mediated cytotoxicity. Our findings from perforin release in the cells treated with hemibodies, raise some questions. Is there any correlation between the content of perforin in hemibody-activated T cells with their cytolytic potency? Is perforin required for initiation of caspase activation? For answering the latter question, inhibition of intracellular perforin release using a specific perforin inhibitor could be helpful.

It is also interesting to analyze the possibility that complementary hemibodies may activate other apoptosis pathways such as FasL-mediated pathways to induce apoptosis in the target cell.

5.2 Conclusion

In summary, we have demonstrated that complementary hemibodies from an atypical synapse and induce higher caspase activity compared to BiTE antibody. We also detected an impaired translocation of ZAP70 from the cytosol to the cell membrane and a calcium flux lower compared to BiTE antibody.

The low levels of perforin in the presence of complementary hemibodies compared to BiTE is maybe due to other apoptosis pathways such as FasL-mediated pathway which play a role in hemibody mediated target cell killing.

The finding that in the presence of complementary hemibodies, target cell-T cell conjugates continuously increase over time suggesting that more conjugates compensate for the the suboptimal synapse, resulting in increased target cell killing.

We have further shown that only under unphysiological hemibody concentration a soluble CD3 molecule can bind to an immobilized hemibody with the complementary hemibody in solution.

In conclusion, these results contribute to the mechanistic understanding of the hemibody technology. They may further help to define requisite parameters for hemibody pairing which facilitate the search of suitable antigen combinations for combinatorial and high precision immunotherapy.

6 References

6.1 Publications

Alam, S. M., Davies, G. M., Lin, C. M., Zal, T., Nasholds, W., Jameson, S. C., . . . Travers, P. J. (1999). Qualitative and quantitative differences in T cell receptor binding of agonist and antagonist ligands. *Immunity, 10*(2), 227-237. doi:10.1016/s1074-7613(00)80023-0

Alarcon, B., Mestre, D., & Martinez-Martin, N. (2011). The immunological synapse: a cause or consequence of T-cell receptor triggering? *Immunology, 133*(4), 420-425. doi:10.1111/j.1365-2567.2011.03458.x

Andreotti, A. H., Schwartzberg, P. L., Joseph, R. E., & Berg, L. J. (2010). T-cell signaling regulated by the Tec family kinase, Itk. *Cold Spring Harb Perspect Biol, 2*(7), a002287. doi:10.1101/cshperspect.a002287

Balagopalan, L., Coussens, N. P., Sherman, E., Samelson, L. E., & Sommers, C. L. (2010). The LAT story: a tale of cooperativity, coordination, and choreography. *Cold Spring Harb Perspect Biol, 2*(8), a005512. doi:10.1101/cshperspect.a005512

Barry, M., & Bleackley, R. C. (2002). Cytotoxic T lymphocytes: all roads lead to death. *Nat Rev Immunol, 2*(6), 401-409. doi:10.1038/nri819

Basu, R., & Huse, M. (2017). Mechanical Communication at the Immunological Synapse. *Trends Cell Biol, 27*(4), 241-254. doi:10.1016/j.tcb.2016.10.005

Bjorkman, P. J., Saper, M. A., Samraoui, B., Bennett, W. S., Strominger, J. L., & Wiley, D. C. (1987). Structure of the human class I histocompatibility antigen, HLA-A2. *Nature, 329*(6139), 506-512. doi:10.1038/329506a0

Bluemel, C., Hausmann, S., Fluhr, P., Sriskandarajah, M., Stallcup, W. B., Baeuerle, P. A., & Kufer, P. (2010). Epitope distance to the target cell membrane and antigen size determine the potency of T cell-mediated lysis by BiTE antibodies specific for a large melanoma surface antigen. *Cancer Immunol Immunother, 59*(8), 1197-1209. doi:10.1007/s00262-010-0844-y

Brischwein, K., Schlereth, B., Guller, B., Steiger, C., Wolf, A., Lutterbuese, R., . . . Baeuerle, P. A. (2006). MT110: a novel bispecific single-chain antibody construct with high efficacy in eradicating established tumors. *Mol Immunol, 43*(8), 1129-1143. doi:10.1016/j.molimm.2005.07.034

Butler, M., & Spearman, M. (2014). The choice of mammalian cell host and possibilities for glycosylation engineering. *Curr Opin Biotechnol, 30*, 107-112. doi:10.1016/j.copbio.2014.06.010

Chakraborty, A. K., & Weiss, A. (2014). Insights into the initiation of TCR signaling. *Nat Immunol, 15*(9), 798-807. doi:10.1038/ni.2940

Chang, J. C. (2016). Cancer stem cells: Role in tumor growth, recurrence, metastasis, and treatment resistance. *Medicine (Baltimore), 95*(1 Suppl 1), S20-25. doi:10.1097/md.0000000000004766

Coloma, M. J., & Morrison, S. L. (1997). Design and production of novel tetravalent bispecific antibodies. *Nat Biotechnol, 15*(2), 159-163. doi:10.1038/nbt0297-159

Courtney, A. H., Lo, W. L., & Weiss, A. (2018). TCR Signaling: Mechanisms of Initiation and Propagation. *Trends Biochem Sci, 43*(2), 108-123. doi:10.1016/j.tibs.2017.11.008

Cullen, S. P., & Martin, S. J. (2009). Caspase activation pathways: some recent progress. *Cell Death Differ, 16*(7), 935-938. doi:10.1038/cdd.2009.59

Das, J., Ho, M., Zikherman, J., Govern, C., Yang, M., Weiss, A., . . . Roose, J. P. (2009). Digital signaling and hysteresis characterize ras activation in lymphoid cells. *Cell, 136*(2), 337-351. doi:10.1016/j.cell.2008.11.051

Davis, S. J., & van der Merwe, P. A. (2006). The kinetic-segregation model: TCR triggering and beyond. *Nat Immunol, 7*(8), 803-809. doi:10.1038/ni1369

Desai, D. M., Sap, J., Silvennoinen, O., Schlessinger, J., & Weiss, A. (1994). The catalytic activity of the CD45 membrane-proximal phosphatase domain is required for TCR signaling and regulation. *Embo j, 13*(17), 4002-4010. Retrieved from https://www.ncbi.nlm.nih.gov/pmc/articles/PMC395320/pdf/emboj00065-0084.pdf

Dreier, T., Lorenczewski, G., Brandl, C., Hoffmann, P., Syring, U., Hanakam, F., . . . Baeuerle, P. A. (2002). Extremely potent, rapid and costimulation-independent cytotoxic T-cell response against lymphoma cells catalyzed by a single-chain bispecific antibody. *Int J Cancer, 100*(6), 690-697. doi:10.1002/ijc.10557

Dustin, M. L., & Long, E. O. (2010). Cytotoxic immunological synapses. *Immunol Rev, 235*(1), 24-34. doi:10.1111/j.0105-2896.2010.00904.x

Dustin, M. L., Olszowy, M. W., Holdorf, A. D., Li, J., Bromley, S., Desai, N., . . . Shaw, A. S. (1998). A novel adaptor protein orchestrates receptor patterning and cytoskeletal polarity in T-cell contacts. *Cell, 94*(5), 667-677. Retrieved from https://www.sciencedirect.com/science/article/pii/S0092867400816086?via%3Dihub

Fooksman, D. R., Vardhana, S., Vasiliver-Shamis, G., Liese, J., Blair, D. A., Waite, J., . . . Dustin, M. L. (2010). Functional anatomy of T cell activation and synapse formation. *Annu Rev Immunol, 28*, 79-105. doi:10.1146/annurev-immunol-030409-101308

Furlan, G., Minowa, T., Hanagata, N., Kataoka-Hamai, C., & Kaizuka, Y. (2014). Phosphatase CD45 both positively and negatively regulates T cell receptor phosphorylation in reconstituted membrane protein clusters. *J Biol Chem, 289*(41), 28514-28525. doi:10.1074/jbc.M114.574319

Galluzzi, L., Vacchelli, E., Bravo-San Pedro, J. M., Buque, A., Senovilla, L., Baracco, E. E., . . . Kroemer, G. (2014). Classification of current anticancer immunotherapies. *Oncotarget, 5*(24), 12472-12508. doi:10.18632/oncotarget.2998

Garboczi, D. N., Ghosh, P., Utz, U., Fan, Q. R., Biddison, W. E., & Wiley, D. C. (1996). Structure of the complex between human T-cell receptor, viral peptide and HLA-A2. *Nature, 384*(6605), 134-141. doi:10.1038/384134a0

Gokbuget, N., Dombret, H., Bonifacio, M., Reichle, A., Graux, C., Faul, C., . . . Bargou, R. C. (2018). Blinatumomab for minimal residual disease in adults with B-cell precursor acute lymphoblastic leukemia. *Blood, 131*(14), 1522-1531. doi:10.1182/blood-2017-08-798322

Griguolo, G., Pascual, T., Dieci, M. V., Guarneri, V., & Prat, A. (2019). Interaction of host immunity with HER2-targeted treatment and tumor heterogeneity in HER2-positive breast cancer. *J Immunother Cancer, 7*(1), 90. doi:10.1186/s40425-019-0548-6

Gunturu, K. S., Woo, Y., Beaubier, N., Remotti, H. E., & Saif, M. W. (2013). Gastric cancer and trastuzumab: first biologic therapy in gastric cancer. *Ther Adv Med Oncol, 5*(2), 143-151. doi:10.1177/1758834012469429

Haas, C., Krinner, E., Brischwein, K., Hoffmann, P., Lutterbuse, R., Schlereth, B., . . . Baeuerle, P. A. (2009). Mode of cytotoxic action of T cell-engaging BiTE antibody MT110. *Immunobiology, 214*(6), 441-453. doi:10.1016/j.imbio.2008.11.014

Hanahan, D., & Weinberg, R. A. (2011). Hallmarks of cancer: the next generation. *Cell, 144*(5), 646-674. doi:10.1016/j.cell.2011.02.013

Hermiston, M. L., Xu, Z., & Weiss, A. (2003). CD45: a critical regulator of signaling thresholds in immune cells. *Annu Rev Immunol, 21*, 107-137. doi:10.1146/annurev.immunol.21.120601.140946

Hoffmann, P., Hofmeister, R., Brischwein, K., Brandl, C., Crommer, S., Bargou, R., . . . Baeuerle, P. A. (2005). Serial killing of tumor cells by cytotoxic T cells redirected with a CD19-/CD3-bispecific single-chain antibody construct. *Int J Cancer, 115*(1), 98-104. doi:10.1002/ijc.20908

Housman, G., Byler, S., Heerboth, S., Lapinska, K., Longacre, M., Snyder, N., & Sarkar, S. (2014). Drug resistance in cancer: an overview. *Cancers (Basel), 6*(3), 1769-1792. doi:10.3390/cancers6031769

Huppa, J. B., & Davis, M. M. (2003). T-cell-antigen recognition and the immunological synapse. *Nat Rev Immunol, 3*(12), 973-983. doi:10.1038/nri1245

James, J. R., & Vale, R. D. (2012). Biophysical mechanism of T-cell receptor triggering in a reconstituted system. *Nature, 487*(7405), 64-69. doi:10.1038/nature11220

Joseph, N., Reicher, B., & Barda-Saad, M. (2014). The calcium feedback loop and T cell activation: how cytoskeleton networks control intracellular calcium flux. *Biochim Biophys Acta, 1838*(2), 557-568. doi:10.1016/j.bbamem.2013.07.009

Keefe, D., Shi, L., Feske, S., Massol, R., Navarro, F., Kirchhausen, T., & Lieberman, J. (2005). Perforin triggers a plasma membrane-repair response that facilitates CTL induction of apoptosis. *Immunity, 23*(3), 249-262. doi:10.1016/j.immuni.2005.08.001

Kohler, G., & Milstein, C. (2005). Continuous cultures of fused cells secreting antibody of predefined specificity. 1975. *J Immunol, 174*(5), 2453-2455.

Kojima, H., Toda, M., & Sitkovsky, M. V. (2000). Comparison of Fas- versus perforin-mediated pathways of cytotoxicity in TCR- and Thy-1-activated murine T cells. *Int Immunol, 12*(3), 365-374. doi:10.1093/intimm/12.3.365

Kontermann, R. E., & Brinkmann, U. (2015). Bispecific antibodies. *Drug Discov Today, 20*(7), 838-847. doi:10.1016/j.drudis.2015.02.008

Lattenmayer, C., Loeschel, M., Schriebl, K., Steinfellner, W., Sterovsky, T., Trummer, E., . . . Kunert, R. (2007). Protein-free transfection of CHO host cells with an IgG-fusion protein: selection and characterization of stable high producers and comparison to conventionally transfected clones. *Biotechnol Bioeng, 96*(6), 1118-1126. doi:10.1002/bit.21183

Lauritsen, J. P., Christensen, M. D., Dietrich, J., Kastrup, J., Odum, N., & Geisler, C. (1998). Two distinct pathways exist for down-regulation of the TCR. *J Immunol, 161*(1), 260-267.

Li, J., Stagg, N. J., Johnston, J., Harris, M. J., Menzies, S. A., DiCara, D., . . . Junttila, T. T. (2017). Membrane-Proximal Epitope Facilitates Efficient T Cell Synapse Formation by Anti-FcRH5/CD3 and Is a Requirement for Myeloma Cell Killing. *Cancer Cell, 31*(3), 383-395. doi:10.1016/j.ccell.2017.02.001

Lin, Y., Pagel, J. M., Axworthy, D., Pantelias, A., Hedin, N., & Press, O. W. (2006). A genetically engineered anti-CD45 single-chain antibody-streptavidin fusion protein for pretargeted radioimmunotherapy of hematologic malignancies. *Cancer Res, 66*(7), 3884-3892. doi:10.1158/0008-5472.Can-05-3443

Locksley, R. M., Reiner, S. L., Hatam, F., Littman, D. R., & Killeen, N. (1993). Helper T cells without CD4: control of leishmaniasis in CD4-deficient mice. *Science, 261*(5127), 1448-1451. doi:10.1126/science.8367726

Loffler, A., Kufer, P., Lutterbuse, R., Zettl, F., Daniel, P. T., Schwenkenbecher, J. M., . . . Bargou, R. C. (2000). A recombinant bispecific single-chain antibody, CD19 x CD3, induces rapid and high lymphoma-directed cytotoxicity by unstimulated T lymphocytes. *Blood, 95*(6), 2098-2103.

Matthews, D. C., Appelbaum, F. R., Eary, J. F., Hui, T. E., Fisher, D. R., Martin, P. J., . . . et al. (1991). Radiolabeled anti-CD45 monoclonal antibodies target lymphohematopoietic tissue in the macaque. *Blood, 78*(7), 1864-1874. Retrieved from http://www.bloodjournal.org/content/bloodjournal/78/7/1864.full.pdf

McCall, M. N., Shotton, D. M., & Barclay, A. N. (1992). Expression of soluble isoforms of rat CD45. Analysis by electron microscopy and use in epitope mapping of anti-CD45R monoclonal antibodies. *Immunology, 76*(2), 310-317. Retrieved from https://www.ncbi.nlm.nih.gov/pmc/articles/PMC1421548/pdf/immunology00105-0136.pdf

McKeithan, T. W. (1995). Kinetic proofreading in T-cell receptor signal transduction. *Proc Natl Acad Sci U S A, 92*(11), 5042-5046. doi:10.1073/pnas.92.11.5042

Millard, P. J., Henkart, M. P., Reynolds, C. W., & Henkart, P. A. (1984). Purification and properties of cytoplasmic granules from cytotoxic rat LGL tumors. *J Immunol, 132*(6),

3197-3204. Retrieved from http://www.jimmunol.org/content/jimmunol/132/6/3197.full.pdf

Monks, C. R., Freiberg, B. A., Kupfer, H., Sciaky, N., & Kupfer, A. (1998). Three-dimensional segregation of supramolecular activation clusters in T cells. *Nature, 395*(6697), 82-86. doi:10.1038/25764

Nagorsen, D., Kufer, P., Baeuerle, P. A., & Bargou, R. (2012). Blinatumomab: a historical perspective. *Pharmacol Ther, 136*(3), 334-342. doi:10.1016/j.pharmthera.2012.07.013

Nowell, P. C. (1976). The clonal evolution of tumor cell populations. *Science, 194*(4260), 23-28. doi:10.1126/science.959840

Offner, S., Hofmeister, R., Romaniuk, A., Kufer, P., & Baeuerle, P. A. (2006). Induction of regular cytolytic T cell synapses by bispecific single-chain antibody constructs on MHC class I-negative tumor cells. *Mol Immunol, 43*(6), 763-771. doi:10.1016/j.molimm.2005.03.007

Palacios, E. H., & Weiss, A. (2004). Function of the Src-family kinases, Lck and Fyn, in T-cell development and activation. *Oncogene, 23*(48), 7990-8000. doi:10.1038/sj.onc.1208074

Penninger, J. M., Irie-Sasaki, J., Sasaki, T., & Oliveira-dos-Santos, A. J. (2001). CD45: new jobs for an old acquaintance. *Nat Immunol, 2*(5), 389-396. doi:10.1038/87687

Rabinowitz, J. D., Beeson, C., Lyons, D. S., Davis, M. M., & McConnell, H. M. (1996). Kinetic discrimination in T-cell activation. *Proc Natl Acad Sci U S A, 93*(4), 1401-1405. doi:10.1073/pnas.93.4.1401

Reich, Z., Boniface, J. J., Lyons, D. S., Borochov, N., Wachtel, E. J., & Davis, M. M. (1997). Ligand-specific oligomerization of T-cell receptor molecules. *Nature, 387*(6633), 617-620. doi:10.1038/42500

Restifo, N. P., Dudley, M. E., & Rosenberg, S. A. (2012). Adoptive immunotherapy for cancer: harnessing the T cell response. *Nat Rev Immunol, 12*(4), 269-281. doi:10.1038/nri3191

Riquelme, E., Carreno, L. J., Gonzalez, P. A., & Kalergis, A. M. (2009). The duration of TCR/pMHC interactions regulates CTL effector function and tumor-killing capacity. *Eur J Immunol, 39*(8), 2259-2269. doi:10.1002/eji.200939341

Rossy, J., Williamson, D. J., & Gaus, K. (2012). How does the kinase Lck phosphorylate the T cell receptor? Spatial organization as a regulatory mechanism. *Front Immunol, 3*, 167. doi:10.3389/fimmu.2012.00167

Russell, J. H., & Ley, T. J. (2002). Lymphocyte-mediated cytotoxicity. *Annu Rev Immunol, 20*, 323-370. doi:10.1146/annurev.immunol.20.100201.131730

Sasaki, T., Sasaki-Irie, J., & Penninger, J. M. (2001). New insights into the transmembrane protein tyrosine phosphatase CD45. *Int J Biochem Cell Biol, 33*(11), 1041-1046. Retrieved from https://www.sciencedirect.com/science/article/pii/S1357272501000759?via%3Dihub

Scharenberg, A. M., Humphries, L. A., & Rawlings, D. J. (2007). Calcium signalling and cell-fate choice in B cells. *Nat Rev Immunol, 7*(10), 778-789. doi:10.1038/nri2172

Schilham, M. W., Fung-Leung, W. P., Rahemtulla, A., Kuendig, T., Zhang, L., Potter, J., . . . Mak, T. W. (1993). Alloreactive cytotoxic T cells can develop and function in mice lacking both CD4 and CD8. *Eur J Immunol, 23*(6), 1299-1304. doi:10.1002/eji.1830230617

Staerz, U. D., Kanagawa, O., & Bevan, M. J. (1985). Hybrid antibodies can target sites for attack by T cells. *Nature, 314*(6012), 628-631. doi:10.1038/314628a0

Stepanek, O., Prabhakar, A. S., Osswald, C., King, C. G., Bulek, A., Naeher, D., . . . Palmer, E. (2014). Coreceptor scanning by the T cell receptor provides a mechanism for T cell tolerance. *Cell, 159*(2), 333-345. doi:10.1016/j.cell.2014.08.042

Strebhardt, K., & Ullrich, A. (2008). Paul Ehrlich's magic bullet concept: 100 years of progress. *Nat Rev Cancer, 8*(6), 473-480. doi:10.1038/nrc2394

Sun, Z. J., Kim, K. S., Wagner, G., & Reinherz, E. L. (2001). Mechanisms contributing to T cell receptor signaling and assembly revealed by the solution structure of an ectodomain fragment of the CD3 epsilon gamma heterodimer. *Cell, 105*(7), 913-923.

Tan, S. Y., & Grimes, S. (2010). Paul Ehrlich (1854-1915): man with the magic bullet. *Singapore Med J, 51*(11), 842-843.

Ueda, H., Tsumoto, K., Kubota, K., Suzuki, E., Nagamune, T., Nishimura, H., . . . Mohoney, W. C. (1996). Open sandwich ELISA: a novel immunoassay based on the interchain interaction of antibody variable region. *Nat Biotechnol, 14*(13), 1714-1718. doi:10.1038/nbt1296-1714

Valitutti, S., Muller, S., Cella, M., Padovan, E., & Lanzavecchia, A. (1995). Serial triggering of many T-cell receptors by a few peptide-MHC complexes. *Nature, 375*(6527), 148-151. doi:10.1038/375148a0

van der Merwe, P. A., & Dushek, O. (2011). Mechanisms for T cell receptor triggering. *Nat Rev Immunol, 11*(1), 47-55. doi:10.1038/nri2887

Varma, R., Campi, G., Yokosuka, T., Saito, T., & Dustin, M. L. (2006). T cell receptor-proximal signals are sustained in peripheral microclusters and terminated in the central supramolecular activation cluster. *Immunity, 25*(1), 117-127. doi:10.1016/j.immuni.2006.04.010

Vigneron, N. (2015). Human Tumor Antigens and Cancer Immunotherapy. *Biomed Res Int, 2015*, 948501. doi:10.1155/2015/948501

Voskoboinik, I., Smyth, M. J., & Trapani, J. A. (2006). Perforin-mediated target-cell death and immune homeostasis. *Nat Rev Immunol, 6*(12), 940-952. doi:10.1038/nri1983

Wacquier, B., Combettes, L., Van Nhieu, G. T., & Dupont, G. (2016). Interplay Between Intracellular Ca(2+) Oscillations and Ca(2+)-stimulated Mitochondrial Metabolism. *Sci Rep, 6*, 19316. doi:10.1038/srep19316

Wang, H., Kadlecek, T. A., Au-Yeung, B. B., Goodfellow, H. E., Hsu, L. Y., Freedman, T. S., & Weiss, A. (2010). ZAP-70: an essential kinase in T-cell signaling. *Cold Spring Harb Perspect Biol, 2*(5), a002279. doi:10.1101/cshperspect.a002279

Wange, R. L., & Samelson, L. E. (1996). Complex complexes: signaling at the TCR. *Immunity, 5*(3), 197-205. doi:10.1016/s1074-7613(00)80315-5

Watkins, N. A., Brown, C., Hurd, C., Navarrete, C., & Ouwehand, W. H. (2000). The isolation and characterisation of human monoclonal HLA-A2 antibodies from an immune V gene phage display library. Tissue Antigens, 55(3), 219-228. Retrieved from https://onlinelibrary.wiley.com/doi/pdf/10.1034/j.1399-0039.2000.550305.x

Yablonski, D., Kuhne, M. R., Kadlecek, T., & Weiss, A. (1998). Uncoupling of nonreceptor tyrosine kinases from PLC-gamma1 in an SLP-76-deficient T cell. *Science, 281*(5375), 413-416. doi:10.1126/science.281.5375.413

Yao, Y., & Dai, W. (2014). Genomic Instability and Cancer. *J Carcinog Mutagen, 5*. doi:10.4172/2157-2518.1000165

Zhang, W., Trible, R. P., Zhu, M., Liu, S. K., McGlade, C. J., & Samelson, L. E. (2000). Association of Grb2, Gads, and phospholipase C-gamma 1 with phosphorylated LAT tyrosine residues. Effect of LAT tyrosine mutations on T cell angigen receptor-mediated signaling. *J Biol Chem, 275*(30), 23355-23361. doi:10.1074/jbc.M000404200

Zugazagoitia, J., Guedes, C., Ponce, S., Ferrer, I., Molina-Pinelo, S., & Paz-Ares, L. (2016). Current Challenges in Cancer Treatment. *Clin Ther, 38*(7), 1551-1566. doi:10.1016/j.clinthera.2016.03.026

6.2 Books and eBooks

Bennett, J. (2015). *Mandell, Douglas, and Bennett's Principles and Practice of Infectious Diseases* (8nd ed.). doi: https://doi.org/10.1016/C2012-1-00075-6

Cooper, GM. (2000). The Cell: A Molecular Approach (2nd ed.). Sunderland (MA), VIC: Sinauer Associates

Kamada, H., Tsunoda, S.-I. (2013). ScienceDirect: Generating functional mutant proteins to create highly bioactive anticancer biopharmaceuticals

Murphy, K. (2011). *Janeway's Immunobiology* (8nd ed.). New York, VIC: Garland Science, Taylor & Francis Group, LLC

Topp, M.S., Gökbuget, N., Kufer, P., Zugmaier, G., Degenhard, E., Neumann, S., Horst, H.A., Viardot, A., Schmid, M., Ottmann, O.G., Schmidt, M., Reinhardt, C.F., Baeuerle, P.A., Nagorsen, D., Hoelzer, D., & Bargou, R.C. (2008). Treatment with Anti-CD19 BiTE Antibody Blinatumomab (MT103 / MEDI-538) Is Able to Eliminate Minimal Residual Disease (MRD) in Patients with B-Precursor Acute Lymphoblastic Leukemia (ALL): First Results of An Ongoing Phase II Study

6.3 Doctoral Dissertations

Banaszek, A. (2013). Dual Antigen-Restricted Complementation of a Two-Part Trispecific Antibody for Targeted Immunotherapy of Blood Cancer (Doctoral dissertaion). Rterieved from https://opus.bibliothek.uni-wuerzburg.de/frontdoor/index/index/searchtype/authorsearch/referee/Harald+Wajant+/rows/10/start/1/subjectfq/Antik%C3%B6rper/docId/9017

Hauff, C. (2009). Aspects of the mode of action of bispecific T cell engager (BiTE) antibodies (Doctoral dissertaion). Rtereived from https://pdfs.semanticscholar.org/b2d5/8bb08265d59e9fdcff8a335b851ac085a303.pdf

6.4 Websites

Ledford, H. (2016, APRIL 14). The next frontier in cancer immunotherapy lies in combining it with other treatments. Scientists are trying to get the mix just right. Nature. Retrieved from https://www.nature.com/news/polopoly_fs/1.19745!/menu/main/topColumns/topLeftColumn/pdf/532162a.pdf?origin=ppub

Structural Biochemistry/Leukemia. (2017, August 16). Wikibooks, The Free Textbook Project. Retrieved from https://en.wikibooks.org/w/index.php?title=Structural_Biochemistry/Leukemia&oldid=3269837

7 Abbreviations

°C	Degree Celsius
µ	micro
AML	acute myeloid leukemia
AIEX	anion exchange chromatography
amp	ampicillin resistance gene
APC	Antigen presenting cell
Approx.	Approximately
AU	Arbitrary units
BiTE	Bispecific T-cell engager
bp	base pairs
BSA	Bovine serum albumin
CD	Cluster of differentiation
CD3	Part of T-cell receptor complex
CDC	complement-dependent cytotoxicity
CDR	complementarity-determining regions
CFU	colony forming unit
C_H	constant heavy
C_L	constant light
Co	cobalt
cspA	cold-shock promoter termed Protein A
DIC	Differential interference contrast

DMSO	dimethyl sulfoxide
DNA	deoxyribonucleic acid
dNTP	deoxyribonucleoside triphosphate
E : T	effector cell to target cell ratio
e.g.	exempli gratia; for example
EDTA	ethylenediaminetetraacetic acid
ELISA	enzyme-linked immunosorbent assay
Fab	fragment antigen-binding
FACS	fluorescence activated cell sorting
FBS	fetal bovine serum
Fc	crystallizable fragment
Fig	Figure
Fluc	Firefly Luciferase
Fwd	Forward
GFP	green fluorescent protein
h	hours
His-tag	polyhistidine-tag
HRP	horseradish peroxidise, enzyme used for TMB/H_2O_2 colour reaction in ELISA
Hygro	Hygromycin
Ig	immunoglobulin
IL	Interleukin
IMAC	immobilized-metal affinity chromatography
IS	Immunological synapse
ITAM	immunoreceptor tyrosine-based activation motif

kDa	kilo Dalton
LacI	Lactose repressor
M	molar concentration
m	milli (10^{-3}) or meter
mAb	monoclonal antibody
MCS	multiple cloning site
MHC	major histocompatibility complex
min	Minute(s)
mol	amount of chemical substance
mRNA	messenger ribonucleic acid
MW	molecular weight
MWCO	molecular weight cut-off
n	nano (10^{-9})
NaCl	sodium chloride
NK	Natural Killer cells
OD_{600}	optical density at 600 nm
Ori	origin of replication
PAGE	polyacrylamide gel electrophoresis
PBMC	peripheral blood mononuclear cells
PBS	phosphate buffered saline
PCR	polymerase chain reaction
Prep	Preparation
Puro	Puromycin
Rev	Reverse
RPM	Revolutions per minute

RT	room temperature
s	second
scFv	single-chain variable-fragment, comprises a monovalent binding site for the antigen
SDS	sodium dodecyl sulphate
SEC	size exclusion chromatography
TAA	tumor-associated antigen
TCR	T-cell receptor
TEMED	N,N,N,N-Tetramethylethylendiamin
TMB	3,3',5,5'-tetramethylbenzidine,colour substrate in ELISA
Tris	tris(hydroxymethyl)aminomethane
Tween	polyoxyethylene sorbitan monolaurate
UTR	Untranslated region
V	Volt
V_H	variable heavy
V_L	variable light
wt	wild type
x g	acceleration of gravity (9.81 m/s_2)
α	anti

8 Annex

8.1 Sequences

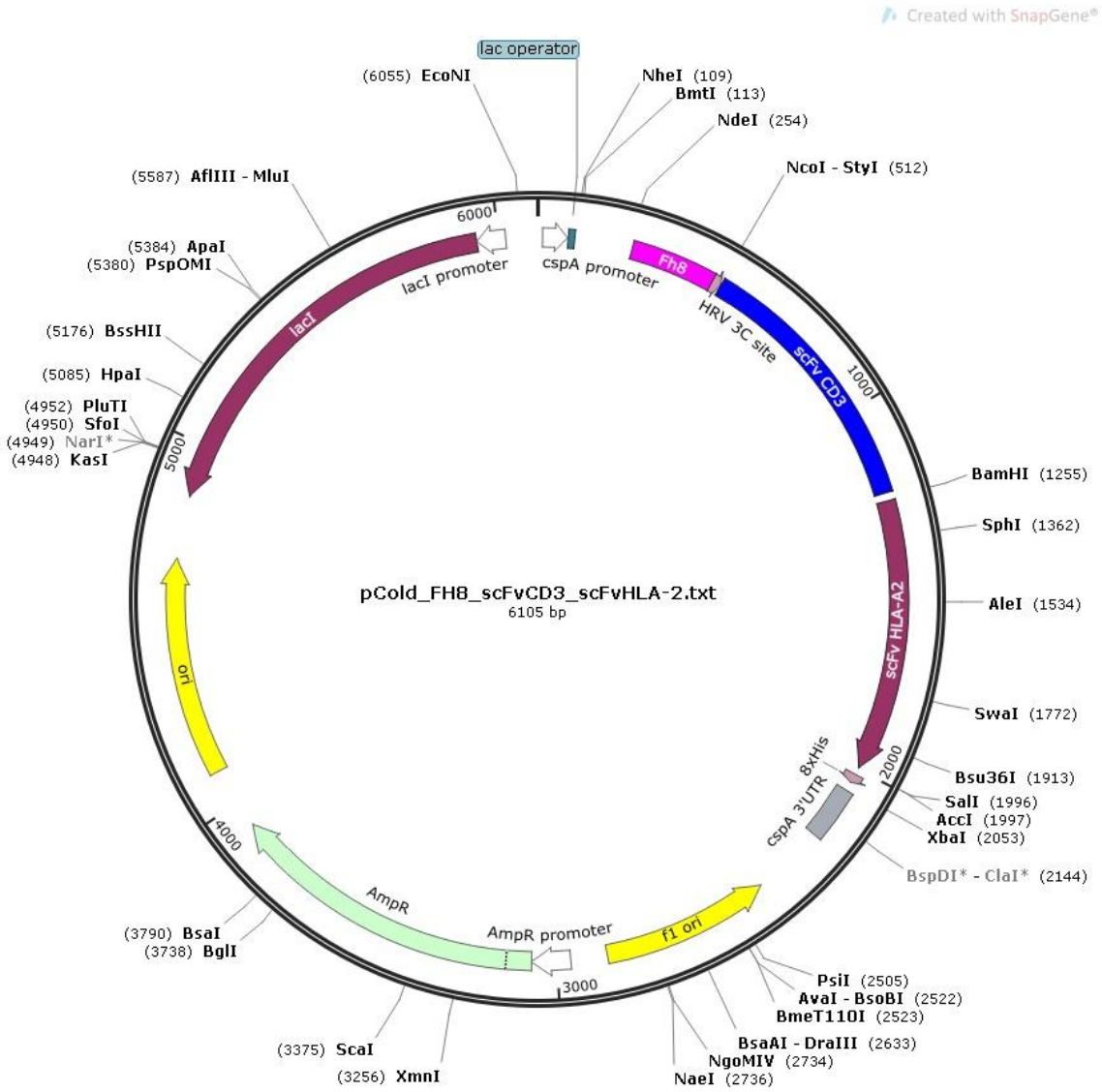

Figure 29: Vector card of the plasmid pCold IV. The positions of cold-shock promotor termed Protein A (cspA) promotor, lac operator are indicated. The DNA of scFvαCD3-scFvαHLA-A2 hemibody was inserted in the multiple cloning site (MCS) via specific restriction sites. The color of the vector card and the corresponding DNA sequence matches. Adapted from the Takara catalog.

8.1.1 scFvαCD3-scFvαHLA-A2

CATATGCCGAGCGTTCAAGAAGTTGAAAAACTGCTGCATGTTCTGGATCGTAATGGTGATGGTAAAGT
TAGCGCAGAAGAACTGAAAGCATTTGCCGATGATAGCAAATGTCCGCTGGATAGCAATAAAATCAAAG
CCTTTATCAAAGAGCACGATAAAAACAAAGATGGCAAACTGGATCTGAAAGAACTGGTTAGCATTCTG
AGCAGCGGTGGTTCAGGTGGTGGTGGCGGTAGCCTGGAAGTTCTGTTTCAGGGTCCCATGGACGTTCA
GCTGGTTCAGAGCGGTGCCGAAGTTAAAAAACCGGGTGCAAGCGTTAAAGTTAGCTGTAAAGCAAGCG
GTTATACCTTTACCCGTTATACCATGCATTGGGTTCGTCAGGCACCGGGTCAGGGTCTGGAATGGATT
GGTTATATCAATCCGAGCCGTGGCTATACCAATTATGCAGATAGCGTGAAAGGTCGCTTTACCATTAC
CACCGATAAAAGCACCAGCACCGCATATATGGAACTGAGCAGCCTGCGTAGCGAAGATACCGCAACCT
ATTATTGTGCACGCTATTATGATGATCACTACTGCCTGGATTATTGGGGTCAGGGCACCACCGTTACC
GTTAGCAGCTCAGGTGGTGGTGGTAGCGGTGGTGGCGGTTCTGGCGGTGGCGGTAGCGATATTGTTCT
GACCCAGAGTCCGGCAACCCTGAGCCTGAGTCCGGGTGAACGTGCCACCCTGAGCTGTCGTGCAAGCC
AGAGCGTTAGCTATATGAATTGGTATCAGCAGAAACCGGGTAAAGCACCGAAACGTTGGATTTATGAT
ACCAGCAAAGTTGCAAGCGGTGTTCCGGCACGTTTTAGCGGTAGCGGTTCAGGTACAGATTATAGCCT
GACCATTAATAGCCTGGAAGCAGAAGATGCAGCCACATATTATTGTCAGCAGTGGTCAAGCAATCCGC
TGACCTTTGGTGGTGGCACCAAAGTTGAAATTAAAGGTAGCGGAGGCGGTGGATCCCAGGTGCAGCTG
GTGCAGTCTGGGGGAGGCGTGGTCCAGCCTGGGGGGTCCCTGAGAGTCTCCTGTGCAGCGTCTGGGGT
CACCCTCAGTGATTATGGCATGCATTGGGTCCGCCAGGCTCCAGGCAAGGGGCTGGAGTGGATGGCTT
TTATACGGAATGATGGAAGTGATAAATATTATGCAGACTCCGTGAAGGGCCGATTCACCATCTCCAGA
GACAACTCCAAGAAAACAGTGTCTCTGCAAATGAGCAGTCTCAGAGCTGAAGACACGGCTGTGTATTA
CTGTGCGAAAAATGGCGAATCTGGGCCTTTGGACTACTGGTACTTCGATCTCTGGGGCCGTGGCACCC
TGGTCACCGTGTCGAGTGGTGGAGGCGGTTCAGGCGGAGGTGGCTCTGGCGGTGGCGGATCGGATGTT
GTGATGACTCAGTCTCCATCCTCCCTGTCTGCATCTGTAGGAGACAGAGTCACCATCACTTGCCAGGC
GAGTCAGGACATTAGCAACTATTTAAATTGGTATCAGCAGAAACCAGGGAAAGCCCCTAAGCTCCTGA
TCTACGATGCATCCAATTTGGAAACAGGGGTCCCATCAAGGTTCAGTGGAAGTGGATCTGGGACAGAT
TTTACTTTCACCATCAGCAGCCTGCAGCCTGAGGATTTTGCAACTTATTACTGCCAACAATATAGTAG
TTTTCCGCTCACTTTCGGCGGAGGGACCAAAGTGGATATCAAAGTCGACGGTGGCGGTGGTAGTCATC
ATCACCACCATCACCATCATTGATAACTGCAGTCTAG

Figure 30: Vector card of the plasmid pRSF DUET. This plasmid has two multiple cloning sites with a T7-Lac promoter and a kanamycin resistance gene. The color of the vector card and the corresponding DNA sequence matches. Vector map is adapted from the company Merck.

8.1.2 3C Protease

GGGGAATTGTGAGCGGATAACAATTCCCCTGTAGAAATAATTTTGTTTAACTTTAATAAGGAGATATA
CCATGGGACCGAATACCGAATTTGCACTGAGCCTGCTGCGTAAAAACATTATGACCATTACCACCTCC
AAAGGCGAATTTACCGGTCTGGGTATTCATGATCGTGTTTGTGTTATTCCGACCCATGCACAGCCTGG
TGATGATGTTCTGGTTAATGGTCAGAAAATTCGCGTGAAAGATAAATACAAACTGGTGGACCCGGAAA
ACATTAATCTGGAACTGACCGTTCTGACCCTGGATCGTAATGAAAAATTTCGTGATATCCGTGGCTTT
ATCAGCGAAGATCTGGAAGGTGTTGATGCAACCCTGGTTGTTCATAGCAATAACTTTACCAACACCAT
TCTGGAAGTTGGTCCGGTTACAATGGCAGGTCTGATTAATCTGAGCAGCACCCCGACCAATCGTATGA
TTCGTTATGATTATGCAACCAAAACCGGTCAGTGTGGTGGTGTTCTGTGTGCAACCGGTAAAATCTTT
GGCATTCATGTTGGTGGCAATGGTCGTCAGGGTTTTAGCGCACAGCTGAAAAAACAGTATTTCGTCGA
AAAACAGTAATAATT

The sequences of produced hemibodies in CHO cells are only shown here in vectors containing hygromycin resistance gene. The same sequence was also inserted in plasmids with puromycin resistance.

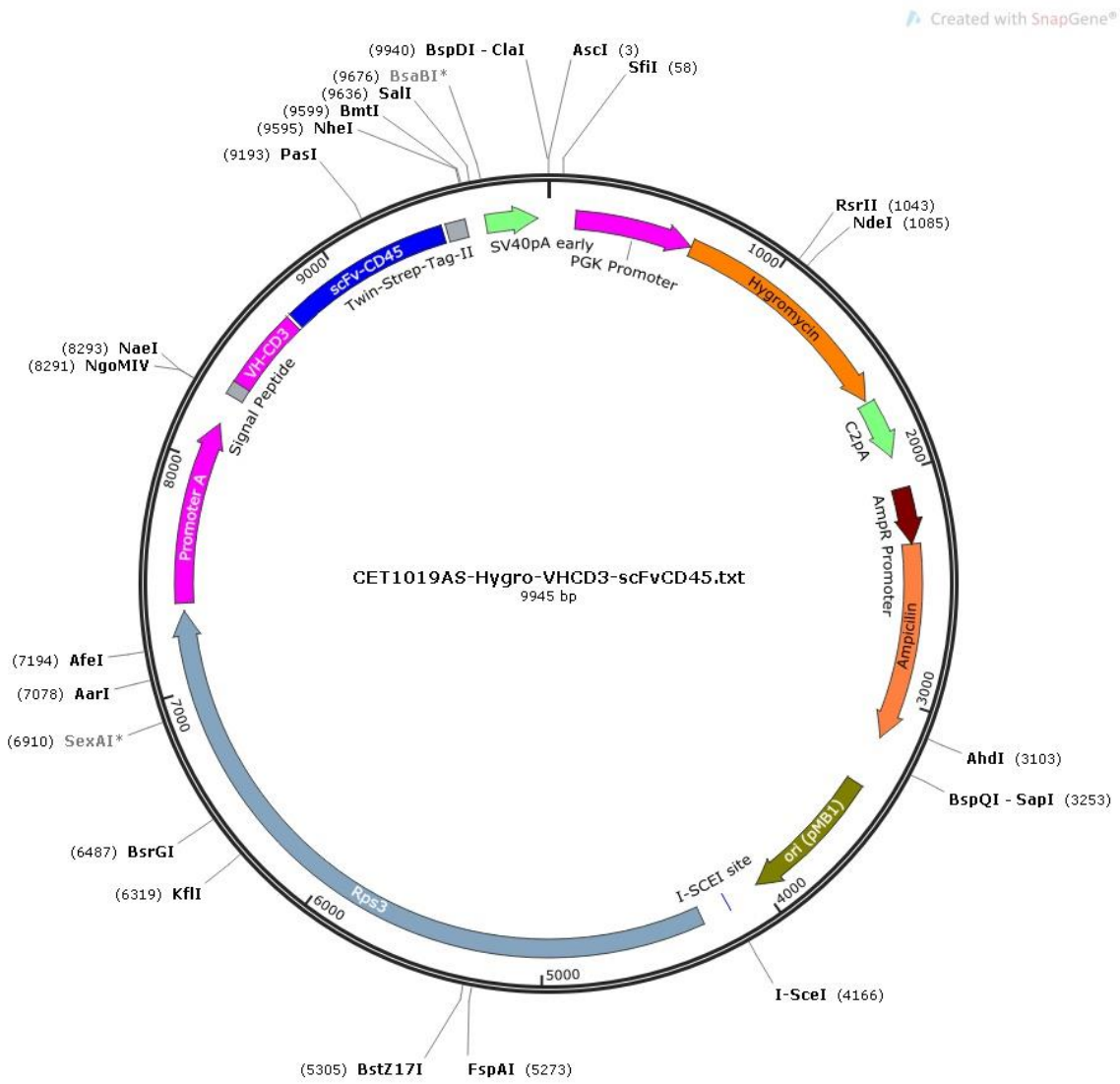

Figure 31: Vector card of the plasmid CET1019AS-hygro vector. The DNA of VHαCD3-scFvαCD45 hemibody was inserted in the multiple cloning site (MCS) via specific restriction sites. The color of the vector card and the corresponding DNA sequence matches. Adapted from the certificate of analysis of UCOER Single Expression Hygromycin Vector Set.

8.1.3 VHαCD3-scFvαCD45

GCCGGCGCCACCATGGAAACAGATACCCTGCTGGTGTTCGTGCTGCTCGTGTGGGTGCCAGCTGGAAA
TGGGGATGTGCAGCTGGTTCAGTCTGGCGCCGAAGTGAAGAAACCTGGCGCCTCTGTGAAGGTGTCCT
GCAAGGCTTCCGGCTACACCTTTACCAGATACACCATGCACTGGGTCCGACAGGCCCCTGGACAAGGA
TTGGAGTGGATCGGCTACATCAACCCCTCTCGGGGCTACACCAACTACGCCGACTCTGTGAAAGGCCG
GTTCACCATCACCACCGACAAGTCCACCTCCACCGCCTACATGGAACTGTCCAGCCTGAGATCTGAGG
ACACCGCCACCTACTACTGCGCCCGGTACTACGACGACCACTACTGCCTGGATTATTGGGGCCAGGGC
ACCACCGTGACAGTTTCTAGCGGAGGCGGAGGATCTCAGGTCCAGCTGGTGGAATCTGGCGGAGGACT
TGTTCAGCCTGGCGGATCCCTGAAGCTGTCTTGTGCCGCCTCTGGCTTCGACTTCTCCCGGTACTGGA
TGTCCTGGGTTCGACAAGCTCCAGGCAAAGGCCTGGAATGGATCGGAGAGATCAACCCTACCTCCTCC
ACCATCAACTTCACCCCTAGCCTGAAGGACAAGGTGTTCATCTCCCGGGACAACGCCAAGAACACCCT
GTACCTGCAGATGTCCAAAGTGCGGAGCGAGGATACCGCTCTGTACTACTGTGCCAGAGGCAACTACT
ACAGATACGGCGACGCCATGGACTACTGGGGACAGGGAACATCTGTGACCGTGTCATCTGGTGGCGGC
GGATCTGGTTCTGGCTCTGGCAATGGATCAGGTGGCGGAGGCTCTGACATCGTGCTGACACAGTCTCC
CGCTTCTCTGGCTGTGTCCCTGGGACAGAGAGCCACCATCTCTTGCCGGGCCTCCAAGTCCGTGTCTA
CCTCCGGCTACTCTTACCTGCACTGGTATCAGCAGAAGCCCGGCCAGCCTCCTAAGCTGCTGATCTAC
CTGGCCTCCAACCTGGAAAGCGGAGTGCCTGCCAGATTTTCCGGCTCTGGATCTGGCACCGACTTCAC
CCTGAACATCCATCCTGTGGAAGAAGAGGACGCTGCTACCTACTATTGCCAGCACTCCAGAGAGCTGC
CCTTCACCTTTGGCTCCGGCACCAAGCTCGAGATCAAGTCCAGCTCCTCCTCCTCTGCTTGGTCCCAT
CCTCAGTTCGAGAAAGGCGGCGGAAGCGGCGGTGGTAGTGGTGGATCTGCTTGGAGTCACCCACAGTT
TGAGAAGTAATAGCTAGC

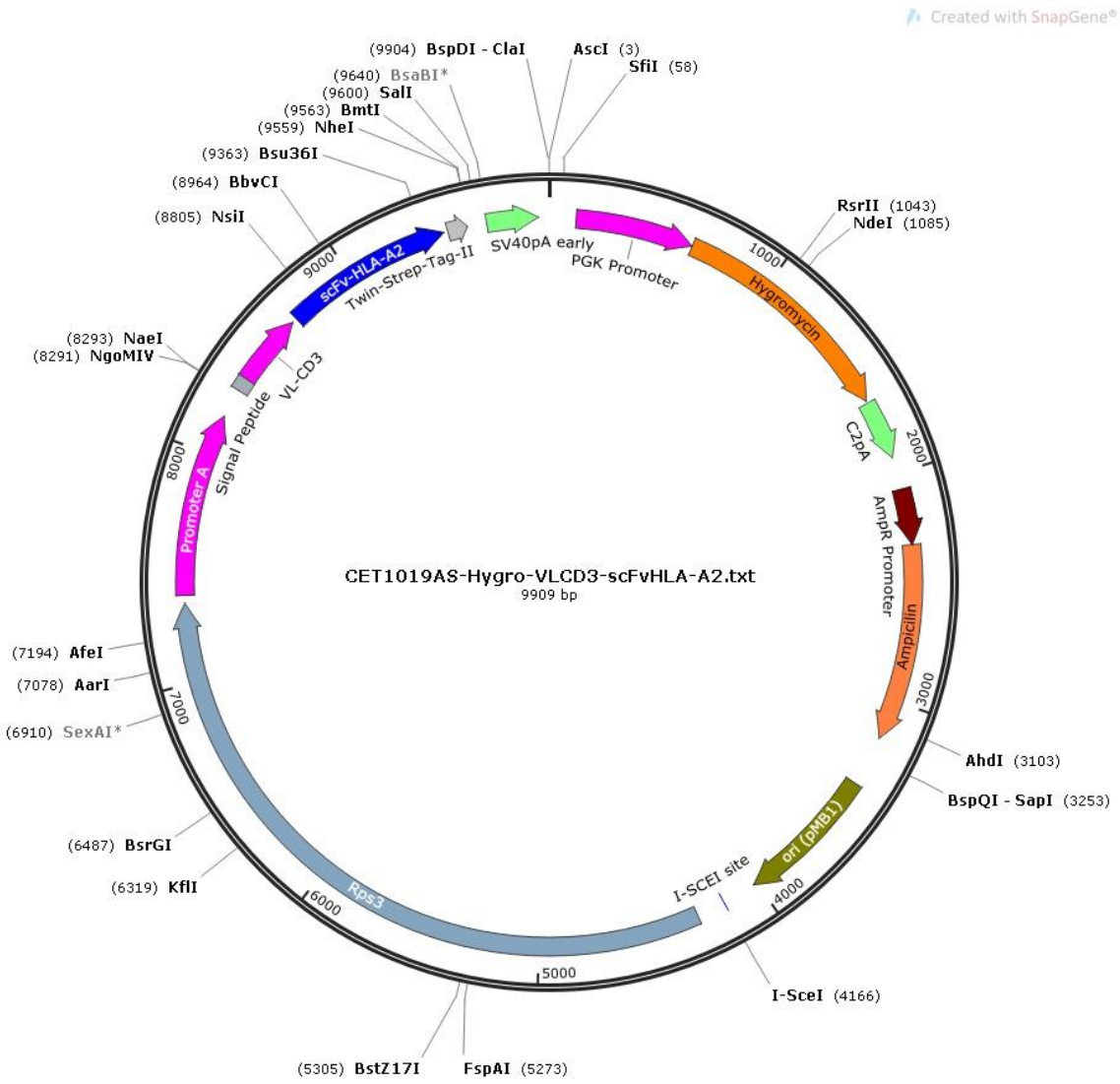

Figure 32: Vector card of the plasmid CET1019AS-hygro vector. The DNA of VLαCD3-scFvαHLA-A2 hemibody was inserted in the multiple cloning site (MCS) via specific restriction sites. The color of the vector card and the corresponding DNA sequence matches. Adapted from the certificate of analysis of UCOER Single Expression Hygromycin Vector Set.

8.1.4 VLαCD3-scFvαHLA-A2

GCCGGCGCCACCATGGAAACAGATACCCTGCTGGTGTTCGTGCTGCTCGTGTGGGTGCCAGCTGGAAA
CGGCGATATCGTGCTGACCCAGTCTCCTGCCACACTGTCACTGTCTCCAGGCGAGAGAGCTACCCTGT
CCTGTAGAGCCTCTCAGTCCGTGTCCTACATGAACTGGTATCAGCAGAAGCCCGGCAAGGCCCCTAAG
CGGTGGATCTACGATACCTCCAAGGTGGCCTCTGGCGTGCCAGCCAGATTTTCTGGCTCTGGATCTGG
CACCGACTACTCCCTGACCATCAACTCCCTGGAAGCCGAGGATGCCGCCACCTACTATTGTCAGCAGT
GGTCTAGCAACCCTCTGACCTTTGGCGGAGGCACCAAGGTGGAAATCAAAGGCTCTGGCGGCGGAGGC
TCTCAGGTTCAGTTGGTTCAAAGCGGAGGCGGCGTTGTGCAACCTGGCGGATCTCTGAGAGTGTCTTG
TGCCGCTTCTGGCGTGACCCTGTCTGACTACGGAATGCATTGGGTTCGACAGGCCCCTGGCAAAGGCC
TGGAATGGATGGCCTTCATCCGGAACGACGGCTCCGACAAGTACTACGCCGACTCCGTGAAGGGCAGA
TTCACCATCTCTCGGGACAACTCCAAGAAAACCGTGTCTCTGCAGATGTCCAGCCTGCGCGCTGAGGA
TACCGCCGTGTACTACTGTGCCAAGAACGGCGAGTCTGGCCCTCTGGACTACTGGTACTTCGACCTGT
GGGGCAGAGGCACCCTGGTCACAGTTAGTTCTGGTGGTGGTGGCTCCGGCAGCGGCTCTGGAAATGGA
TCTGGTGGCGGAGGATCCGACGTCGTGATGACTCAGAGCCCTAGCTCTCTGTCTGCCTCCGTGGGCGA
CAGAGTGACCATTACCTGTCAGGCCAGCCAGGACATCTCCAACTACCTCAATTGGTATCAACAAAAGC
CTGGGAAAGCTCCCAAGCTGCTGATCTACGACGCCAGCAATCTGGAAACCGGCGTGCCCTCTAGATTC
TCCGGATCTGGCTCCGGAACCGACTTTACCTTTACAATCAGCTCCCTGCAGCCTGAGGACTTCGCTAC
CTATTACTGCCAGCAGTACAGCTCCTTTCCACTGACATTTGGAGGCGGAACAAAAGTGGATATCAAGC
GGTCCTCCTCCAGCTCCTCCGCTTGGTCCCATCCTCAGTTCGAGAAAGGCGGAGGTTCAGGCGGAGGA
AGCGGCGGATCTGCTTGGAGCCATCCACAGTTTGAAAAGTAATAGCTAGCG